

# 1 Eruptive history and $^{40}\text{Ar}/^{39}\text{Ar}$ geochronology of the Milos volcanic 2 field, Greece 3

4 Xiaolong Zhou<sup>1</sup>, Klaudia Kuiper<sup>1</sup>, Jan Wijbrans<sup>1</sup>, Katharina Boehm<sup>1</sup>, Pieter Vroon<sup>1</sup>

5 <sup>1</sup>Department of Earth Sciences, VU University Amsterdam, De Boelelaan 1085, 1081 HV Amsterdam, The Netherlands.

6 Correspondence to: Xiaolong Zhou (z.x.l.zhou@vu.nl)

7 **Abstract.** High-resolution geochronology is essential to determine the growth-rate of volcanoes, which is one of the key factors  
8 to establish the periodicity of explosive volcanic eruptions. However, there are less high-resolution eruptive histories ( $>10^6$   
9 years) determined for long-lived submarine arc volcanic complexes than for subaerial complexes, since the submarine  
10 volcanoes are far more difficult to observe than subaerial ones. In this study, high-resolution geochronology and major element  
11 data are presented for Milos Volcanic Field (VF) in the South Aegean Volcanic Arc, Greece. The Milos VF has been active  
12 for over 3 Myrs, and the first two million years of its eruptive history occurred in a submarine setting that has emerged above  
13 sea level nowadays. The long submarine volcanic history of the Milos VF makes it an excellent natural laboratory to study the  
14 growth-rate of a long-lived submarine arc volcanic complex. This study reports twenty-one new high-precision  $^{40}\text{Ar}/^{39}\text{Ar}$  ages  
15 and major element compositions for eleven volcanic units of the Milos VF. This allows us to refine the volcanic evolution of  
16 Milos into nine phases and five volcanic quiescence periods of longer than 200 kyrs, on the basis of age, composition, volcano  
17 type and location. Phase 1-5 (~3.34-1.60 Ma) contributed ~85% by volume to the Milos VF, whereas the volcanoes of Phase  
18 6-9 only erupted small volumes (2-6 km<sup>3</sup> in DRE) rhyolitic magmas. Although there are exceptions of the felsic cone volcanoes  
19 of Phase 1-2, in general the Milos VF becomes more rhyolitic in composition from Phase 1 to Phase 9. In particular, the last  
20 three phases (Phase 7-9) only contain rhyolites. Moreover, the high-resolution geochronology suggests that there are divide the  
21 Milos volcanic history into at least three periods of different long term volumetric volcanic output rate ( $Q_v$ ). Period I (~3.3-  
22 2.36 Ma) and III (1.48 Ma-present) have low  $Q_v$  of  $0.9 \pm 0.5 \times 10^{-5} \text{ km}^3 \cdot \text{yr}^{-1}$  and  $0.25 \pm 0.05 \times 10^{-5} \text{ km}^3 \cdot \text{yr}^{-1}$ , respectively. Period  
23 II (2.36 - 1.48 Ma) has a 3-12 times higher  $Q_v$  of  $3.0 \pm 1.7 \times 10^{-5} \text{ km}^3 \cdot \text{yr}^{-1}$ . The  $Q_v$  of the Milos VF is 2-3 orders of magnitude  
24 lower than the average for rhyolitic systems and continental arcs. Most of the effusive eruptions of Period II are probably  
25 derived from magma chambers in the upper crust, whereas the more pumiceous units of Period I and III are probably related  
26 to lower crustal hot-zone.

Commented [MOU1]: Fix Abstract after the text has been revised

## 27 1 Introduction

28 Short-term eruptive histories and compositional variations of lavas and pyroclastic deposits of many arc volcanic fields are  
29 well established. However, high-resolution eruptive histories that extend back  $> 10^5$ - $10^6$  years have been determined only for  
30 a handful of long-lived subaerial arc volcanic complexes. Some examples are: Mount Adams (Hildreth and Lanphere, 1994),  
31 Tatará-San Pedro (Singer et al., 1997), Santorini (Druitt et al., 1999), Montserrat (Cole et al., 2002), Mount Baker (Hildreth  
32 et al., 2003a), Katmai (Hildreth et al., 2003b), and Ceboruco-San Pedro (Frey et al., 2004). In order to establish the growth  
33 rate of volcanic complexes and to disentangle the processes which are responsible for the eruption, fractionation, storage and  
34 transport of magmas over time, comprehensive geological studies are required. These include detailed field mapping, sampling,  
35 high-resolution geochronology and geochemical analysis. Based on these integrated studies, the growth-rate of volcanoes can  
36 be determined to establish the periodicity of effusive and (explosive) volcanism.

37 The Milos Volcanic Field (VF) is a long-lived volcanic complex which has been active for over 3 Myrs. The Milos VF erupted  
38 for a significant part of its life below sea level, similar to the other well studied volcanic structures in the eastern Mediterranean  
39 (Fytikas et al., 1986; Stewart and McPhie, 2006). The eruptive history of the Milos VF has been examined with a broad range

Commented [MOU2]: why is effusive volcanism eliminated? most big volcanoes grow by means of both explosive and effusive eruptions.

40 of the chronostratigraphic techniques such as K-Ar, U-Pb, fission track,  $^{14}\text{C}$  and biostratigraphy (e.g. Angelier et al., 1977,  
41 Fytikas et al., 1976, 1986, Traineau and Dalabakis, 1989, Matsuda et al., 1999, Stewart and McPhie, 2006, Van Hinsbergen et  
42 al., 2004 and Calvo et al., 2012). However, most of the published ages have been measured using the less precise K-Ar or  
43 fission track methods, and modern, high precision  $^{40}\text{Ar}/^{39}\text{Ar}$  ages for the Milos VF have not been published so far. In this  
44 study, (1) we provide high-precision  $^{40}\text{Ar}/^{39}\text{Ar}$  geochronology of key volcanic units of the Milos VF and (2) refine the  
45 stratigraphic framework of the Milos VF with the new high-precision  $^{40}\text{Ar}/^{39}\text{Ar}$  ages and major element composition. (3) We  
46 also quantify and constrain the compositional and volumetric temporal evolution of volcanic products of the Milos VF.

### 47 1.1 Geological setting

48 The Milos VF is part of the South Aegean Volcanic Arc (SAVA), an arc which was formed in the eastern Mediterranean by  
49 subduction of the African plate beneath the Aegean microplate (Figure 1, Nicholls, 1971; Spakman et al., 1988; Duermeijer et  
50 al., 2000; Pe-Piper and Piper, 2007; Rontogianni et al., 2011). The present-day Benioff zone is located approximately 90 km  
51 underneath the Milos VF (Hayes et al., 2018). The upper plate is influenced by extensional tectonics (e.g. McKenzie, 1978;  
52 Pe-Piper and Piper, 2013), which is evident on the island of Milos as horst and graben structures (Figure 2).

53 The Milos VF is exposed on the islands of the Milos archipelago: Milos, Antimilos, Kimolos and Polyegos. The focus of this  
54 study is Milos with a surface area of 151 km<sup>2</sup> for the main island. The geology and volcanology of Milos have been extensively  
55 studied in the last 100 years. The first geological map was produced by Sonder (1924). This work was extended by Fytikas et  
56 al. (1976) and Angelier et al. (1977) and subsequent publications by Fytikas (Fytikas, 1989; Fytikas et al., 1986). Interpretations  
57 based on volcanic facies of the complete stratigraphy were made by Stewart and McPhie (Stewart and McPhie, 2003, 2006).  
58 More detailed studies of single volcanic centres (e.g. Bombarda volcano and Fyriplaka complex) were published by Campos  
59 Venuti and Rossi (1996) and Rinaldi et al. (2003). Milos has also been extensively studied for its epithermal gold  
60 mineralization, that has been summarized by Alfieris et al. (2013). Milos was known during the Neolithic period for its export  
61 of high quality obsidian. Today the main export product is kaolinite, that is mined from hydrothermally altered felsic volcanic  
62 units in the centre of the island (e.g. Alfieris et al. 2013).

63 The geology of Milos can be divided into four main units: (1) metamorphic basement, (2) Neogene sedimentary rocks, (3)  
64 volcanic sequences and (4) the alluvial cover. The metamorphic basement crops out at the southwest, south and southeast of  
65 Milos (Figure 3) and is also found as lithic blocks in many volcanic units as lithics. The metamorphic rocks include lawsonite-  
66 free jadeite eclogites, lawsonite eclogites, glaucophane schists, quartz-muscovite-chlorite and chlorite-amphibole schists  
67 (Fytikas et al., 1976, 1986; Grasemann et al., 2018; Kornprobst et al., 1979). The exposed units belong to the Cycladic  
68 Blueschist Unit (Lower Cycladic nappe), whereas eclogite pebbles in the green lahar unit (e.g. Fytikas, 1977) are derived from  
69 the Upper Cycladic Nappe (Grasemann et al., 2018).

70 On top of this metamorphic basement Neogene fossiliferous marine sedimentary rocks were deposited (e.g. Van Hinsbergen  
71 et al. 2004). This sedimentary sequence can be divided into a lower unit A and upper unit B and that that is unconformable  
72 overlain by volcanoclastic sediments (Van Hinsbergen et al., 2004). Unit A is 80 m thick and consists of fluvial-lacustrine,  
73 brackish and shallow marine conglomerate, sandstone, dolomite and limestone. Unit B is 25-60 m thick and consists of a  
74 sandstone overlain by a succession of alternating marls and sapropels, suggesting a deeper marine setting (Van Hinsbergen et  
75 al., 2004). Five volcanic ash layers that contain biotite are found in this Neogene sedimentary rock sequence either suggesting  
76 that volcanic eruptions in small volume already occurred in the Milos area, or that these ash layers are derived from larger  
77 eruptions of volcanic centres further away from Milos (van Hinsbergen et al., 2004). Age determinations by bio-magneto- and  
78 cyclo-stratigraphy suggested that deposition of Unit A started at approximately 5 Ma, and that Milos subsided 900 m in 0.6  
79 million years (Van Hinsbergen et al. 2004) due to extension. This subsidence happened ca 1.0-1.5 Myrs before the onset of  
80 the main phase of Pliocene- recent volcanism on Milos.

Commented [MOU3]: What is this?

81 The Pliocene-recent volcanic sequence of Milos has been subdivided into different units by Angelier et al. (1977) and Fytikas  
82 et al. (1986). In addition, Stewart and McPhie (2006) provided a detailed facies analysis of the different volcanic units. The  
83 subdivision by Angelier et al. (1977) is not constrained well due to their limited amount of age data. The subdivision of volcanic  
84 units by Fytikas et al. (1986) and facies descriptions of Stewart and McPhie (2006) are summarized below. It is important to  
85 note that according to Stewart and McPhie (2006), the five volcanic cycles described by Fytikas et al. (1986) are difficult to  
86 match with existing age data and the continuous progression in volcanic construction (Fig. 4). For example, the first phase of  
87 Fytikas et al. (1986), the Basal Pyroclastic Series, contains the large pumice cone-crypto dome volcanoes according to Stewart  
88 and McPhie (2006). Two of these pumice-cone crypto dome volcanoes are much younger and intercalated between the  
89 Complex of Domes and Lava Flows (CDLF) of Fytikas et al. (1986).

90 The first volcanic unit deposited in the Milos area is the Basal Pyroclastic Series (BPS) (Fytikas et al., 1986) or submarine  
91 felsic cryptodome-pumice cone volcanoes (Stewart and McPhie, 2006, Figure 2-4). This unit consist of thickly bedded pumice  
92 breccia with a rhyolitic-dacitic composition. These rhyolites-dacites are aphyric or contain quartz-feldspar±biotite phenocrysts.  
93 Graded sandstone and bioturbated and fossil rich (in-situ bivalve shells) mudstone are intercalated, indicating a marine  
94 environment and a water depth of several hundreds of meters (e.g. Stewart, 2003; Stewart and McPhie, 2006), whereas later  
95 degassed magmas with a similar composition intruded as sills and cryptodomes. The BPS has been strongly affected by  
96 hydrothermal fluids, especially the proximal deposits (e.g. Kiliias et al., 2001).

97 The second volcanic unit was named the Complex of Domes and Lava Flows (CDLF, Fytikas et al., 1986) and the volcanic  
98 facies of this unit is described as the submarine dacitic and andesitic domes by Stewart and McPhie (2006). This phase of  
99 effusive submarine volcanism was predominantly andesitic/dacitic in composition and produced microcrystalline rocks with  
100 phenocrysts of pyroxene, amphibole, biotite and plagioclase. The eruption centres were mainly located along NNE faults and  
101 formed up to 300 m thick deposits extending over areas of 2.5 to 10 km around the eruption centres. In the north-eastern part  
102 of Milos, an andesitic scoria cone provided scoria lapilli and bombs to deeper water settings. Sandstone intercalated in the  
103 CDLF contains both igneous and metamorphic minerals suggesting input from the basement. Rounded pebbles of rhyolite and  
104 dacite indicate that some of the volcanic deposits were above sea level, or in very shallow, near shore environments (e.g.  
105 Stewart and McPhie, 2006).

106 The third volcanic unit is called the Pyroclastic Series and Lava Domes (PSLD) by Fytikas et al. (1986) and belongs to  
107 submarine-to-subaerial dacitic and andesitic lava domes of Stewart and McPhie (2006). This highly variable group is  
108 dominated by rhyolitic, dacitic and andesitic lavas, domes, pyroclastic deposits and felsic pumiceous sediments (Stewart and  
109 McPhie, 2006). Thickness varies between 50-200 m, and the deposits are located in the eastern and northern parts of Milos  
110 (Figure 2 and 3). The initial pyroclastic layers were subaqueously deposited and the extrusion of a dome resulted in deposition  
111 of talus around the margins by mass flow. On top of the dome sand- and siltstone with fossils (Ostrea fossil assemblage) and  
112 traction-current structures suggest that the top of the dome was above wave base. The youngest deposits of this unit are dacitic  
113 and andesitic lavas and domes. These domes generated subaerial block-and-ash flow and surge deposits. Paleosols within these  
114 deposits are a clear indicator that some areas were above sea level. The last unit of the PSLD is represented by large subaerial  
115 rhyolitic lava that contain quartz and biotite phenocrysts and is found near Halepa in the south-central part of Milos.

116 The fourth unit consists of the subaerially constructed rhyolitic Complexes of Trachilas and Fyriplaka (CTF) (Fytikas et al.,  
117 1986), which Stewart and McPhie (2006) interpreted as subaerial rhyolitic lava-pumice cones. These two volcanic complexes  
118 are built from rhyolitic pumice deposits and lavas that contain quartz and biotite phenocrysts (10-20 modal %). The deposits  
119 have a maximum thickness of 120 m and decrease to several meters thickness in the distal parts. Basement-derived schist is  
120 found as lithic clasts (Fytikas et al., 1986). In addition, the Kalamos rhyolitic lava dome that outcrops on the southern coast of  
121 Milos produced a lava that spread westwards to the Fyriplaka beach (Figure 2). This lava belongs to this fourth phase and is  
122 probably derived from an older volcano and not the Fyriplaka complex (Campos Venuti and Rossi, 1996).

123 The fifth volcanic unit comprises deposits from phreatic activity, especially in the northern part of the Zefiria Graben and near  
124 Agia Kiriaki (Figure 2 of Stewart and McPhie, 2006). Many overlapping craters are surrounded by lithic breccias that are  
125 composed of variably altered metamorphic basement clasts and volcanic clasts. This phreatic activity has continued into  
126 historic times (Trainau and Dalabakis, 1989). Fytikas et al. (1986) described this unit as “green lahar”, although indicated that  
127 this deposit is not a lahar but the product of phreatic eruptions in the last 0.2 Ma.

## 128 1.2 Previous geochronological studies

129 Previous geochronological work is summarised in Table 1. Angelier et al. (1977) reported six K-Ar ages (0.95-2.50 Ma). These  
130 ages were used in combination with field observations to divide the Milos volcanic succession into four units. However, the  
131 samples from Fyriplaka, the fourth unit, were too young to be dated by Angelier et al. (1977). Fytikas et al. (1976, 1986)  
132 published 16 K-Ar ages for Milos (0.09-3.50 Ma) including an age of 0.09-0.14 Ma for the Fyriplaka complex. Fytikas et al.  
133 (1986) also obtained 3 K-Ar ages for Antimilos ( $0.32 \pm 0.05$  Ma), Kimolos ( $3.34 \pm 0.06$  Ma) and Polyegos ( $2.34 \pm 0.17$  Ma).  
134 Trainau and Dalabakis (1989) dated the very young phreatic deposits by  $^{14}\text{C}$  dating and found ages between 200 BC and 200  
135 AD. Matsuda et al. (1999) published two K-Ar ages of  $0.8 \pm 0.1$  (MI-1) and  $1.2 \pm 0.1$  Ma (MI-4) for the Plakes dome that was  
136 also studied by Fytikas et al. (1986). Bigazzi and Radi (1981) published two fission track ages of  $1.54 \pm 0.18$  and  $1.57 \pm 0.15$   
137 Ma for obsidians of Bombarda-Adamas and Demenaghaki, respectively. Later fission track studies by Arias et al. (2006) ( $1.57$   
138  $\pm 0.12$  and  $1.60 \pm 0.06$  Ma) confirmed these ages. The fission track ages are younger than the K-Ar ages given by Angelier et  
139 al. (1977;  $1.84 \pm 0.08$  Ma for Demenaghaki) and Fytikas et al. (1986;  $1.71 \pm 0.05$  Ma for Bombarda). In the most recent  
140 geochronological study of the Milos VF, Stewart and McPhie (2006) published 4 SHRIMP U/Pb zircon ages: Triades dacite  
141 facies ( $1.44 \pm 0.08$  and  $2.18 \pm 0.09$  Ma), Kalogeros cryptodome ( $2.70 \pm 0.04$  Ma) and the Fylakopi Pumice Breccia ( $2.66 \pm$   
142  $0.07$  Ma). All uncertainties reported here are 1 standard deviation uncertainties as reported in the original publications, except  
143 for the  $^{14}\text{C}$  ages for which uncertainties were not specified.

## 144 2 Methods

### 145 2.1 Mineral separation and sample preparation

146 Samples were collected from all major volcanic units on Milos island as based on the studies of Fytikas et al. (1986), Stewart  
147 and McPhie (2006) and our own observations in the field. Photos of the sample locations and thin sections can be found in the  
148 supplementary material I. Approximately 2 kg of fresh juvenile pyroclastic material or lava was sampled from each unit.  
149 Samples were cut in  $\sim 5$  cm<sup>3</sup> cubes using a diamond saw to remove potentially altered surfaces and obtain the fresh interior  
150 parts. These cubes were ultra-sonicated for 30 minutes in demi-water to remove dust and seawater and dried in an oven  
151 overnight at 50 °C. Dry sample cubes were crushed in a steel jaw crusher, and this fraction was split into two portions of  
152 roughly equal size. One of them was powdered in an agate shatter box and agate ball mill to a grain size of less than 2  $\mu\text{m}$  for  
153 the major-element analysis. The second fraction was sieved to obtain a grain size of 250-500  $\mu\text{m}$  for  $^{40}\text{Ar}/^{39}\text{Ar}$  dating.  
154 Heavy liquids density separation techniques (IJlst, 1973) were used to purify mineral separates (groundmass, biotite, amphibole)  
155 required for the  $^{40}\text{Ar}/^{39}\text{Ar}$  dating. Different densities of heavy liquids were used to obtain groundmass ( $2700 \leq \rho \leq 3000$  kg.m<sup>-3</sup>),  
156 biotite ( $2900 \leq \rho \leq 3100$  kg.m<sup>-3</sup>) and/or amphibole ( $\sim 3100 \leq \rho \leq 3200$  kg.m<sup>-3</sup>). A Franz Isodynamic Magnet separator was  
157 used to remove the magnetic minerals from the non-magnetic minerals and groundmass. The samples for  $^{40}\text{Ar}/^{39}\text{Ar}$  analysis  
158 were purified by handpicking under a binocular optical microscope to select mineral grains without visible alteration and  
159 inclusions.

Commented [MOU4]: clarify - I presume you mean juvenile clasts such as pumice clasts from pyroclastic deposits? or do you mean lithified/welded pyroclastic deposits?

## 160 2.2 <sup>40</sup>Ar/<sup>39</sup>Ar dating

161 The mineral and groundmass samples were wrapped in either 6- or 9-mm aluminium foil and packed in 20 mm aluminium  
162 cups, that were vertically stacked. Based on stratigraphy and previous geochronological constraints >1 Ma samples and the <1  
163 Ma samples were irradiated for respectively 7 and 1 hours in irradiation batches VU108 and VU110 in the CLICIT facility of  
164 the OSU TRIGA reactor. The neutron flux for all irradiations was monitored by standard bracketing using the Drachenfels  
165 sanidine (DRA; 25.52 ± 0.08 Ma, modified from Wijbrans et al., 1995 and calibrated relative to Kuiper et al., 2008) and Fish  
166 Canyon Tuff sanidine (FCs; 28.201 ± 0.023 Ma, Kuiper et al., 2008) with Min et al. (2000) decay constants.

167 In total 24 samples (8 groundmasses, 15 biotites and 2 amphiboles, for sample G15M0026 both biotite and amphibole were  
168 analysed) were measured by either <sup>40</sup>Ar/<sup>39</sup>Ar fusion and/or incremental heating techniques. For incremental heating  
169 experiments 80-100 grains per sample were loaded into a 25-hole (surface per hole ~36 mm<sup>2</sup>) copper tray together with single  
170 grain standards in ~12 mm<sup>2</sup> holes. The tray was prebaked in vacuum (10<sup>-5</sup>-10<sup>-6</sup> mbar) at 250 °C overnight to remove  
171 atmospheric argon and subsequently baked overnight at 120 °C in the ultra-high vacuum sample chamber (<5\*10<sup>-9</sup> mbar) and  
172 purification system connected to a Thermo Scientific Helix MC mass spectrometer.

173 Samples and standards ~~are~~were heated with a focused laser beam at 8 % power using a 50W CW CO<sub>2</sub> laser. The released gas  
174 was cleaned by exposure to a cold trap cooled by a Lauda cooler at -70 °C, a SAES NP10 at 400 °C, Ti sponge at 500 °C and  
175 cold SAES ST172 Fe-V-Zr sintered metal. The five isotopes of argon ~~are~~were measured simultaneously on five different  
176 collectors: <sup>40</sup>Ar on the H2-Faraday, <sup>39</sup>Ar on the H1-Faraday or the H1-CDD, <sup>38</sup>Ar on the AX-CDD, <sup>37</sup>Ar on the L1-CDD and  
177 <sup>36</sup>Ar on the L2-CDD for 15 cycles with 33 seconds integration time (CDD: compact discrete dynodes). The Faraday cups on  
178 H2 and H1 ~~are~~were equipped with 10<sup>13</sup> Ohm amplifiers. Procedural blanks were measured every 2 or 3 analyses in different  
179 sequences, and air-shots were measured every 8-12 hours to correct the instrumental mass discrimination. Gain between  
180 different collectors ~~is~~was monitored by measuring CO<sub>2</sub> on mass 44 in dynamic mode on all collectors. Gain ~~is~~was generally  
181 stable over periods of weeks. Note, that because samples, standards and air calibration runs are measured during the same  
182 period, gain correction does not substantially change the final age results. The raw mass spectrometer data output was  
183 converted by an in-house designed Excel macro script to be compatible with the ArArCalc 2.5 data reduction software  
184 (Koppers, 2002). The atmospheric air value of 298.56 from Lee et al. (2006) is used in the calculations. The correction factors  
185 for neutron interference reactions are (2.64 ± 0.02) x 10<sup>-4</sup> for (<sup>36</sup>Ar/<sup>37</sup>Ar)<sub>ca</sub>, (6.73 ± 0.04) x 10<sup>-4</sup> for (<sup>39</sup>Ar/<sup>37</sup>Ar)<sub>ca</sub>, (1.21 ± 0.003)  
186 x 10<sup>-2</sup> for (<sup>38</sup>Ar/<sup>39</sup>Ar)<sub>K</sub> and (8.6 ± 0.7) x 10<sup>-4</sup> for (<sup>40</sup>Ar/<sup>39</sup>Ar)<sub>K</sub>. All uncertainties are quoted at the 1σ level and include all analytical  
187 errors (i.e. blank, mass discrimination and neutron interference correction and analytical error in J-factor, the parameter  
188 associated with the irradiation process).

189 A reliable plateau age is defined as experiments with at least 3 consecutive steps overlapping at 2-sigma, containing >50% of  
190 the <sup>39</sup>Ar<sub>K</sub>, a Mean Square Weighted Deviate (MSWD) value <2.5, and with an <sup>40</sup>Ar/<sup>36</sup>Ar inverse isochron intercept that does  
191 not deviate from atmospheric argon at 2-sigma. All the inverse isochron ages used the same steps as used in the weighted mean  
192 ages, and all relevant analytical data for the age calculations following standard practices (Schaen et al., 2020) can be found  
193 in in the supplementary material II.

## 194 2.3 ~~Major element analysis~~Whole-rock major element analysis by XRF

195 Major-element concentrations were measured by X-ray fluorescence spectroscopy (XRF) on a Panalytical AxiosMax. A  
196 Panalytical Eagon2 was used to create 40mm fused glass beads of Li<sub>2</sub>B<sub>4</sub>O<sub>7</sub>/LiBO<sub>2</sub> (65.5:33.5%, Johnson & Johnson  
197 Spectroflux 110) with a 1:6 dilution sample-flux ratio that were molten at 1150 °C. Sample powders were ignited at 1000 °C  
198 for 2 hours to determine loss on ignition (LOI) before being mixed with the Li<sub>2</sub>B<sub>4</sub>O<sub>7</sub>/LiBO<sub>2</sub> flux. Interference corrected spectra  
199 intensities were converted to oxide-concentrations against a calibration curve consisting of 30 international standards. The  
200 precision, expressed as the coefficient of variation (CV), is better than 0.5%. The accuracy, as measured on the international  
201 standards AGV-2, BHVO-2, BCR-2 and GSP-2 was better than 0.7% (1 RSD) (supplementary material III).

202 **2.4 Rock textural analysis and eruption volume calculations**

203 The crystallinity and vesicularity were estimated with Image-J software by scanning the thin section of each sample 4-6 times  
204 to cover the entire area. For the crystallinity only the phenocrysts were considered, crystals smaller than 50 µm were included  
205 in the groundmass. The estimations of crystallinity and vesicularity on the older samples (>1.0 Ma) of Milos VF are all from  
206 lava and domes. The younger samples (<1.0 Ma) are from pumiceous pyroclastic units. The other old pumices of the Profitis  
207 Illias and Filakopi volcanoes are not included in this study due to the severe alteration that prevents the collection of reliable  
208 geochemical and geochronological data on these samples. The mean value and standard deviation of the crystallinity and  
209 vesicularity were also calculated.

210 The minimum and/or maximum eruption volume of each volcano during each eruption period is derived from the ranges of  
211 thickness and surface areas that are reported in Campos and Rossi (1996) and Stewart and McPhie (2006). We converted these  
212 volumes to Dense Rock Equivalent (DRE) based on the magma type of different deposits. This analysis only includes the  
213 onshore deposits and results in a smaller estimate for larger pyroclastic volumes. The DRE volume is calculated using the  
214 equation of (Crosweller et al., 2012):

215 
$$DRE (km^3) = \frac{tephra\ vol (km^3) \times tephra\ density (kg/m^3)}{magma\ density (kg/m^3)}$$

216 Tephra density is assumed to be 1000 kg/m<sup>3</sup> (Crosweller et al., 2012). Magma density varies depending on the magma type.  
217 Here we used 2300 kg/m<sup>3</sup> for rocks with a SiO<sub>2</sub> range of 65-77 wt.% and 2500 kg/m<sup>3</sup> for all samples with SiO<sub>2</sub> < 65 wt.%  
218 (Table 4 for major-element composition). DRE corresponds to the unvesiculated erupted magma volume and DRE volumes  
219 are converted to include vesicularity. Therefore, we did not convert the volume of some cryptodome and lavas from Profitis  
220 Illias (G15M0017), Triades (G15M0021-24), Dhemenehaki (G15M0032B) and Halepa (G15M0013) to the DRE since they  
221 contain less than 5% vesicles.

222 **3 Results**

223 **3.1 <sup>40</sup>Ar/<sup>39</sup>Ar age results**

224 In this section, we present our groundmass, biotite and amphibole <sup>40</sup>Ar/<sup>39</sup>Ar results for eleven volcanic units of Milos. The  
225 <sup>40</sup>Ar/<sup>39</sup>Ar ages range from 0.06 to 4.10 Ma and cover most of the major volcanic units of Milos. Table 2 and 3 show the  
226 <sup>40</sup>Ar/<sup>39</sup>Ar results of incremental heating steps and single grain fusion analyses, respectively. Note that the Irr-ID column in  
227 these two Tables represents the irradiation ID of the analytical experiment (e.g. VU108-, VU110-) and the top right superscripts  
228 (G, B, A, O) in the sample IDs (e.g., G15M0029<sup>G</sup>, G15M0021<sup>B</sup>) refer to groundmass, biotite, amphibole and obsidian.

229 **3.1.1 Groundmass <sup>40</sup>Ar/<sup>39</sup>Ar plateau and/or isochron ages**

230 All groundmass samples yielding <sup>40</sup>Ar/<sup>39</sup>Ar plateau and isochron ages with more than 50% <sup>39</sup>Ar<sub>K</sub> and less than 2.5 MSWD  
231 included in their age spectrum are shown in Figure 4 and reported in Table 2. The <sup>40</sup>Ar/<sup>36</sup>Ar isochron intercepts do not deviate  
232 from atmospheric argon at the 2-sigma level, unless stated otherwise (Table 3). Sample G15M0016 was collected from an  
233 extrusive dyke at Klefiko in the southwest of Milos (Figure 2). Three incremental heating experiments were performed on the  
234 groundmass of this sample (Figure 5A). The first experiment (VU108-Z8a) produced a weighted mean age of 2.71 ± 0.02 Ma  
235 (MSWD 2.31; <sup>39</sup>Ar<sub>K</sub> 79.6%; inverse isochron age 2.65 ± 0.10 Ma). The other two, VU108-Z8a\_4 and VU108-Z8b\_1, have  
236 plateau ages of 2.61 ± 0.03 Ma (MSWD 0.93; <sup>39</sup>Ar<sub>K</sub> 57.4%; inverse isochron age 2.69 ± 0.10 Ma) and 2.67 ± 0.01 Ma (MSWD  
237 1.50; <sup>39</sup>Ar<sub>K</sub> 65.57%; inverse isochron age 2.55 ± 0.05 Ma), respectively. The three experiments are remarkably similar.  
238 Although the amount of radiogenic <sup>40</sup>Ar is low (<20%), a combined age of 2.66 ± 0.01 Ma is considered to be best estimate  
239 with a relatively high MSWD value (2.51).

Commented [MOU5]: doesnt make sense; dykes by definition are intrusions

240 Two lava samples, G15M0019 and G15M0020, were collected from Kontaro in north-eastern Milos (Figure 2). Three replicate  
241 incremental heating steps experiments of groundmass from sample G15M0019 (VU108-Z6a\_4; VU108-Z6a\_5 and VU108-  
242 Z6b\_1, Figure 5B) were performed that are not reproducible. Their plateau ages range from 1.55 Ma to 1.62 Ma with relatively  
243 high MSWD (3.8-4.5), 56-95% of the total  $^{39}\text{Ar}_K$ , 34-53% of radiogenic  $^{40}\text{Ar}$ , 0.88-1.02 of K/Ca and an atmospheric isochron  
244 intercept of 297-315. We consider the isochron age from the last experiment (VU108-Z6b\_1) as the only reliable age ( $1.48 \pm$   
245  $0.02$  Ma, MSWD 0.44) because of the least scatter in this experiment, and therefore the best estimate for the eruption age.  
246 Three replicate incremental heating steps experiments of groundmass from sample G15M0020 (VU108-Z5a\_5; VU108-Z5b\_1  
247 and VU108-Z5b\_2, Figure 5C) were analysed. These experiments are similar at the lower temperature heating steps. They  
248 produced statistically meaningful plateau ages ranging from 1.52-1.56 Ma with 41-62% of the total  $^{39}\text{Ar}_K$ , 18-48% of  
249 radiogenic  $^{40}\text{Ar}$ , 1.51-1.73 of K/Ca and an atmospheric isochron intercept of 295-300. Their combined weighted mean age is  
250  $1.54 \pm 0.01$  Ma (MSWD 3.06;  $^{39}\text{Ar}_K$  57.32%) with 25.31% of  $^{40}\text{Ar}^*$ .  
251 Sample G15M0032B (obsidian) was collected from a pumice cone volcano at Demeneghaki (Figure 2). One incremental  
252 heating experiment of this sample (VU108-Z18, Figure 5D) yielded a plateau age of  $1.825 \pm 0.002$  Ma (MSWD 0.91;  $^{39}\text{Ar}_K$   
253 98.6%). The  $^{40}\text{Ar}^*$  is 93.86%. The inverse isochron age is identical to the weighted mean plateau age  $1.825 \pm 0.002$  Ma. The  
254 age of  $1.825 \pm 0.002$  Ma is considered the best estimate for the eruption age of the Demeneghaki obsidian.

### 255 3.1.2 Groundmass $^{40}\text{Ar}/^{39}\text{Ar}$ plateau and/or isochron ages (25-40% $^{39}\text{Ar}_K$ released)

256 The results shown in Figure 5 did not yield weighted mean plateau according to standard criteria including  $^{39}\text{Ar}_K > 50\%$ , but  
257 still provide some useful age information. Sample G15M0017 was collected from a cryptodome of the Profitis Illias volcano  
258 of southwestern Milos (Figure 2). Three replicate incremental heating experiments, VU108-Z7a, VU108-Z7a\_4 and VU108-  
259 Z7b\_1, have been performed on this sample which resulted in disturbed age spectra (Figure 6A). The consecutive lower  
260 temperature steps of all experiments define ages of  $< 2.5$  Ma, which is much younger than the ages of the submarine pyroclastic  
261 products of the lower series at Kleftiko and/or Profitis Illias (3.0-3.5 Ma, Fytikas et al., 1986 and Stewart and McPhie, 2006).  
262 At the consecutive higher temperature heating steps, these experiments yielded  $3.64 \pm 0.08$  Ma ( $^{40}\text{Ar}/^{36}\text{Ar}$  293.87  $\pm$  4.77;  
263 VU108-Z7a),  $4.10 \pm 0.06$  Ma ( $^{40}\text{Ar}/^{36}\text{Ar}$  298.44  $\pm$  15.51; VU108-Z7a\_4) and  $3.41 \pm 0.05$  Ma ( $^{40}\text{Ar}/^{36}\text{Ar}$  295.97  $\pm$  7.34; VU108-  
264 Z7b\_1). The total fusion and inverse isochron ages of the three experiments gave large ranges of 2.25-3.23 and 3.68-4.14 Ma,  
265 respectively, and none of these high temperature heating steps produced a statistical plateau (all MSWD  $> 2.0$ ). The amount  
266 of radiogenic  $^{40}\text{Ar}$  of both  $^{40}\text{Ar}/^{39}\text{Ar}$  result from our sample and K-Ar from previous studies (Fytikas et al., 1986) is rather low  
267 ( $< 15\%$ ) for a sample of this age based on our laboratory experience. Therefore, the estimated age range for the oldest volcanic  
268 products of the Milos VF should be confirmed by other dating techniques.

269 Sample G15M0015 is also a cryptodome breccia from Profitis Illias (Figure 2). Two replicate incremental step heating  
270 experiments were performed on the groundmass of this sample (VU108-Z9a and VU108-Z9b\_1, Figure 6B). Experiment  
271 VU108-Z9a groundmass shows a disturbed age spectrum with ages increasing from  $\sim 3$  Ma in the initial heating steps to  $\sim 3.2$   
272 Ma followed by a decrease to  $\sim 3$  Ma in the high temperature heating steps. The consecutive heating steps only exist at the  
273 lower temperature steps yielding a "plateau" of  $3.12 \pm 0.02$  Ma (MSWD 9.07). Due to the excess argon ( $^{40}\text{Ar}/^{36}\text{Ar}$  304.19  $\pm$   
274 1.25 comprising 43.07% of the released  $^{39}\text{Ar}_K$ ), the inverse isochron of  $3.06 \pm 0.02$  Ma (MSWD 0.01) is more reliable for this  
275 analysis. The inverse isochron age of the second groundmass (VU108-Z9b\_1) is identical at  $3.04 \pm 0.02$  Ma (MSWD 1.14;  
276  $^{39}\text{Ar}_K$  27.00%) and  $^{40}\text{Ar}/^{36}\text{Ar}$  of 293.83  $\pm$  1.38 obtained at high temperature steps. The two experiments are remarkably similar.  
277 Although the sample does not formally fulfil the definition of a plateau age comprising  $> 50\%$   $^{39}\text{Ar}_K$  released, a combined age  
278 of  $3.06 \pm 0.02$  Ma (MSWD 1.14;  $^{39}\text{Ar}_K$  22.79%,  $^{40}\text{Ar}^*$  41.77%) most likely represents the eruption age. This  $^{40}\text{Ar}/^{36}\text{Ar}$  age is  
279 consistent with the K-Ar age from the same lithology of  $3.08 \pm 0.08$  Ma (Fytikas et al. 1986).

280 Sample G15M0029 is an andesite collected from Korakia in the northeast of Milos (Figure 2). Two incremental heating  
281 experiments (VU108-Z16a and VU108-Z16b\_1, Figure 6C) were performed on this sample. The two experiments are

282 remarkably similar with a decreasing age from ~2.85 Ma at the lower temperature heating steps to 2.65 Ma at the higher  
283 temperatures. The higher temperature heating steps of both experiments yielded weighted mean plateau ages of  $2.67 \pm 0.01$   
284 Ma (MSWD 0.96;  $^{39}\text{Ar}_k$  23.61%,  $^{40}\text{Ar}^*$  56.34%; inverse isochron age  $2.68 \pm 0.02$  Ma) and  $2.69 \pm 0.01$  Ma (MSWD 1.32;  
285  $^{39}\text{Ar}_k$  27.08%,  $^{40}\text{Ar}^*$  55.78%; inverse isochron age  $2.67 \pm 0.03$  Ma). The isochron intercepts for both experiments are  
286 atmospheric. The combined age of  $2.68 \pm 0.01$  Ma should be considered with caution due to the rather low amount of released  
287  $^{39}\text{Ar}$  (23-28%).

### 288 3.1.3 Single biotite grain $^{40}\text{Ar}/^{39}\text{Ar}$ fusion and/or isochron ages

289 Results of nine single fusion experiments are given in Figure 7. Nine or ten replicate single fusion experiments were conducted  
290 on 5-10 grains biotite per fusion. Sample G15M0006 is from a solid in-situ dacite with columnar joints from the Kalogeros  
291 cryptodome in the northeast of Milos (VU108-Z11, Figure 7A). The sample shows a weighted mean age of  $2.72 \pm 0.01$  Ma  
292 with 9 out of 10 total fusion experiments (MSWD 1.95; 9/10) with an average 47.9% of radiogenic  $^{40}\text{Ar}$ . The inverse isochron  
293 age is  $2.62 \pm 0.04$  Ma (MSWD 0.99). Note that excess argon ( $^{40}\text{Ar}/^{36}\text{Ar}$  310.2  $\pm$  4.0) is present, hence the inverse isochron age  
294 is younger compared to the weighted mean age. The isochron age of  $2.62 \pm 0.04$  Ma is considered as the best estimate for the  
295 emplacement age.

296 Sample G15M0025 was collected from the Mavros Kavos lava dome located in the west of Milos (Figure 2). The biotite of  
297 this sample (VU108-Z2, Figure 7B) shows a weighted mean age of  $2.36 \pm 0.01$  Ma (MSWD 0.70; 9/10;  $^{40}\text{Ar}^*$  37.60%, inverse  
298 isochron age  $2.34 \pm 0.04$  Ma) with an  $^{40}\text{Ar}/^{36}\text{Ar}$  intercept of  $300.6 \pm 3.5$ . The age of  $2.36 \pm 0.01$  Ma is considered the best  
299 eruption age estimate for this sample.

300 Sample G15M0023 and -24 are from the Triades lava dome of the northeast of Milos (Figure 2). A mafic enclave G15M0022  
301 (host rock G15M0021) was collected from a lava near Cape Vani (Figure 2). The total fusion experiments of the biotites show  
302 that their initial  $^{40}\text{Ar}/^{36}\text{Ar}$  estimates overlap with air (296-300). The total fusion ages gave the best estimates for their eruption  
303 ages of 2.10-2.13 Ma using 22 out of 31 fusions with a range of radiogenic  $^{40}\text{Ar}$  between 30-36% (Figure 7B).

304 Sample G15M0013 is from the rhyolitic Halepa lava dome in the south of Milos (Figure 2). The total fusion experiment  
305 (VU108-Z13, Figure 7C) on biotite of this sample produced a weighted mean age of  $1.04 \pm 0.01$  Ma (MSWD 1.62; 9/10,  $^{40}\text{Ar}^*$   
306 26.3%; inverse isochron age  $1.02 \pm 0.04$  Ma) with an initial  $^{40}\text{Ar}/^{36}\text{Ar}$  estimate of  $299.8 \pm 4.1$ . The best estimate for the  
307 eruption age of the Halepa rhyolite is  $1.04 \pm 0.01$  Ma.

308 Sample G15M0034 and 35 were collected from a lava dome located southeast of the Trachilas cone (Figure 2). Nine total  
309 fusion experiments (VU108-Z21, Figure 7C) were performed on biotite of sample G15M0035 and yielded  $0.63 \pm 0.02$  Ma  
310 (MSWD 1.26; 6/9;  $^{40}\text{Ar}^*$  4.9%; inverse isochron age  $0.77 \pm 0.13$  Ma). The atmospheric isochron intercept overlaps with air at  
311 2-sigma ( $296.4 \pm 1.7$ ). The 4.9% of radiogenic  $^{40}\text{Ar}$  is so low that we should consider the age of  $0.63 \pm 0.02$  Ma with caution.  
312 For biotite of sample G15M0034 (VU108-Z20, Figure 7C) one total fusion experiment produced a weighted mean age of  $0.51$   
313  $\pm 0.02$  Ma (MSWD 0.95; 6/10;  $^{40}\text{Ar}^*$  3.5%; inverse isochron age  $0.61 \pm 0.08$  Ma) with an atmospheric isochron intercept. The  
314 age of  $0.51 \pm 0.02$  Ma also needs to be considered as possibly suspect due to the low amount of radiogenic  $^{40}\text{Ar}$ .

315 Sample G15M0033 was collected from the Kalamos lava along the coast of the southwest of the Fyriplaka rhyolitic complex  
316 (Figure 2). Biotite of this sample (VU108-Z19, Figure 7C) yielded  $0.412 \pm 0.004$  Ma (MSWD 1.10; 8/10; inverse isochron  
317 age  $0.39 \pm 0.02$  Ma) with ~22.2% of radiogenic  $^{40}\text{Ar}$  which is considered as the eruption age for the Kalamos lava.

### 318 3.1.4 Multiple biotite grain $^{40}\text{Ar}/^{39}\text{Ar}$ incremental heating plateau and/or isochron ages

319 Figure 8 displays the biotite  $^{40}\text{Ar}/^{39}\text{Ar}$  ages measured by the incremental heating steps method. Sample G15M0021 is the host  
320 lava of mafic enclave G15M0022. Twelve replicate total fusion experiments of its biotite (VU110-Z4, Table 3) produced an  
321 age of  $2.48 \pm 0.04$  Ma (MSWD 1.49; 4/12,  $^{40}\text{Ar}^*$  36.09%; inverse isochron age  $3.44 \pm 0.46$  Ma). Although this suggests a  
322 correct age, the large analytical error of each fusion ( $>0.3$  Ma on average) and poor reproducibility (4/12) of this experiment



323 probably results in an unreliable age. Therefore, two more incremental heating experiments were performed on this sample  
324 (VU110-Z4\_2 and VU110-Z4\_2b, Figure 8A), that gave an age of  $1.97 \pm 0.01$  Ma (MSWD 1.66;  $^{39}\text{Ar}_K$  63.8%,  $^{40}\text{Ar}^*$  54.7%;  
325 inverse isochron age  $1.97 \pm 0.03$  Ma) and  $2.01 \pm 0.01$  Ma (MSWD 6.76;  $^{39}\text{Ar}_K$  75.39%,  $^{40}\text{Ar}^*$  57.84%; inverse isochron age  
326  $2.04 \pm 0.05$  Ma), respectively. The scatter in the latter is too high to define a reliable plateau age and the first incremental  
327 heating experiment is considered as the best estimate of the eruption age of this sample.

328 Sample G15M0007 was collected from the rhyolitic ~~Trachilas~~ Trachilas complex in the north of Milos (Figure 2). Twenty-two  
329 total fusion (VU110-Z12, Table 3) and two incremental heating experiments (VU110-Z12a and 12b, Figure 8B) were  
330 performed on biotite of this sample. The total fusion experiments did not result in a reliable age due to the large errors of single  
331 steps ( $\pm 0.19$  Ma on average) and the rather low amount of radiogenic  $^{40}\text{Ar}$  (9.1%). On the other hand, the first incremental  
332 heating experiment produced a plateau age of  $0.30 \pm 0.01$  Ma (MSWD 4.61;  $^{39}\text{Ar}_K$  56.60%; inverse isochron age  $0.28 \pm 0.05$   
333 Ma) including 14.51% of radiogenic  $^{40}\text{Ar}$ . The second incremental heating experiment yielded a plateau of  $0.317 \pm 0.004$  Ma  
334 (MSWD 1.29;  $^{39}\text{Ar}_K$  74.05%; inverse isochron age  $0.31 \pm 0.03$  Ma) with a higher amount of radiogenic  $^{40}\text{Ar}$  (18.30%). The  
335 isochron intercepts of both incremental heating experiments are atmospheric. The second experiment is the best estimate for  
336 the eruption age, since it contained the largest amount of radiogenic  $^{40}\text{Ar}$  and has a better reproducibility of single heating  
337 steps.

338 Three pumice clasts (G15M0008-9 and G15M0012) were sampled from different layers of the Fyriplaka complex (Figure 2).  
339 The first incremental step heating experiment of biotite from sample G15M0009 (VU110-Z23a, Figure 8C) gave negative ages  
340 at the lower temperature heating steps. Four consecutive higher temperature heating steps seem to define a “plateau” of  $0.11$   
341  $\pm 0.02$  Ma (MSWD 1.37) only using 18.33% of the total  $^{39}\text{Ar}_K$  with 1.65% of radiogenic  $^{40}\text{Ar}$ . The second experiment (VU110-  
342 Z23b) also yielded a “plateau” of  $0.11 \pm 0.03$  Ma (MSWD 6.77) at higher temperature heating steps including 41.05% of the  
343 total  $^{39}\text{Ar}_K$  and 3.13% of radiogenic  $^{40}\text{Ar}$ . The significantly larger error of the isochron age may be due to the clustering of data  
344 close to zero on the y-axis. The two experiments (VU110-Z23a and Z23b) are comparable. The combined age of  $0.11 \pm 0.02$   
345 (MSWD 3.5) is consistent with the age of 0.09-0.14 Ma from Fytikas et al. (1986). Although only 29.50% of the released  $^{39}\text{Ar}_K$   
346 was used for this sample, we believe this age is the eruption age of this layer in the Fyriplaka complex.

347 For biotite of sample G15M0012 both incremental step heating experiments are comparable. Both of them yielded plateau  
348 ages of  $0.05 \pm 0.01$  Ma (VU110-Z24a; MSWD 3.09;  $^{39}\text{Ar}_K$  38.89%,  $^{40}\text{Ar}^*$  2.89%; inverse isochron age  $0.14 \pm 0.03$  Ma) and  
349  $0.09 \pm 0.02$  Ma (VU110-Z24b; MSWD 8.16;  $^{39}\text{Ar}_K$  48.04%,  $^{40}\text{Ar}^*$  4.59%; inverse isochron age  $0.09 \pm 0.05$  Ma) at higher  
350 temperature heating steps (Figure 8C). The clustering of data points of experiment VU110-Z24a could result in the lower  
351 initial estimate of  $^{40}\text{Ar}/^{36}\text{Ar}$  ( $285.98 \pm 4.76$ ). However, the combined age of  $0.07 \pm 0.01$  Ma, using 43.53% of the total  $^{39}\text{Ar}_K$   
352 with an atmospheric isochron intercept ( $295.67 \pm 7.39$ ), could be the representative age of eruption.

353 Biotite of sample G15M0008 did not result in a reliable plateau in the first incremental step heating experiment (VU110-Z22a,  
354 Figure 8C) but shows a very disturbed age spectrum. The second experiment (VU110-Z22b) yielded  $0.062 \pm 0.003$  Ma (MSWD  
355 0.91) using 71.81% of the total  $^{39}\text{Ar}_K$  with 2.69% of radiogenic  $^{40}\text{Ar}$  as the best estimate of the eruption age.

### 356 3.1.5 Multiple amphibole grain $^{40}\text{Ar}/^{39}\text{Ar}$ multi-grain incremental heating plateau and/or isochron ages

357 There are only two amphibole samples that yielded  $^{40}\text{Ar}/^{36}\text{Ar}$  plateau and/or isochron ages (Figure 9A and B). Sample  
358 G15M0004 was collected from the pyroclastic series of Adamas from the PSLD (Fytikas et al., 1986), to the north of Bombarda  
359 (Figure 2). Two replicate heating experiments of G15M0004 amphibole (VU108-Z10\_1 and VU108-Z10\_2) were performed  
360 yielding  $2.99 \pm 0.11$  Ma (MSWD 1.00;  $^{39}\text{Ar}_K$  87.31%,  $^{40}\text{Ar}^*$  16.36%; inverse isochron age  $7.89 \pm 2.46$  Ma) and  $2.86 \pm 0.09$   
361 Ma (MSWD 1.50;  $^{39}\text{Ar}_K$  86.18%,  $^{40}\text{Ar}^*$  17.58%; inverse isochron age  $0.70 \pm 0.29$  Ma). The variable atmospheric isochron  
362 intercept of both experiments ( $^{40}\text{Ar}/^{36}\text{Ar}$   $202.39 \pm 48.47$  and  $348.91 \pm 27.33$ ) is due to clustering of the data points. Note that  
363 also the amount of radiogenic  $^{40}\text{Ar}$  is rather low (~17%). The two experiments are remarkably similar. A combined inverse

364 isochron age of  $1.95 \pm 0.45$  Ma (MSWD 1.17;  $^{40}\text{Ar}/^{36}\text{Ar}$  319.51  $\pm$  14.70) is considered the best estimate, but ideally this age  
365 should be checked by other techniques.  
366 Sample G15M0026 is from the same location as sample G15M0025, which gives us the opportunity to compare the biotite age  
367 with the amphibole age. One total fusion experiment of biotite (VU108-Z1b) yielded a weighted mean age of  $2.35 \pm 0.01$  Ma  
368 (MSWD 1.36;  $^{40}\text{Ar}^*$  38.6%). The atmospheric isochron intercept is low ( $^{40}\text{Ar}/^{36}\text{Ar}$  292.01  $\pm$  2.92), the inverse isochron age of  
369  $2.42 \pm 0.04$  Ma (MSWD 0.93) is considered the best result from the biotite. Two incremental heating experiments for  
370 amphibole (VU108-Z1b\_1 and VU108-Z1b\_2) gave plateau ages of 2.67-2.70 Ma which are much higher values than the  
371 biotite inverse isochron ages (2.28-2.31 Ma). This result could be caused by the high  $^{40}\text{Ar}/^{36}\text{Ar}$  isochron intercepts (>320) with  
372 large uncertainties of  $\sim 29$ . Therefore, on the basis of the remarkable similarity of the two experiments, the combined inverse  
373 isochron age of  $2.31 \pm 0.28$  Ma (MSWD 0.93,  $^{39}\text{Ar}_K$  71.36%,  $^{40}\text{Ar}^*$  34.97%) is considered as the best estimate from amphibole  
374 which overlaps with the biotite age of  $2.42 \pm 0.03$  Ma. This biotite age of  $2.42 \pm 0.03$  Ma is considered to be the best approximation  
375 of the eruption age.

### 376 3.2 Major element results

377 Major-element results are given in Table 4. The major element compositions range from 54 to 78 wt.%  $\text{SiO}_2$  (basaltic-andesite-  
378 rhyolite to dacite-rhyolite, see Figure 10A). The most felsic samples ( $\text{SiO}_2 > 75$  wt.%) belong to the Fyriplaka and Trachilas  
379 complexes. Our data overlap with those of previous studies and display a similar range in  $\text{SiO}_2$ - $\text{K}_2\text{O}$  (Francalanci and Zellmer,  
380 2019 and reference therein). The samples of Polyegos are similar to the Fyriplaka and Trachilas complexes, whereas the older  
381 Milos samples overlap with Kimolos and Antimilos (Fytikas et al., 1986, Francalanci et al., 2007).  
382 Although some samples of Antimilos are tholeiitic, all of the Milos volcanic units belong to the calc-alkaline and medium to  
383 high-K series (Figure 10B). A mafic inclusion, sample G15M0022, has high  $\text{K}_2\text{O}$  (6%), similar to sample G15M0021 (7.2  
384 wt.%). Both of them were collected from the Vani Cape area (Fig. 2). The  $\text{SiO}_2$  wt.% versus our  $^{40}\text{Ar}/^{39}\text{Ar}$  ages diagram (Figure  
385 11A) shows that there is a tendency of the volcanic units to become more felsic over time. In the diagram with  $\text{K}_2\text{O}/\text{SiO}_2$   
386 versus age there is no significant change (Figure 11CB).

### 387 3.3 Variations of rock texture and eruption volume with ages

388 Figure 11DC and ED show the variations of crystallinity and vesicularity of the studied samples versus the  $^{40}\text{Ar}/^{39}\text{Ar}$  ages.  
389 There is lack of geochemical and petrological data of the old-pumice deposits of the Profitis Ilias (>3.0 Ma). Apart from the  
390 other old pumiceous pyroclastic units, Trachilas and Fyriplaka complexes (<1.0 Ma), Profitis Ilias (>3.0 Ma) and Filakopi  
391 (~2.66 Ma) volcanoes, has low crystallinity (<10%) and high vesicularity (10-100%) based on the data of Stewart (2003).  
392 Before 1.48 Ma, the crystallinity of the Milos volcanic units is relatively high (10-40%) and vesicularity varies between 1-  
393 10%. Since after 1.48 Ma, the lava unit of the Halepa dome and the young pumiceous unit of Trachilas and Fyriplaka  
394 complexes (<1.0 Ma) have low the vesicularity (0.1-10%) and crystallinity (<10%+0-40%), and the high vesicularity (10-  
395 100%) tends to become higher with younger deposits. The volcanic complex of Milos was largely (~85% by volume)  
396 constructed before ~1.486 Ma (Figure 11A2). During 1.4859-0.06 Ma-present, only a small volume (~15%) of rhyolitic magma  
397 was added from different eruption vents. The ratio of eruption volume of Milos VF in submarine to subaerial is 6-8. At least  
398 approximately  $12 \text{ km}^3$  in DRE (minimum) has been added by submarine volcanism, whereas  $\sim 2 \text{ km}^3$  was subaerially added.

### 399 4 Discussion

400 In this section, our  $^{40}\text{Ar}/^{39}\text{Ar}$  results are compared with previously published geochronological data, and subsequently used to  
401 refine the stratigraphy of the Milos VF. In the last part, we will discuss the temporal variations in major elements and the  
402 volumetric volcanic output rate of the Milos VF.

Commented [MOU6]: excluding all these parts of the sequence means the conclusion is meaningless "vesicularity (0.1-10%) and crystallinity (10-40%) tends to become higher with younger deposits"

Commented [MOU7]: this result is meaningless because you have no data on the submarine part of the volcanic edifice

403 **4.1 Comparison with the previous geochronological studies on the Milos VF**

404 ~~K~~-Ar ages may show undesirable and unresolvable scatter due to various problems: (1) in accurate determination of radiogenic  
405 argon due to either incorporation of excess argon or incomplete degassing of argon during the experiments; (2) inclusion of  
406 cumulate or wall rock phenocrysts in bulk analyses; (3) disturbance of a variety of geological processes such as slow cooling,  
407 thermal reheating; (4) unrecognized heterogeneities due to separate measurements of potassium and argon content by different  
408 methods; (5) requirement of relatively large quantities (milligrams) of pure sample (e.g. Lee, 2015). In addition to these  
409 methodological issues, in the case of Milos we observe that hydrothermal alteration caused substantial kaolinitisation, in  
410 particular the felsic volcanic samples, that most likely has affected the K-Ar systematics. Some of these issues are also valid  
411 for the  $^{40}\text{Ar}/^{39}\text{Ar}$  method, however, the K-Ar method does not allow testing if ages are compromised.

412  $^{40}\text{Ar}/^{39}\text{Ar}$  ages only need isotopes of argon to be measured from a single aliquot of sample with the same equipment that can  
413 eliminate some of the problems with sample inhomogeneity. Furthermore, step heating and multiple single fusion experiments  
414 can shed light on sample inhomogeneity due to partial alteration effects. The high sensitivity of modern noble gas mass  
415 spectrometers for  $^{40}\text{Ar}/^{39}\text{Ar}$  measurements results in very small sample amounts needed for analysis, that can yield more  
416 information on the thermal or alteration histories than larger samples. Moreover, other argon isotopes ( $^{36}\text{Ar}$ ,  $^{37}\text{Ar}$  and  $^{38}\text{Ar}$ ) can  
417 be used to infer some information about the chemical compositions (i.e. Ca and Cl) of samples. A high-resolution laser  
418 incremental heating method of  $^{40}\text{Ar}/^{39}\text{Ar}$  dating allows us to resolve the admixture of phenocryst-hosted inherited  $^{40}\text{Ar}$  in the  
419 final temperature steps of the incremental step heating experiments. More than half of our  $^{40}\text{Ar}/^{39}\text{Ar}$  ages derived for this study  
420 are based on this method. All incremental step heating experiments are reproducible, except for the sample G15M0017 which  
421 gave the oldest age. The total fusion experiments of this study gave at least five times smaller analytical uncertainty (1SE on  
422 average  $\leq 0.01$  Ma) than the previous studies using conventional K-Ar (Angelier et al., 1977; Fytikas et al., 1976, 1986; Matsuda  
423 et al., 1999) and SHRIMP U/Pb zircon methods (Stewart and McPhie, 2006). Fission track dating on obsidians of the Milos  
424 VF produced two ages (Bigazzi and Radi, 1981; Arias et al., 2006) which seems to overlap with the K-Ar and  $^{40}\text{Ar}/^{39}\text{Ar}$  ages,  
425 but with larger uncertainty. U/Pb zircon ages could indicate the timing of zircon formation at high temperature ( $>1000$  °C) in  
426 magma chambers significantly prior to volcanic eruption (e.g. Flowers et al., 2005). On the other hand, the lower closure  
427 temperature of K-rich minerals ( $<700$  °C) makes the K-Ar and  $^{40}\text{Ar}/^{39}\text{Ar}$  ages better suited to determine the timing of extrusion  
428 of volcanic products (e.g. Grove and Harrison, 1996; Cassata and Renne, 2013).

429 The MSWD value, as a measure of the scatter of the individual step ages, is based on the error enveloping around the data  
430 point. The decrease in error will automatically cause an increase in MSWD (e.g. York, 1968; Wendt and Carl, 1991). The  
431 MSWD values reported in this study are relatively high. In part this is caused by the fact that modern multi-collector mass  
432 spectrometers used for  $^{40}\text{Ar}/^{39}\text{Ar}$  dating can measure the isotope ratios very precisely, which in turn would ~~result in the increase~~  
433 ~~the~~ MSWD. It will be more valuable and challenging to find a plateau or isochron age which meets the MSWD criteria ( $<2.5$ )  
434 by modern multi-collector  $^{40}\text{Ar}/^{39}\text{Ar}$  dating than by K-Ar or  $^{40}\text{Ar}/^{39}\text{Ar}$  dating using a single detector instrument (e.g. Mark et  
435 al., 2009).

436 Potential drawbacks of the  $^{40}\text{Ar}/^{39}\text{Ar}$  method are its dependence on neutron irradiation causing the production of interfering  
437 argon isotopes that needs to be corrected for. The uncertainty in ages of standards that are required to quantify the neutron flux  
438 also need to be incorporated in the final ages as are uncertainties related to decay constants (supplementary material II). Finally,  
439 recoil can occur during irradiation. Minerals such as biotite can be prone to recoil, yielding slightly older ages (e.g. Hora et  
440 al., 2010).

441 Figure 13 compares previous published K-Ar, U/Pb zircon and ~~fission track ages~~ from the same volcanic units with the new  
442  $^{40}\text{Ar}/^{39}\text{Ar}$  data of this study. In general, there is a good agreement, however, six ages out of twenty-three differ significantly  
443 from previous studies that will be discussed below.

444 The obsidian fission track ages (Bigazzi and Radi, 1981; Arias et al., 2006) for the Dhemenehaki volcano are 0.25 My younger  
445 than the K-Ar ages (1.84 Ma, Angelier et al., 1977) and the  $^{40}\text{Ar}/^{39}\text{Ar}$  age of this study (1.825 Ma, G15M0032B). The good

Commented [MOU8]: Text 394-430 is irrelevant here. It reads like thesis review. It should be greatly reduced in length and put in the Introduction, as a defence of the  $^{40}\text{Ar}/^{39}\text{Ar}$  method

Commented [MOU9]: not in caption or labelled on figure

446 agreement between the K-Ar and  $^{40}\text{Ar}/^{39}\text{Ar}$  ages suggests that the fission track ages record another, lower temperature event,  
447 than the K-Ar and  $^{40}\text{Ar}/^{39}\text{Ar}$  ages. In addition, the larger uncertainty of fission track ages ( $>0.05$  Ma) also overlaps with the  
448  $^{40}\text{Ar}/^{39}\text{Ar}$  age at 2-sigma. We assume that the  $^{40}\text{Ar}/^{39}\text{Ar}$  age is the correct extrusion age for the obsidian of the Dhemenehaki  
449 volcano.

450 Angelier et al. (1977) reported one dacite sample in the northwest of Milos with an age of 1.71 Ma (Angelier\_3, location 3 on  
451 Figure 3 of Angelier et al., 1977). Argon loss could result in these ages (Angelier\_3-5 in Figure 13) being younger than our  
452  $^{40}\text{Ar}/^{39}\text{Ar}$  groundmass ages of  $1.97 \pm 0.01$  Ma (dacite sample G15M0021 and -22).

453 The amphibole of sample G15M0004 of the Adamas dacitic lava dome, located ~1 km north of rhyolitic Bombarda volcano,  
454 gave an inverse isochron age of  $1.95 \text{ Ma} \pm 0.45 \text{ Ma}$ . This age overlaps with the K-Ar age for the Adamas lava dome of  $2.03 \pm$   
455  $0.06 \text{ Ma}$  (dacite M 66) of Fytikas et al. (1986). The large analytical uncertainty of our sample G15M0004 is caused by a  
456 combination of low  $^{40}\text{Ar}^*$  yields and clustering of data points that define the inverse isochron showing excess argon was  
457 identified by the  $^{40}\text{Ar}/^{39}\text{Ar}$  method ( $^{40}\text{Ar}/^{36}\text{Ar}$   $319.51 \pm 14.70$ ), whereas the presence of excess argon cannot be tested by the  
458 K-Ar technique, implying that the Fytikas et al. (1986) might be slightly old.

459 The Korakia andesite has an age of  $1.59 \pm 0.25 \text{ Ma}$  (M 103, Fytikas et al., 1986) and was deposited in a submarine-subaerial  
460 environment on top of the Sarakiniko Formation that was dated based on paleomagnetic polarity in combination with a K-Ar  
461 age (1.80-1.85 Ma, Stewart and McPhie, 2003 and reference therein). The much older  $^{40}\text{Ar}/^{39}\text{Ar}$  groundmass age ( $2.68 \pm 0.01$   
462 Ma) of Korakia andesite sample G15M0029 is unreliable and it could indicate the emplacement age of the Kalogeros  
463 cryptodome ( $2.70 \pm 0.04 \text{ Ma}$ , Stewart and McPhie, 2006) or represents a geological meaningless age with only 23-27% of the  
464 total  $^{39}\text{Ar}$  released in the "plateau". In this case, the K-Ar age of  $1.59 \pm 0.25 \text{ Ma}$  is considered as the likely eruption age for the  
465 Korakia andesite although its argon loss or excess Ar component is unknown.

466 We obtained  $^{40}\text{Ar}/^{39}\text{Ar}$  ages of 3.41-4.10 Ma and  $3.06 \pm 0.02 \text{ Ma}$ , respectively, from the groundmasses of dacite samples  
467 G15M0017 and G15M0015 in the southwest of Milos (Figure 2 and 14B). Both of ~~them~~ these samples are ~~from~~ derived from  
468 the coherent dacite facies of the rhyolitic Profitis Illias volcano based on the Figure 11 of Stewart and McPhie (2006). Sample  
469 G15M0015 yielded much higher radiogenic  $^{40}\text{Ar}$  (41.77%) than that of sample G15M0017 ( $<10\%$  of  $^{40}\text{Ar}^*$ ), and the rhyolite  
470 sample M 164 from Fytikas et al. (1986) (23.5% of  $^{40}\text{Ar}^*$ ) gave an estimate the eruptive age of  $3.08 \pm 0.08 \text{ Ma}$  to the Profitis  
471 Illias volcano which is much younger than that given by our sample G15M0017 (Figure 13). Therefore, we considered our  
472  $^{40}\text{Ar}/^{39}\text{Ar}$  ages of  $3.06 \pm 0.02 \text{ Ma}$  is the best estimate of the emplacement age of the coherent dacite facies of Profitis Illias  
473 volcano.

474 A basaltic andesite dyke near Klefiko on the south-western coast of Milos has a K-Ar age of  $3.50 \pm 0.14 \text{ Ma}$  which only gave  
475 13.9% of  $^{40}\text{Ar}^*$  (Fytikas et al. 1986). This age is significantly older than the eruptive ages of Profitis Illias volcano which they  
476 intrude (Stewart, 2003). Although containing relatively low  $^{40}\text{Ar}^*$  (16.87%), our  $^{40}\text{Ar}/^{39}\text{Ar}$  age of  $2.66 \pm 0.01 \text{ Ma}$  with 67.27%  
477 of  $^{40}\text{Ar}^*$  from the groundmass of basaltic andesitic sample G15M0016 of the dyke near Klefiko is probably an accurate  
478 intrusion age.

#### 479 4.2 The published ages of the other volcanic units

480 Unfortunately, we were not able to date all key volcanic units of the Milos VF. This has three reasons (1) we did not collect  
481 samples from all units; (2) some of the collected samples were not fresh enough after inspection of thin sections; and (3) some  
482 of the  $^{40}\text{Ar}/^{39}\text{Ar}$  data indicates that the K-Ar decay system was disturbed. Therefore, ~~in order to construct~~ we include published  
483 age information to establish a complete high-resolution geochronology ~~on~~ for the Milos VF.

484 The published volcanic units that we include ~~They~~ are the Profitis Illias volcano ( $3.08 \pm 0.08 \text{ Ma}$  with 23.5 (%), Fytikas et al.,  
485 1986), the Mavro Vouni lava dome ( $2.50 \pm 0.09 \text{ Ma}$  with 55.2  $^{40}\text{Ar}^*$  (%), Anglier et al., 1977) in the south-western part of  
486 Milos, the Bombarda volcano ( $1.71 \pm 0.05 \text{ Ma}$  with 24.3  $^{40}\text{Ar}^*$  (%), Fytikas et al., 1986), the Plakes volcano ( $0.97 \pm 0.06 \text{ Ma}$   
487 with 10.2  $^{40}\text{Ar}^*$  (%), Fytikas et al., 1986, and 0.8-1.2 Ma with 5.4-11.9  $^{40}\text{Ar}^*$  (%) Matsuda et al. 1999), ~~and the scoria cone in~~

Commented [MOU10]: not on fig 13

488 the north-east. Scoria deposits are found that Stewart and McPhie (2006) attributed to an andesitic scoria cone between Milos  
489 and Kimolos that was produced in-submarine, and maybe occasionally above sea level. No age data for this deposit has  
490 been published so far. However, ~~But the~~ stratigraphic position of this scoria deposit is between MIL 365 (2.66 Ma, Stewart  
491 and McPhie, 2006) and M103 (1.59 Ma, Fytikas et al., 1986), which is shown in Figure 10 of Stewart and McPhie (2006).  
492 Therefore, this scoria cone was likely active in the north-eastern part of the Milos VF between 2.6 and 1.6 Ma.  
493 In addition, Fytikas et al. (1986) also analysed a pumice from the Sarakiniko pumice deposits eastward of Adamas (1.85 ± 0.10  
494 Ma with 13.6 <sup>40</sup>Ar\* (%), Fytikas et al., 1986) ~~deposits eastward of Adamas~~ (Fig. 2). This unit belongs ~~is a~~ to the reworked  
495 pyroclastic sediment of the Adamas lava dome (Rinaldi and Venuti, 2003). Therefore, the K-Ar age from the Sarakiniko unit  
496 ~~was is~~ not considered as an eruption age in this study. We did not sample the neighbouring islands of the Milos VF and also  
497 did not attempt to date the products of the recent phase of phreatic activity that Traineau and Dalabakis (1989) obtained <sup>14</sup>C  
498 ages of 200 BC and 200 AD.

Commented [MOU11]: this is not a sentence

#### 499 4.3 Implications for the stratigraphy of the Milos VF

##### 500 4.3.1. Start of volcanism in the Milos VF.

501 Figures 13 and 14 summarize our stratigraphic interpretation of the Milos VF based on our new <sup>40</sup>Ar/<sup>39</sup>Ar ages in  
502 combination with previously published stratigraphic, biostratigraphic, fission track, <sup>14</sup>C, K-Ar and U-Pb ages. We did not  
503 consider the Matsuda et al. (1999) data as the fission-track ages seem to be offset to other dating techniques ages obtained  
504 from the same deposits (see section 4.1 above). The exact start of volcanism in the Milos VF is still unclear since these older  
505 deposits are strongly hydrothermally altered. Van Hinsbergen et al. (2004) reported five ash layers in the Pliocene sedimentary  
506 rocks of southern Milos, ranging between 4.5-3.7 Ma in age, based on biostratigraphy, magnetostratigraphy and astronomical  
507 dating. In a slightly wider circle around Milos island, the 6.943 ± 0.005 Ma a1-tephra event recorded in several locations on  
508 nearby Crete (Rivera et al., 2011), shows that explosive volcanism along the Aegean arc, possibly on Milos, already occurred  
509 during the Messinian. These ash beds cannot be traced to currently exposed centres in the Milos VF and could conceivably be  
510 related to volcanic centres further north (Antiparos and Patmos), which were active during this time interval (Vougioukalakis  
511 et al., 2019).

Commented [MOU12]: I have not tried to correct this text because it needs major revision. The main problem is that the authors misunderstand what their dates actually mean.

1. The notion of successive "phases" is misleading because of the implication that the phases are periods of continuous volcanism. The dated eruption events in fact occupy geological "instants", the longest activity being that of large

Commented [MOU13]: given that you do not present any volcanological data, most of the volcanological interpretations of the units should be removed from this section.

512 Biostratigraphy shows that the youngest layer with dateable fossils (bio-event, the last common occurrence of  
513 *Sphenolithus* spp., Van Hinsbergen et al., 2004) in the Neogene sedimentary rocks is 3.61 Ma old (GTS2020, Raffi et al.,  
514 2020). The diatomite Unit II from Calvo et al. (2012) on top of the oldest volcanoclastic deposit from the north-eastern coast  
515 of Milos is constrained within 2.83-3.19 Ma. These data suggest that the oldest products must be older than 2.83 Ma and  
516 younger than 3.61 Ma. Our oldest <sup>40</sup>Ar/<sup>39</sup>Ar ages of this study displayed a wide range of 3.41-4.10 Ma that are probably not  
517 correct due to alteration of the samples. Alteration might induce Ar loss and that would imply that the age is even older than  
518 3.4-4.1 Ma. The age of 3.50 ± 0.14 Ma given by Fytikas et al. (1986) for an andesitic pillow lava or dyke has been discussed  
519 above and probably belongs to a series of basaltic andesite intrusions in the younger dacitic-rhyolitic deposits of Profitis Illias  
520 (~3.08 Ma, Fytikas et al., 1986), and therefore the 3.5 Ma age is probably not correct (e.g. Stewart, 2003). Fytikas et al. (1986)  
521 measured one sample from Kimolos (Figure 2 and 3) with an age of 3.34 Ma. Furthermore, Ferrara et al. (1980) reported an  
522 age of 3.15 Ma for a lithic clast derived from the Petalia intrusion in the Kastro volcanoclastics of Polyegos. If we assume that  
523 this reported age is a cooling age, volcanism in the Milos VF must have started before 3.15 Ma. Although age constraints for  
524 the start of volcanism on Milos both from the Neogene sedimentary rocks and the dated volcanic samples are poor, the evidence  
525 at this stage would suggest that volcanism in the Milos VF started ~3.3 Ma ago.

##### 526 4.3.2. Periods with different volumetric output.

527 The volume estimates of the Milos VF are hampered by limited exposure of several volcanic units and unknown age  
528 relationships. Therefore, not all units can be attributed to a certain volcano. Furthermore, we also do not know how much  
529

530 volcanic material was lost through transport by air, sea currents and erosion. Given the large errors on these estimates, we only  
531 considered the rough difference in density between extruded magma and the calculated DRE values. The volumetric  
532 contributions of the islands Polygos, Kimolos and Antimilos are not considered here. Therefore, the discussion here only  
533 provides a first order estimate of the onshore extruded magma volume. Taken into account all these limitations, our age data  
534 and the volume estimates by Stewart and McPhie (2006) likely indicate at least three periods of different long term volumetric  
535 volcanic output rates ( $Q_v$ ) throughout the Milos volcanic activity of ~3.3 - 0.00 Ma. We propose to divide the Milos volcanic  
536 activity of ~3.3-0.00 Ma into three periods based on the long-term volumetric volcanic output rate ( $Q_v$ ). We define a "Period"  
537 as a time interval where the  $Q_v$  is significantly different from the average output rate of the Milos VF over the last 3.3 Ma.  
538 Figure 11 shows that the  $Q_v$  can be subdivided into two slow growth periods (I and III) and one period (II) during which the  
539  $Q_v$  was much higher significantly larger.

540 The lower boundary of Period I is based on our estimate of the first volcanic units of Milos at ~3.3 Ma. These first  
541 units have been deposited in the SW of Milos between ~3.3 and 3.08 Ma (see above) that were mapped as large pumiceous  
542 deposits of the basal pyroclastic series by Fytikas et al. (1986) and the felsic pumice cone/cryptodome facies by Stewart and  
543 McPhie (2006). These deposits have a minimum thickness of 120m. The estimates of the DRE volume and  $Q_v$  of these earliest  
544 volcanic deposits are hampered by the lack of precise age information, the high degree of alteration and structural complexities.  
545 Therefore, we only calculated the  $Q_v$  of Period I since 3.08 Ma from which the eruption products are mainly dacitic-rhyolitic  
546 in composition (Table 5, Fig 11), and the first products that can be reliably dated are cryptodomes (3.06 Ma, sample G15M0015)  
547 and dikes (2.66 Ma, sample G15M0016) into the older basal pyroclastic series of Fytikas et al. (1986) or the units of Profitis  
548 Ilias volcano of Stewart and McPhie (2006, 3.08 Ma) in the SW of Milos. This was followed by the formation of the submarine  
549 Fylakopi pumice cone volcano at 2.66 Ma (Stewart and McPhie, 2006) and Kalogeros cryptodome at 2.62 Ma (sample  
550 G15M0006) in the north-eastern part of Milos. These two pumice cone volcanoes contributed 3-11 km<sup>3</sup> DRE in volume to the  
551 Milos VF. The last two volcanic activities of Period I occurred in the SW (Mavro Vauni, 2.50 Ma, Angelier et al., 1977) and  
552 west of Milos (Mavros Kavos, 2.36 Ma, this study), respectively, which produced two high-aspect-ratio andesitic-dacitic lava  
553 domes with a total volume of 1-3 km<sup>3</sup> DRE (Stewart and McPhie, 2006). During Period I, which lasted ~ 1 Myr, the estimated  
554  $Q_v$  is  $0.9 \pm 0.5 \times 10^{-5} \text{ km}^3 \cdot \text{yr}^{-1}$ .

555 The change from Period I to II is based on the sharp increase in  $Q_v$  of Figure 11 at 2.13 Ma. During this period the  $Q_v$   
556 ( $3.0 \pm 1.7 \times 10^{-5} \text{ km}^3 \cdot \text{yr}^{-1}$ ) increased by a factor of ~3 compared to the Period I and III. This Period II starts with the extrusions  
557 of the dacitic-rhyolitic Triades lava dome in the north-west and dacitic Adamas lava dome in the north-east of Milos and is  
558 followed by the rhyolitic Dhemenehaki pumice cone/cryptodome and the Bombardo volcano in the north-east of Milos. For  
559 the Bombarda centre a large age range is reported in the literature (1.71-2.15 Ma, Fig. 13B). We were not successful to date  
560 samples from the Bombarda centre, but Rinaldi and Campos Venuti (2003) reported that an age of 1.71 Ma is the best  
561 approximation based on other stratigraphic information. For the Dhemenehaki centre, we obtained a <sup>40</sup>Ar/<sup>39</sup>Ar age of  $1.825$   
562  $\pm 0.002$  Ma from obsidian. The Triades, Adamas, -Dhemenehaki and Bombarda centres all developed in a submarine setting,  
563 as the intercalated sediments from the northern coast of Milos show (Calvo et al., 2012; see Fig. 14). The last two volcanic  
564 expressions in Period II consists of two submarine-to-subaerial lava dome extrusions, Kantaro (1.59 Ma, Fytikas et al., 1987)  
565 and Korakia (1.48 Ma, this study) in the north-west and north-east of Milos, respectively. The products of these two centres  
566 are andesitic-dacitic in composition. All volcanic centres of Period II produced 8-30 km<sup>3</sup> DRE in volume for the Milos VF.  
567 Each dome of Period II has a massive core and flow banded rind surrounded by an in-situ autobreccia zone (Stewart and  
568 McPhie, 2006).

569 Period III starts with a time interval of 0.4 Ma with no eruptions and has a very low  $Q_v$  of  $0.25 \pm 0.05 \times 10^{-5} \text{ km}^3 \cdot \text{yr}^{-1}$ .  
570 The boundary between Period II and III can be placed at the last eruption of Period II, at the start of the first eruption in the  
571 low output interval, or halfway in between. The difference between those options is not significant, given the large uncertainties  
572 of the volume estimates (Fig. 12), and therefore we have decided to start Period III directly after the last eruption of the high

573 Q<sub>c</sub> of Period II. The composition of nearly all Period III volcanic products is rhyolitic, an~~the~~ exception is the dacitic Plakes  
574 lava dome (Fig. 12). The Plakes lava dome is probably the last volcano erupting at ~0.97 Ma (Fytikas et al., 1987) in a  
575 submarine environment in the north of Milos, whereas the other lava dome in Period III, Halepa, produced rhyolitic lavas in a  
576 subaerial setting in the south (Stewart and McPhie, 2006). The Halepa and Plakes domes contributed 1-3 km<sup>3</sup> DRE in volume  
577 to the Milos VF and were followed by a 0.3 Ma interval with no or limited volcanic eruptions. Two subaerial pumice cone  
578 volcanoes with biotite bearing rhyolites were constructed during the last 0.6 Ma: Trachilias and Fyriplaka complexes. The  
579 Trachilias complex was active for approximately 300 kyr (0.63-0.32 Ma) in the northern part of Milos. The evolution of this  
580 complex starts with phreatic eruptions which became less explosive over time (Fytikas et al., 1986). During the last eruption  
581 (0.317 ± 0.004 Ma) phase of volcanic activity at the Trachilias complex rhyolitic pumices filled up the crater area and did  
582 breach the northern tuff cone walls. This phaseThe Trachilias complex only added a small volume (1-2 km<sup>3</sup> DRE) of material  
583 to the Milos VF. The Kalamos lava dome was also extruded in the south of Milos (Fig. 2) contemporaneously with the  
584 Trachilias complex.

585 The youngest volcanic activity of Milos (0.11 Ma-present), is characterized by subaerial eruptions of biotite phyric  
586 rhyolite from the Fyriplaka complex in the south of Milos, and was studied in detail by Campos Venuti and Rossi (1996). This  
587 complex is constructed on a paleosol that developed in a phreatic deposit (“Green Lahar”, Fytikas et al., 1986) or lies directly  
588 on the metamorphic basement. Campos Venuti and Rossi (1996) indicated that the stratigraphic order is: Fyriplaka and Gheraki  
589 tuff rings, Fyriplaka lava flow, composed tuff cone of Tsigrado-Provatas. The tuff ring of Fyriplaka was divided into three  
590 members, with on top the deposits of the Tsigrado tuff cone. The total estimated volume of volcanic material is 0.18 km<sup>3</sup> DRE.  
591 The boundary between the Fyriplaka and Tsigrado tuff cones is characterized by a marked erosive unconformity. The  
592 composition of these young volcanic products of this phase is very constant (Fig. 10-11), this was also noted by Fytikas et al  
593 (1986) and Campos Venuti and Rossi (1996). The products from Fyriplaka and Tsigrado cones are covered with a paleosol  
594 rich in archaeological remains and a phreatic deposit consisting largely of greenschist metamorphic fragments. According to  
595 Campos Venuti and Rossi (1996), the Fyriplaka cone was quickly built by phreatic and phreatomagmatic eruptions, as there  
596 are no paleosols observed between the different units. However, our data do suggest a large range in ages between 0.11 and  
597 0.06 Ma. Fytikas et al. (1986) also reported a range between 0.14 and 0.09 Ma. These ages are inconsistent with the “Green  
598 Lahar” age of 27 kyrs (Principe et al., 2002), suggesting that the “Green Lahar” deposit consists of many different phreatic  
599 eruption layers that were formed during a time interval of more than 0.4 Ma, as the Kalamos lava is underlain by a green  
600 phreatic eruption breccia (Campos Venuti and Rossi 1996). We, therefore, conclude that phreatic eruptions occurred for more  
601 than 400 kyr, predominately in the eastern part of Milos until historical times (200 BC – 200 AD, Traineau and Dalabakis,  
602 1989).

#### 603 4.3.3. Temporal evolution of the magma plumbing system of the Milos VF.

604 Figure 11 shows several of the temporal petrographic and major-element variations during the evolution of the Milos VF. The  
605 chemistry of the magmas did not change significantly between the three different periods, for example, the K<sub>2</sub>O/SiO<sub>2</sub> ratio is  
606 constant (0.05 ± 0.02) with one exception, sample G15M0021 collected near Cape Vani which is altered by hydrothermal  
607 processes (e.g. Alfieris et al. 2013). The volcanic units of Period III are dominantly rhyolitic in composition, whereas during  
608 Period I and II the compositions of volcanic units range between basaltic-andesite~~ie~~ to rhyolite~~ie~~. The crystallinity of the  
609 volcanic products is low (<10 vol.%) during Period III because most of these products are pumiceous. Although there is also  
610 a large number of pumiceous units of low crystallinity produced by Profitis Illias and Fylakopi volcanoes during Period I  
611 (Stewart and McPhie, 2006), the crystallinity of the other products of Period I and most of Period II units are much higher (20-  
612 40 vol.%) than that of Period III. In addition, we observed that the volcanic products of Period II have the lowest vesicularity  
613 (<10 vol.%), compared to the highly variable vesicularity of Period I (1-50 vol.%) and the high value for Period III (10-100  
614 vol.%). These observations are consistent with the type of volcanic structures. Period I and III contain large explosive pumice  
615

616 cone volcanoes, whereas Period II is dominated by effusive dome extrusions. The extrusion of crystal-rich, outgassed and thus  
617 viscous residual magmas in large volumes during Period II is similar to the description for the effusive volcanism of the  
618 Methana VF (Popa et al., 2020). Popa et al. (2020) suggested that the critical factor controlling the effusive-explosive  
619 transitions of Methana is the crystallinity of the erupted material based on their petrological data. The crystallinity has a higher  
620 influence on the bulk viscosity of magma than the other factors (e.g. water content and composition; Popa et al., 2020). A  
621 higher crystallinity results in a slower ascent velocity of magma and enhances the formation of permeable pathways in the  
622 conduit for the gas, which promotes the outgassing of the magmas and leads to effusive behaviour. Lower crystallinity (<30  
623 vol.%) of the magmas results in explosive eruptions and has the opposite effect on outgassing, which causes high vesicularity  
624 of the eruption products.

625 Popa et al. (2020) showed that different magma plumbing systems are responsible for the explosive (crystal-poor) and effusive  
626 (crystal-rich) eruptions of Methana (Popa et al., 2020, their Fig. 13). For the effusive lava domes of Period II, the composition  
627 mainly ranges from basaltic-andesitic to dacitic, and the petrological observations of the dacite sample G15M0019 and -20 of  
628 the Kantaro dome show the presence of olivine-clinopyroxene-orthopyroxene cumulates and amphibole-biotite reaction rims  
629 (supplementary material I). The andesite of the Korakia dome (G15M0029) has a groundmass of acicular plagioclase and  
630 plagioclase phenocrysts with sieve textures. These petrological observations suggest large scale magma mixing between felsic  
631 and more mafic magma, consistent with the hybridized magmas of the effusive events on Methana (e.g. Popa et al., 2020). The  
632 pumiceous units of the explosive volcanoes on Milos during Period I and III could be caused by mafic magmas that intrudes a  
633 magma reservoir filled with felsic magma. This is consistent with the suggestion of Fytikas et al. (1986) that the main location  
634 of feeding magma for the Milos VF is in the lower part of the crust from Pliocene to Pleistocene ( $\approx$ Period I).

635 It is noteworthy that the value of the  $Q_e$  ( $0.2-4.7 \times 10^{-5} \text{ km}^3 \cdot \text{yr}^{-1}$ ) for the Milos VF is at least 2-3 orders lower than the average  
636 for rhyolitic systems ( $4.0 \times 10^{-3} \text{ km}^3 \cdot \text{yr}^{-1}$ ) and the mean for continental arcs ( $\sim 70 \times 10^{-3} \text{ km}^3 \cdot \text{yr}^{-1}$ ) with a range of  $8 \times 10^{-6} -$   
637  $9 \times 10^{-2} \text{ km}^3 \cdot \text{yr}^{-1}$  (White et al., 2006). Milos overlaps with the lowest  $Q_e$  values of the study of White et al. (2006). For the  
638 magma supply rate underneath the Milos VF, although no data are available for the ratio between intruded magma in the crust  
639 below Milos and extruded volcanics (I:E), White et al. (2006) argue that a ratio of 5:1 is probably a realistic estimate for most  
640 volcanic centres and that this ratio can be higher in volcanic centres constructed on continental crust. This would result in a  
641 magma supply rate from the mantle beneath the Milos VF in the order of  $0.1-3.3 \times 10^{-4} \text{ km}^3 \cdot \text{yr}^{-1}$ . Compared with other SAVA  
642 volcanic centres, Druitt et al. (2019) reported a long-term average magma supply rate of approximately  $1 \times 10^{-3} \text{ km}^3 \cdot \text{yr}^{-1}$   
643 beneath the Kameni islands of Santorini, which is comparable to that of the Milos. Besides the case of Santorini VF, no other  
644 information on the long-term average magma supply rate of other volcanic centres of the SAVA is available to our knowledge.  
645 Given that the island of Milos is approximately 15 km long (W-E), this results in a magma production rate over the last  $\sim 3.34$   
646 Ma of approximately  $0.7-22 \text{ km}^3 \cdot \text{km}^{-1} \cdot \text{Myr}^{-1}$ . Although this magma production rate per km are length is the onshore estimate  
647 for the Milos VF, it is still significant lower than for oceanic arcs:  $157-220 \text{ km}^3 \cdot \text{Myr}^{-1} \cdot \text{km}^{-1}$  (Jicha and Jagoutz, 2015). For  
648 continental arcs the long-term magma production rate is more difficult to establish because magmatism is cyclic, and short  
649 periods (5-20 Ma) of intense magmatism ("flare ups") with  $85 \text{ km}^3 \cdot \text{km}^{-1} \cdot \text{Myr}^{-1}$  are alternating with periods of 25-50 Ma of low  
650 magma production rate of  $20 \text{ km}^3 \cdot \text{km}^{-1} \cdot \text{Myr}^{-1}$  (e.g. Jicha and Jagoutz, 2015). The periods of low magma production overlap  
651 with the magma production rates beneath the Milos VF over the past  $\sim 3.34$  Ma.

#### 652 4.3 Implications for the stratigraphy of the Milos VF

653 Figures 14 and 15 summarize our stratigraphic interpretation of the Milos VF based on our new  $^{40}\text{Ar}/^{39}\text{Ar}$  ages in combination  
654 with previously published facies analysis by Stewart and McPhie (2006) and biostratigraphic, fission track,  $^{14}\text{C}$ , K-Ar and U-  
655 Pb ages. We propose to divide the volcanic activity in the Milos VF into 9 distinct phases and 5 periods of quiescence. Here  
656 we define a "phase" as a period of the Milos VF that one type of volcano was active (e.g. pumice cone/cryptodome, lava dome,  
657 tuff cone) in a certain area of the Milos VF (NW, NE, SE or SW part) (Fig. 2 and 15). In addition, we use the chemical

**Commented [MOU14]:** Highlighted "one type of volcano was active" and "chemical composition of the volcanic units as an extra distinguishing characteristic" with a comment of "volcanic phases" in figure 15 show any connections or relationship. eg. "phase 4" groups rhyolite and andesite and "phase 2" groups a cryptodome and pumice cone. what you define as "phases" are in fact the dates at which single volcanic centres were active.



658 composition of the volcanic units as an extra-distinguishing characteristic (e.g. andesite, dacite and rhyolite). The lower and  
659 upper boundary of these phases are based on the  $^{40}\text{Ar}/^{39}\text{Ar}$  data of this study, in combination with previously published age  
660 data (Fig. 14). The errors of the previously published K-Ar data for volcanic units not dated in the present study result in  
661 estimates for some events that are probably longer than they in reality were. Most of the time the Milos VF was in quiescence,  
662 and there are periods during which long breaks are recorded in the stratigraphic succession. In this study we define a period of  
663 volcanic quiescence if this period is longer than 200 kyrs. We did not consider the Matsuda et al. (1999) fission track ages to  
664 define the periods for quiescence, as the fission track ages seem to be offset to other dating techniques ages obtained from the  
665 same deposits (see discussion above). Figure 15 shows that there are five periods of no, or limited volcanic activity on Milos,  
666 between phases 1-2 (Q1), 3-4 (Q2), 6-7 (Q3), 7-8 (Q4) and 8-9 (Q5). These periods are also visible in the published age data,  
667 with two above mentioned exceptions from Matsuda et al. (1999). However, this does not mean that during the periods of these  
668 volcanic quiescence no eruptions occurred the Milos VF, as in Q2 probably the Polyegos lava dome was formed, and in Q5  
669 the domes of Antimilos were extruded (Fig. 15).

670 The exact start of volcanism in the Milos VF is still unclear since these older deposits are strongly hydrothermally altered. Van  
671 Hinsbergen et al. (2004) reported 5 ash layers in the Pliocene sedimentary rocks of southern Milos, ranging between 4.5-3.7  
672 Ma in age, based on biostratigraphy, magnetostratigraphy and astronomical dating. In a slightly wider circle around Milos  
673 island, the  $6.943 \pm 0.005$  Ma a1 tephra event recorded in several locations on nearby Crete (Rivera et al., 2011), shows that  
674 explosive volcanism along the Aegean arc, possibly on Milos, already occurred during the Messinian. These ash beds cannot  
675 be traced to currently exposed centres in the Milos VF and could conceivably be related to volcanic centres further north  
676 (Antiparos and Patmos), which were active during this time interval (Vougioukalakis et al., 2019). Biostratigraphy shows that  
677 the youngest layer with dateable fossils (bio-event, the last common occurrence of *Sphenolithus* spp., Van Hinsbergen et al.,  
678 2004) in the Neogene sedimentary rocks is 3.54 Ma old (GTS2012, Gradstein et al., 2012). The diatomite Unit II from Calvo  
679 et al. (2012) on top of the oldest volcanoelastic deposit from the north-eastern coast of Milos is constrained within 2.83-3.19  
680 Ma. These data suggest that the oldest products must be older than 2.83 Ma and younger than 3.54 Ma. Our oldest  $^{40}\text{Ar}/^{39}\text{Ar}$   
681 ages of this study displayed a wide range of 3.41-4.10 Ma that, are probably not correct due to the alteration of the samples.  
682 Alteration might induce Ar loss and that would imply that the age is even older than 3.4-4.1 Ma. The age of  $3.50 \pm 0.14$  Ma  
683 given by Fytikas et al. (1986) for an andesite pillow lava or dyke has been discussed above and probably belongs to a series  
684 of basaltic andesite intrusions in the younger dacitic-rhyolitic deposits of Profitis Illias ( $\sim 3.08$  Ma, Fytikas et al., 1986), and  
685 therefore the 3.5 Ma age is probably not correct (e.g. Stewart, 2003). Fytikas et al. (1986) measured one sample from Kimolos  
686 (Figure 2 and 3) with an age of 3.34 Ma. Furthermore, Ferrara et al. (1980) reported an age of 3.15 Ma for a lithic elast derived  
687 from the Petalia intrusion in the Kastro volcanoelastics of Polyegos. If we assume that this reported age is a cooling age,  
688 volcanism in the Milos VF must have started before 3.15 Ma. Although age constraints for phase 1 both from the Neogene  
689 sedimentary rocks and the dated volcanic samples are poor, the evidence at this stage would suggest that phase 1, and hence  
690 volcanism in the Milos VF started around  $\sim 3.34$  Ma ago.

691 Phase 1 ( $\sim 3.34$ - $3.06$  Ma) is similar to the basal pyroclastic series of Fytikas et al., 1986, and the submarine felsic  
692 cryptodome/pumice cone facies of Stewart and McPhie (2006). We note that two submarine felsic cryptodome/pumice cone  
693 volcanoes (Dhemenghaki and Bombara) were active during phase 5 (see below). This point was also noted by Stewart and  
694 McPhie, who stated that the cycles of Fytikas et al. (1986) were actually interfingering with other "cycles". The Phase 1  
695 deposits are deposited conformably and unconformably on the Neogene sedimentary rocks (Van Hinsbergen et al., 2004). East  
696 of the Fyriplaka Fault (Figure 2), the phase 1 deposits overlie unconformably the Mesozoic metamorphic basement (Stewart,  
697 2003). The stratigraphic columns (after Stewart and McPhie, 2006, Fig. 14B) show that a mixture of felsic pumice and  
698 sandstone ( $\sim 100$  m thick) was deposited between the Profitis Illias dacite ( $3.06 \pm 0.02$  Ma) and the Kleftiko andesitic or basaltic  
699 andesitic dyke ( $2.66 \pm 0.01$  Ma), suggesting at least one pulse of volcanic activity between 2.66 and 3.06 Ma or erosion  
700 products from the previous eruptions. Submarine eruptions occurred during this phase from broadly circular submarine pumice

701 eones with dacitic to rhyolitic magma compositions (Stewart and McPhie, 2006). The products are thick intervals of felsic  
702 pumice breccia that were either formed by gravity currents or deposition of pumices from suspension. These pumice breccias  
703 were later intruded by dacitic to rhyolitic cryptodomes and sills (Stewart and McPhie, 2006). The main eruption centre of this  
704 phase is the Profitis Ilias volcano (Fig. 2). The amount of volcanic material that phase 1 contributed to the Milos VF is difficult  
705 to establish, since the volcanic rocks are strongly weathered (e.g. Fytikas et al., 1986; Stewart and McPhie, 2006).  
706 Phase 2 (2.66–2.50 Ma) was considered as a phase because of a long volcanic quiescence period (Q1) of 0.3 Ma after phase 1.  
707 The Fylakopi pumice cone volcano and Kalogeros cryptodome of phase 2 in the north-eastern part of Milos, were probably  
708 simultaneously active from 2.66 to 2.62 Ma. These pumice cone/cryptodome volcanoes are comparable to the Profitis Ilias  
709 volcano of phase 1 (Figure 14B). All of the deposits of phase 1 and 2 were submarine, most of them below wave base (up to  
710 several hundred meters water depth), although maybe some volcanic structures were large enough to become subaerial that  
711 were subsequently quickly eroded (Stewart and McPhie, 2006). These two phases could contribute 3–12 km<sup>2</sup> DRE to the Milos  
712 VF (Fig. 12).  
713 Phase 3 (2.50–2.36 Ma) forms together with phase 4 the “complex of domes and lava flows” defined by Fytikas et al. (1986)  
714 (Fig. 4 and 15). This phase includes the Mavros Kavos and Mavro Vouni domes in the south-western part of Milos. These  
715 domes form high aspect ratio deposits with a roughly concentric structure of a coherent core, 30–40 m thick layer which is  
716 flow-banded and a monomeric breccia (Stewart and McPhie, 2006). The deposits of these domes intrude and overlie the phase  
717 1 and 2 deposits. The composition of the deposits is andesitic-dacitic (this study and Stewart and McPhie, 2006). These deposits  
718 are interpreted as submarine domes, which were extruded onto the sea floor or into shallow unconsolidated pumice-rich  
719 sediments. The volume estimate of these deposits was only approximately 1–2 km<sup>2</sup> DRE.  
720 Phase 4 (2.13–1.90 Ma) started after a volcanic quiescence period of ~200 kyrs (Q2) since phase 3. Phase 4 has similar  
721 submarine dome extrusions as phase 3, but the volcanism of phase 4 moved to the north-western (Triades lava dome) and  
722 north-eastern (Adamas lava dome) parts of the Milos VF. Approximately 4–13 km<sup>2</sup> DRE was added to the Milos VF during  
723 this phase.  
724 Phase 5 (1.90–1.60 Ma) consists of two rhyolitic pumice cone/cryptodome structures (Dhemenghaki and Bombarda) in the  
725 north-eastern part of Milos and are similar to the phase 1–2 volcanism. For the Bombarda centre a large age range is reported  
726 in the literature (1.71–2.15 Ma, Fig. 14B). We were not successful to date samples from the Bombarda centre, but Rinaldi and  
727 Campos Venuti (2003) reported that an age of 1.71 Ma is the best approximation based on other stratigraphic information. For  
728 the Dhemenghaki centre we reported a <sup>40</sup>Ar/<sup>39</sup>Ar age of 1.825 ± 0.002 Ma from an obsidian. These centres all developed in a  
729 submarine setting, as the intercalated sediments from the northern coast of Milos show (Diatomite layer III in Fig. 2 and 3 of  
730 Calvo et al., 2012). This phase contains the same volcano type as the phase 1 and 2, but is constructed from rhyolitic material  
731 only. This phase resulted in an addition of approximately 5–18 km<sup>2</sup> DRE to the Milos VF.  
732 Phase 6 (1.60–1.48 Ma) consists of two submarine to subaerial lava dome extrusions (Kantaro and Korakia in the northwest  
733 and northeast of Milos, respectively) that are dacitic and andesitic in composition. The petrological observations of the dacite  
734 sample G15M0019 and 20 of the Kantaro dome show the presences of the olivine-clinopyroxene-orthopyroxene cumulates  
735 and the amphibole-biotite reaction rims (supplementary material I). The andesite of Korakia dome (G15M0029) has a  
736 groundmass of acicular plagioclase and plagioclase phenocrysts with sieve textures. In addition, the intermediate composition  
737 of phase 6 is similar to that of phase 1–3. These petrological and geochemical characters of phase 6 indicate the magma mixing  
738 in these andesitic-dacitic units, that a mafic magma from the deep crust likely injected into the shallow chamber beneath the  
739 Kantaro and Korakia domes.  
740 During phase 6, volcanism on Milos began to change to subaerial by the formation of these domes (e.g. Stewart and McPhie,  
741 2006). These domes structures have the characteristics of subaerial domes with an extent of 2.5–10 km<sup>2</sup> and are maximal 250–  
742 350 m thick in the proximal part (Stewart and McPhie, 2006). Single domes have a massive core and flow-banded rind

Commented [MOU15]: this makes no sense; eruptions last days, weeks, months, years, perhaps decades but definitely not tens of thousands of years

743 surrounded by an in situ autobreccia zone. Phase 6 volcanic units only added a small volume of 0.5–2.5 km<sup>3</sup> DRE to the Milos  
744 VF (Figure 12). This phase is followed by a period of no volcanic activity of approximately 400 kyrs (Q3 in Figure 15).  
745 Phase 7 (1.04–0.97 Ma) contains two eruption centres. The older one produced the subaerial rhyolitic lavas of Halepa (1.04 ±  
746 0.01 Ma) in the south of Milos, which has similar geochemical characteristics to that of phase 5. The second eruption centre is  
747 the dacitic Plakes dome in the north of Milos (0.97 ± 0.06 Ma, Fytikas et al., 1986), of which the geochemical character is  
748 comparable to that of phase 6. We include them into one phase since their eruptive ages are so closed, even though the  
749 geochemical characteristics of both domes are different. Fytikas et al. (1986) included these in the PSLD (Figure 14A and 15).  
750 The Plakes volcano is probably the last volcano erupting in a submarine environment on Milos, whereas the rhyolitic lavas of  
751 Halepa are subaerial (Stewart and McPhie, 2006). Also, this phase is small in volume (1–3 km<sup>3</sup>, Figure 12) and is followed by  
752 the fourth period of quiescence (Q4 in Figure 15) of approximately 300 kyrs.  
753 Phase 8 (0.63–0.32 Ma) consists of two subaerial eruption centres with biotite-bearing rhyolites. The first one, described by  
754 Campos Venuti and Rossi (1996) is the Kalamos lava dome (0.412 ± 0.004 Ma) that underlies the Fyriplaka complex deposits  
755 at Fyriplaka beach (phase 9, see below). The Trachilas complex in the northern part of Milos was active for approximately 300  
756 kyrs (0.63–0.32 Ma). The evolution of this complex starts with phreatic eruptions which became less explosive over time  
757 (Fytikas et al., 1986). In the last phase rhyolitic lavas filled up the crater area and did breach the northern tuff cone walls. This  
758 phase only added a small volume (1–2 km<sup>3</sup> DRE) of material to the Milos VF. Between phase 8 and 9 there is another  
759 quiescence period (Q5) of ~200 kyrs (Fig. 15).  
760 The youngest phase, 9 (0.11 Ma present), is characterized by subaerial eruptions of biotite phyric rhyolite from the Fyriplaka  
761 complex and was studied in detail by Campos Venuti and Rossi (1996). This complex is constructed on a paleosol that  
762 developed in a phreatic deposit (“Green Lahar”, Fytikas et al., 1986) or lies directly on the metamorphic basement. Campos  
763 Venuti and Rossi (1996) indicated that the stratigraphic order is: Fyriplaka and Gheraki tuff rings, Fyriplaka lava flow,  
764 composed tuff cone of Tsigrado Provatas. The tuff ring of Fyriplaka was divided into 3 members, with on top the deposits of  
765 the Tsigrado tuff cone. The total estimated volume of volcanic material is 0.18 km<sup>3</sup> DRE. The boundary between the Fyriplaka  
766 and Tsigrado tuff cones is characterized by a marked erosive unconformity. The composition of the volcanic products of this  
767 phase is very constant (Fig. 10–11), this was also noted by Fytikas et al. (1986) and Campos Venuti and Rossi (1996). The  
768 products from Fyriplaka and Tsigrado cones are covered with a paleosol rich in archaeological remains and a phreatic deposit  
769 consisting largely of greenschist metamorphic fragments. According to Campos Venuti and Rossi (1996), the Fyriplaka cone  
770 was quickly built by phreatic and phreatomagmatic eruptions, as there are no paleosols observed between the different units.  
771 However, our data do suggest a large range in ages between 0.11 and 0.06 Ma. Fytikas et al. (1986) also reported a range  
772 between 0.14 and 0.09 Ma. These ages are inconsistent with the “Green Lahar” age of 27 kyrs (Principe et al., 2002), suggesting  
773 that the “Green Lahar” deposit consists of many different phreatic eruption layers that were formed over a period of more than  
774 0.4 Ma, as the Kalamos lava of phase 8 is underlain by a green phreatic eruption breccia (Campos Venuti and Rossi 1996).  
775 We therefore conclude that between phase 8 and 9 phreatic eruptions occurred, predominately in the eastern part of Milos until  
776 historical times (200 BC–200 AD, Traineau and Dalabakis, 1989).

#### 777 4.4 Temporal variations in the major element composition of the volcanic units of the Milos VF

778 Alteration of the submarine deposits is widespread on Milos, and although we tried to sample material as fresh as possible,  
779 there are still indications that some of our samples are not pristine. This is clearly demonstrated in the SiO<sub>2</sub> versus K<sub>2</sub>O and  
780 BaO diagrams (Fig. 16A and B). Two samples G15M0022 and 21 of the Triades lava dome of phase 4, have anomalously  
781 high BaO (~0.35 wt. %) and K<sub>2</sub>O (6–7 wt. %) contents, despite these samples have a relatively low LOI (<0.2 wt. %). We will  
782 not discuss these samples below. Some volcanic units (Profitis Ilias, Mavro Vouni and Bombarda) are not shown in Figures  
783 16 as we were unable to obtain fresh samples and published data are lacking. The major element compositions of the volcanic

Commented [MOU16]: Reduce this section to a few sentences. Fig6 shows very clearly that there are no compositional trends with time. Plus you have not presented data in support of the petrological interpretations

784 units of Filakopi and Plakes can be obtained from Stewart and McPhie (2003) and Fytikas et al. (1986), respectively, and are  
785 shown in Figure 16 together with our data.

786 The pumice cone/cryptodome volcanic units of phase 1-3 and the dome lavas of phase 4-7 are similar in composition. The  
787 SiO<sub>2</sub> content of the cryptodome units of phase 1-3 shows a narrow range of 64-70 wt.%, excluding the basaltic andesitic sample  
788 G15M0016 (SiO<sub>2</sub>: 55.72 wt.%) of the dyke near Kleftiko. The CaO content of the cryptodome units decreased from 5.9 to 2.9  
789 wt.% from Phase 1 to 3, whereas the Na<sub>2</sub>O content increased from 3.3 to 4.2 wt.%. In addition, the petrographic observations  
790 of these rocks suggest a pyroxene- amphibole sequence of crystallization from phase 1 to 3 (supplementary material I). In  
791 combination with the intermediate composition, the fractionation process of phase 1-3 in these cryptodome and dome units  
792 could be fed by a magma system in the relatively deep crust. This hypothesis is in agreement with the modelling results of  
793 Fytikas et al. (1986) for the Pliocene volcanic cycles of the Milos VF. However, the limited compositional data of the  
794 pumiceous units of the Profitis Illias (-3.08 Ma) and Mavro Vouni (2.50 Ma) volcanoes inhibit us to fully discuss the  
795 geochemical characters of the first three phases of the Milos VF.

796 The volcanic units of phase 8 and 9 both are rhyolitic (SiO<sub>2</sub> wt.%>72) in composition, but their geochemical characteristics  
797 are different. There are subtle differences between TiO<sub>2</sub>/Fe<sub>2</sub>O<sub>3</sub> and CaO/Al<sub>2</sub>O<sub>3</sub> ratios, suggesting that the fractionation or  
798 resorption of biotite and the presence of oxide minerals could explain these subtle differences.

799 Although rhyolites have erupted throughout the whole history of the Milos VF, the volumes were most pronounced during  
800 phase 1. However, during phase 2-9 there is a clear shift to smaller volumes of magma and the tendency to become more felsic  
801 over time (Fig. 12).

#### 802 4.5 Temporal variations in the volumetric volcanic output rate of the Milos VF.

803 The volume estimates of the Milos VF are hampered by limited exposure of several volcanic units and unknown age  
804 relationships. Therefore, not all units can be attributed to a certain volcano. Furthermore, we also do not know how much  
805 volcanic material was lost through transport by air, sea currents and erosion. Given the large errors on these estimates, we only  
806 considered the rough difference in density between extruded magma and the calculated DRE values. The volumetric  
807 contributions of the islands Polygos, Kimolos and Antimilos are not considered here. Therefore, the discussion here only  
808 provides a first order estimate of the onshore extruded magma volume. Taken into account all these limitations, our age data  
809 and the volume estimates by Stewart and McPhie (2006) likely indicate at least three periods of different long term volumetric  
810 volcanic output rates (Q<sub>v</sub>): 0.5-1.8×10<sup>-6</sup> km<sup>3</sup>/yr of Phase 1-3 (-3.34-2.36 Ma), 2.0-6.6×10<sup>-6</sup> km<sup>3</sup>/yr of Phase 4-5 (2.13-1.60  
811 Ma) and 0.2-0.4×10<sup>-6</sup> km<sup>3</sup>/yr of Phase 6-9 (1.60 Ma-present) (Fig. 12). This suggests that the Milos VF has a low long term  
812 Q<sub>v</sub> of 0.2-6.6×10<sup>-6</sup> km<sup>3</sup>/yr. This is at least 2-3 orders lower than the average for rhyolitic systems (4.0×10<sup>-3</sup> km<sup>3</sup>/yr) and the  
813 mean for continental arcs (-70×10<sup>-3</sup> km<sup>3</sup>/yr) with a range of 8×10<sup>-6</sup>—9×10<sup>-2</sup> km<sup>3</sup>/yr (White et al., 2006). Milos overlaps  
814 with the lowest Q<sub>v</sub> values of the study of White et al. (2006). There are large variations in Q<sub>v</sub> in the Milos VF: during phase 5  
815 (1.90-1.60 Ma) the Q<sub>v</sub> is relatively high, whereas the last 1.6 Myrs (phase 6-9) the volumetric volcanic output rate is more than  
816 an order of magnitude lower.

817 No data are available for the ratio between intruded magma in the crust below Milos and extruded volcanics (I:E). White et al.  
818 (2006) argue that a ratio of 5:1 is probably a realistic estimate for most volcanic centres and that this ratio can be higher in  
819 volcanic centres constructed on continental crust. This would result in a magma supply rate from the mantle beneath the Milos  
820 VF in the order of 0.1-3.3×10<sup>-4</sup> km<sup>3</sup>.yr<sup>-1</sup>. Compared with other SAVA volcanic centres, Druitt et al. (2019) reported a long-  
821 term average magma supply rate of approximately 1×10<sup>-3</sup> km<sup>3</sup>.yr<sup>-1</sup> beneath the Kameni islands of the caldera of Santorini.  
822 Considering our estimate of the volcanic volume on the Milos VF is the minimum value, this rate is comparable to that of the  
823 Milos. Besides the case of Santorini VF, no other information on the long-term average magma supply rate of other volcanic  
824 centres of the SAVA is available to our knowledge.

§25 Given that the island of Milos is approximately 15 km long (W-E), this results in a magma production rate over the last ~3.34  
§26 Ma of approximately  $0.7\text{--}22\text{ km}^3\cdot\text{km}^{-1}\cdot\text{Myr}^{-1}$ . Although this magma production rate per km are length is the onshore estimate  
§27 for the Milos VF, it is still significant lower than for oceanic arcs:  $157\text{--}220\text{ km}^3\cdot\text{Myr}^{-1}\cdot\text{km}^{-1}$  (Jicha and Jagoutz, 2015). For  
§28 continental arcs the long-term magma production rate is more difficult to establish because magmatism is cyclic, and short  
§29 periods (5–20 Ma) of intense magmatism (“flare ups”) with  $85\text{ km}^3\cdot\text{km}^{-1}\cdot\text{Myr}^{-1}$  are alternating with periods of 25–50 Ma of low  
§30 magma production rate of  $20\text{ km}^3\cdot\text{km}^{-1}\cdot\text{Myr}^{-1}$  (e.g. Jicha and Jagoutz, 2015). The periods of low magma production overlap  
§31 with the magma production rates beneath the Milos VF over the past ~3.34 Ma.

## §32 5 Conclusion

§33 This study reports twenty-one new  $^{40}\text{Ar}/^{39}\text{Ar}$  ages and major element data for 10 volcanic units of the Milos Volcanic Field.

§34 In combination with previously published age data, geochemistry and facies analysis the following points can be made.

- §35 (1) The exact age of the start of volcanism in the Milos VF is still unclear due to the high degree of alteration of the oldest  
§36 deposits. The best estimate is based on our new  $^{40}\text{Ar}/^{39}\text{Ar}$  ages, published K-Ar data and nannofossil biozones is  
§37 between 3.5 and 3.15 Ma.
- §38 (2) Based on the long-term volumetric volcanic output rate, ~~wethe divided the Milos~~ volcanic history of the Milos VF  
§39 can be divided into two slow growth periods, Period I (~3.3–2.36 Ma) and III (1.48 Ma–present), and one relatively  
§40 fast growth period, Period II (2.36–1.48 Ma).
- §41 (3) Period I and III are dominated by low crystallinity, highly vesicular pumice deposits, whereas Period II is  
§42 characterised by dominantly dome extrusions with low versicular, high crystallinity products.
- §43 (4) Large scale magma mixing between felsic and more mafic magma in the upper crust underneath Milos probably result  
§44 in the high crystallinity of the effusively eruptive units of Period II. During Period I and III, the pumiceous units of  
§45 the explosive volcanoes on Milos could be caused by mafic magma from deep that intrudes a magma reservoir filled  
§46 with felsic magma. The evolution of the Milos VF volcanic rocks changed over time in composition from basaltic-  
§47 andesite-rhyolite volcanism to mainly rhyolite. The long term volumetric volcanic output rate of Milos is  $0.2\text{--}4.7 \times 10^{\text{--}}$   
§48  $5\text{ km}^3\cdot\text{yr}^{-1}$ , 2–3 orders of magnitude lower than the average for rhyolitic systems and continental arcs.

§49 The long term volumetric volcanic output rate ( $Q_v$ ) of Milos is  $0.2\text{--}6.6 \times 10^{\text{--}5}\text{ km}^3/\text{yr}$ , 2–3 orders of magnitude lower than the  
§50 average for rhyolitic systems and continental arcs.

§51 Phase 1 (~3.34–3.06 Ma) and Phase 2 (2.66–2.50 Ma) contain the same volcano type, submarine pumice cone/cryptodome, but  
§52 the volcanic units of phase 1 and 2 are located in the south-western and north-eastern parts of the Milos VF, respectively.

§53 There is a long quiescence period of ~400 kyrs between phase 1 and 2.

§54 Phase 3 (2.50–2.36 Ma) resulted in the construction of submarine andesitic-dacitic domes in the south-western part of the Milos  
§55 VF. The lavas of phase 3 are extruded onto the seafloor or intruded in soft pumice rich sediments of phase 1. After phase 3, a  
§56 period of ~200 kyrs of volcanic quiescence followed.

§57 Phase 4 (2.13–1.90 Ma), Phase 5 (1.90–1.60 Ma) and Phase 6 (1.60–1.48 Ma) volcanism took place in the north-eastern and  
§58 north-western parts of the Milos VF. Phase 4 and 6 consist of andesitic to dacitic domes, whereas Phase 5 is comprised of  
§59 rhyolitic pumice cone/cryptodome volcanoes. Phase 6 contains the oldest subaerial dacitic dome (Kantaro dome). After phase  
§60 6, there is a ~400 kyrs interval of no or limited volcanic eruptions.

§61 Phase 7 (1.04–0.97 Ma) consists of two subaerial volcanic units: the rhyolitic Halepa and the dacitic Plakes lava domes in the  
§62 southern and northern parts of the Milos VF, respectively. Between phase 7 and 8 is a period of volcanic quiescence of ~350  
§63 kyrs.

864 Phase 8 (0.63–0.32 Ma) covers the formation period of the subaerial rhyolitic Trachilas complex in the north-eastern part of  
865 the Milos VF and the rhyolitic Kalamos lava in the southeast. A ~200kyrs period of volcanic quiescence occurred between  
866 phase 8 and 9.

867 Phase 9 (0.11 Ma–present) consists of subaerial rhyolitic lava and pyroclastic deposits of the Fyriplaka complex in the south-  
868 eastern part of the Milos VF. During phase 8 and 9 there could be a few phreatic eruptions, mainly in the south-eastern part of  
869 Milos. The different volcanic locations and geochemical characters between phase 8 and 9 suggest the different magma sources  
870 for these two phases.

871 During the evolution of the Milos VF volcanic rocks changed over time in composition from more mafic basaltic-andesite-  
872 rhyolite volcanism to mainly rhyolite. The volcanic complex of Milos was largely (~85% by volume) constructed during ~3.34–  
873 1.6 Ma. From 1.6 Ma to present, only small volumes of rhyolitic magma were added from different eruption vents. The long  
874 term volumetric volcanic output rate ( $Q_v$ ) of Milos is  $0.2–6.6 \times 10^{-5} \text{ km}^3/\text{yr}$ , 2–3 orders of magnitude lower than the average for  
875 rhyolitic systems and continental arcs.

## 876 Acknowledgement

877 We would like to thank Roel van Elsas with the assistance of rock crushing and mineral separation. Kiki Dings helped with  
878 the XRF bead preparation and measurements. Lara Borst and Onno Postma assisted with the  $^{40}\text{Ar}/^{39}\text{Ar}$  dating. We acknowledge  
879 the Greek Institute of Geology and Mineral Exploration (IGME) for permission to conduct fieldwork on Milos. Xiaolong Zhou  
880 would like to acknowledge a grant no. 201506400055 from the China Scholarship Council (CSC). The  $^{40}\text{Ar}/^{39}\text{Ar}$  facility of the  
881 VU is covered by NWO grant 834.09.004. This research benefitted from funding from the European Research Council under  
882 the European Union's Seventh Framework Programme (FP7/2007-2013)/ERC grant agreement n° 319209. A previous version  
883 of this manuscript greatly benefitted from a very detailed and constructive review by Dr. J. McPhie. A second review by Dr J.  
884 McPhie and Dr. J-F. Wotzlaw helped to clarify the interpretation of the geochronology of Milos. We thank Drs. J. Nadden, J.  
885 Miles and S Tapster for pointing out mistakes in our figures.

886  
887

888 **References**

- 889 Alfieris, D., Voudouris, P. and Spry, P. G.: Shallow submarine epithermal Pb-Zn-Cu-Au-Ag-Te mineralization on western  
890 Milos Island, Aegean Volcanic Arc, Greece: Mineralogical, geological and geochemical constraints, *Ore Geol. Rev.*, 53,  
891 159–180, doi:10.1016/j.oregeorev.2013.01.007, 2013.
- 892 Angelier, J., Cantagrel, J.-M. and Vilminot, J.-C.: Neotectonique cassante et volcanisme plio-quadernaire dans l'arc egeen  
893 interne; l'île de Milos (Grèce), *Bull. la Société Géologique Fr.*, 7(1), 119–124, 1977.
- 894 Arias, A., Oddone, M., Bigazzi, G., Di Muro, A., Principe, C. and Norelli, P.: New data for the characterization of Milos  
895 obsidians, *J. Radioanal. Nucl. Chem.*, 268(2), 371–386, doi:10.1007/s10967-006-0183-9, 2006.
- 896 Berger, G. W. and York, D.: Geothermometry from  $40\text{Ar}/39\text{Ar}$  dating experiments, *Geochim. Cosmochim. Acta*, 45(6), 795–  
897 811, doi:10.1016/0016-7037(81)90109-5, 1981.
- 898 Bigazzi, G. and Radi, G.: Datazione con le tracce di fissione per l'identificazione della provenienza dei manufatti di  
899 ossidiana, *Riv. di Sci. Preist.*, 36/1–2, 223–250, 1981.
- 900 Calvo, J. P., Triantaphyllou, M. V., Regueiro, M. and Stamatakis, M. G.: Alternating diatomaceous and volcanoclastic  
901 deposits in Milos Island, Greece. A contribution to the upper Pliocene-lower Pleistocene stratigraphy of the Aegean Sea,  
902 *Palaeogeogr. Palaeoclimatol. Palaeoecol.*, 321–322, 24–40, doi:10.1016/j.palaeo.2012.01.013, 2012.
- 903 Campos Venuti, M. and Rossi, P. L.: Depositional facies in the Fyriplaka rhyolitic tuff ring, Milos Island (Cyclades, Greece),  
904 *Acta Vulcanol.*, 8, 173–192, 1996.
- 905 Cassata, W. S. and Renne, P. R.: Systematic variations of argon diffusion in feldspars and implications for  
906 thermochronometry, *Geochim. Cosmochim. Acta*, 112, 251–287, doi:10.1016/j.gca.2013.02.030, 2013.
- 907 Cole, P. D., Calder, E. S., Sparks, R. S. J., Clarke, A. B., Druitt, T. H., Young, S. R., Herd, R. A., Harford, C. L. and Norton,  
908 G. E.: Deposits from dome-collapse and fountain-collapse pyroclastic flows at Soufrière Hills Volcano, Montserrat, *Geol.*  
909 *Soc. London, Mem.*, 21(1), 231–262, 2002.
- 910 Crossweller, H. S., Arora, B., Brown, S. K., Cottrell, E., Deligne, N. I., Guerrero, N. O., Hobbs, L., Kiyosugi, K., Loughlin,  
911 S. C. and Lowndes, J.: Global database on large magnitude explosive volcanic eruptions (LaMEVE), *J. Appl. Volcanol.*,  
912 1(1), 4, 2012.
- 913 Druitt, T. H., Edwards, L., Mellors, R. M., Pyle, D. M., Sparks, R. S. J., Lanphere, M., Davies, M. and Barreiro, B.:  
914 Santorini Volcano, *Geol. Soc. Mem.*, 19 [online] Available from: <http://pubs.er.usgs.gov/publication/70094778>, 1999.
- 915 Druitt, T. H., Pyle, D. M. and Mather, T. A.: Santorini Volcano and its Plumbing System, *Elements*, 15(3), 177–184,  
916 doi:10.2138/gselements.15.3.177, 2019.
- 917 Duermeijer, C. E., Nyst, M., Meijer, P. T., Langereis, C. G. and Spakman, W.: Neogene evolution of the Aegean arc:  
918 Paleomagnetic and geodetic evidence for a rapid and young rotation phase, *Earth Planet. Sci. Lett.*, 176(3–4), 509–525,  
919 doi:10.1016/S0012-821X(00)00023-6, 2000.
- 920 Ferrara, G., Fytikas, M., Giuliani, O. and Marinelli, G.: Age of the formation of the Aegean active volcanic arc, *Thera*  
921 *Aegean world II*, 2, 37–41, 1980.
- 922 Flowers, R. M., Bowring, S. A., Tulloch, A. J. and Klepeis, K. A.: Tempo of burial and exhumation within the deep roots of  
923 a magmatic arc, Fiordland, New Zealand, *Geology*, 33(1), 17–20, doi:10.1130/G21010.1, 2005.
- 924 Francalanci, L. and Zellmer, G. F.: Magma Genesis at the South Aegean Volcanic Arc, *Elements*, 15(3), 165–170,  
925 doi:10.2138/gselements.15.3.165, 2019.
- 926 Francalanci, L., Vougioukalakis, G. E., Fytikas, M., Beccaluva, L., Bianchini, G. and Wilson, M.: Petrology and  
927 volcanology of Kimolos and Polyegos volcanoes within the context of the South Aegean arc, Greece, *Spec. Pap. Soc. Am.*,  
928 418, 33, 2007.
- 929 Frey, H. M., Lange, R. A., Hall, C. M. and Delgado-Granados, H.: Magma eruption rates constrained by  $40\text{Ar}/39\text{Ar}$   
930 chronology and GIS for the Ceboruco-San Pedro volcanic field, western Mexico, *Bull. Geol. Soc. Am.*, 116(3–4), 259–276,

931 doi:10.1130/B25321.1, 2004.

932 Fytikas, M., Giuliani, O., Innocenti, F., Marinelli, G. and Mazzuoli, R.: Geochronological data on recent magmatism of the  
933 Aegean Sea, *Tectonophysics*, 31(1–2), T29–T34, doi:10.1016/0040-1951(76)90161-X, 1976.

934 Fytikas, M., 1977. *Geology and Geothermics of Milos Island*. Thesis, Thessaloniki University, 228 pp. (in Greek with  
935 English summary).

936 Fytikas, M., Innocenti, F., Kolios, N., Manetti, P., Mazzuoli, R., Poli, G., Rita, F. and Villari, L.: Volcanology and petrology  
937 of volcanic products from the island of Milos and neighbouring islets, *J. Volcanol. Geotherm. Res.*, 28(3–4), 297–317,  
938 doi:10.1016/0377-0273(86)90028-4, 1986.

939 Fytikas, M.: Updating of the geological and geothermal research on Milos island, *Geothermics*, 18(4), 485–496,  
940 doi:10.1016/0375-6505(89)90051-5, 1989.

941 Grasemann, B., Huet, B., Schneider, D. A., Rice, A. H. N., Lemonnier, N. and Tschegg, C.: Miocene postorogenic extension  
942 of the Eocene synorogenic imbricated Hellenic subduction channel: New constraints from Milos (Cyclades, Greece), *Bull.*  
943 *Geol. Soc. Am.*, 130(1–2), 238–262, doi:10.1130/B31731.1, 2018.

944 Grove, M. and Harrison, T. M.:  $^{40}\text{Ar}^*$  diffusion in Fe-rich biotite, *Am. Mineral.*, 81(7–8), 940–951, 1996.

945 Hayes, G. P., Moore, G. L., Portner, D. E., Hearne, M., Flamme, H., Furtney, M. and Smoczyk, G. M.: Slab2, a  
946 comprehensive subduction zone geometry model, *Science* (80-. ), 362(6410), 58–61, doi:10.1126/science.aat4723, 2018.

947 Hildreth, W. and Lanphere, M. A.: Potassium-argon geochronology of a basalt-andesite-dacite arc system: The Mount  
948 Adams volcanic field, Cascade Range of southern Washington, *Geol. Soc. Am. Bull.*, 106(11), 1413–1429, 1994.

949 Hildreth, W., Fierstein, J. and Lanphere, M.: Eruptive history and geochronology of the Mount Baker volcanic field,  
950 Washington, *Geol. Soc. Am. Bull.*, 115(6), 729–764, 2003a.

951 Hildreth, W., Lanphere, M. A. and Fierstein, J.: Geochronology and eruptive history of the Katmai volcanic cluster, Alaska  
952 Peninsula, *Earth Planet. Sci. Lett.*, 214(1–2), 93–114, doi:10.1016/S0012-821X(03)00321-2, 2003b.

953 Van Hinsbergen, D. J. J., Snel, E., Garstman, S. A., Marunțeanu, M., Langereis, C. G., Wortel, M. J. R. and Meulenkamp, J.  
954 E.: Vertical motions in the Aegean volcanic arc: Evidence for rapid subsidence preceding volcanic activity on Milos and  
955 Aegina, *Mar. Geol.*, 209(1–4), 329–345, doi:10.1016/j.margeo.2004.06.006, 2004.

956 Hora, J. M., Singer, B. S., Jicha, B. R., Beard, B. L., Johnson, C. M., de Silva, S. and Salisbury, M.: Volcanic biotite-  
957 sanidine  $^{40}\text{Ar}/^{39}\text{Ar}$  age discordances reflect Ar partitioning and pre-eruption closure in biotite, *Geology*, 38(10), 923–926,  
958 doi:10.1130/G31064.1, 2010.

959 IJlst, L.: A laboratory overflow-centrifuge for heavy liquid mineral separation, *Am. Mineral.*, 58, 1088–1093, 1973.

960 Jicha, B. R. and Jagoutz, O.: Magma production rates for intraoceanic arcs, *Elements*, 11(2), 105–112,  
961 doi:10.2113/gselements.11.2.105, 2015.

962 Kiliyas, S. P., Naden, J., Cheliotis, I., Shepherd, T. J., Constandinidou, H., Crossing, J. and Simos, I.: Epithermal gold  
963 mineralisation in the active Aegen volcanic arc: The Profitis Ilias deposits, Milos Island, Greece, *Miner. Depos.*, 36(1), 32–  
964 44, doi:10.1007/s001260050284, 2001.

965 Koppers, A. A. P.: ArArCALC-software for  $^{40}\text{Ar}/^{39}\text{Ar}$  age calculations, *Comput. Geosci.*, 28(5), 605–619,  
966 doi:10.1016/S0098-3004(01)00095-4, 2002.

967 Kornprobst, J., Kienast, J.-R. and Vilminot, J.-C.: The high-pressure assemblages at Milos, Greece, *Contrib. to Mineral.*  
968 *Petrol.*, 69(1), 49–63, doi:10.1007/bf00375193, 1979.

969 Kuiper, K. F., Deino, A., Hilgen, F. J., Krijgsman, W., Renne, P. R. and Wijbrans, J. R.: Synchronizing Rock Clocks of  
970 Earth History, *Science* (80-. ), 320(5875), 500–504, doi:10.1126/science.1154339, 2008.

971 Lee, J. K. W.: Ar–Ar and K–Ar Dating BT - *Encyclopedia of Scientific Dating Methods*, edited by W. Jack Rink and J. W.  
972 Thompson, pp. 58–73, Springer Netherlands, Dordrecht., 2015.

973 Lee, J. Y., Marti, K., Severinghaus, J. P., Kawamura, K., Yoo, H. S., Lee, J. B. and Kim, J. S.: A redetermination of the



974 isotopic abundances of atmospheric Ar, *Geochim. Cosmochim. Acta*, 70(17), 4507–4512, doi:10.1016/j.gca.2006.06.1563,  
975 2006.

976 Mark, D. F., Barfod, D., Stuart, F. M. and Imlach, J.: The ARGUS multicollector noble gas mass spectrometer: Performance  
977 for 40Ar/39Ar geochronology, *Geochemistry, Geophys. Geosystems*, 10(10), 1–9, doi:10.1029/2009GC002643, 2009.

978 Matsuda, J., Senoh, K., Maruoka, T., Sato, H. and Mitropoulos, P.: K-Ar ages of the Aegean the volcanic rocks and arc-  
979 trench system their implication for the arc-trench system, *Geochem. J.*, 33, 369–377, 1999.

980 McKenzie, D.: Active tectonics of the Alpine—Himalayan belt: the Aegean Sea and surrounding regions, *Geophys. J. Int.*,  
981 55(1), 217–254, 1978.

982 Meulenamp, J. E., Wortel, M. J. R., van Wamel, W. A., Spakman, W. and Hoogerduyn Strating, E.: On the Hellenic  
983 subduction zone and the geodynamic evolution of Crete since the late Middle Miocene, *Tectonophysics*, 146(1–4), 203–215,  
984 doi:10.1016/0040-1951(88)90091-1, 1988.

985 Min, K., Mundil, R., Renne, P. R. and Ludwig, K. R.: A test for systematic errors in 40Ar/39Ar geochronology, *Geochim.*  
986 *Cosmochim. Acta*, 64(1), 73–98, 2000.

987 Nicholls, I. A.: Santorini volcano, greece - tectonic and petrochemical relationships with volcanics of the Aegean region,  
988 *Tectonophysics*, 11(5), 377–385, doi:10.1016/0040-1951(71)90026-6, 1971.

989 Pe-Piper, G. and Piper, D. J. W.: The South Aegean active volcanic arc: relationships between magmatism and tectonics,  
990 *Dev. Volcanol.*, 7(C), 113–133, doi:10.1016/S1871-644X(05)80034-8, 2005.

991 Pe-Piper, G. and Piper, D. J. W.: Neogene backarc volcanism of the Aegean: New insights into the relationship between  
992 magmatism and tectonics, *Geol. Soc. Am. Spec. Pap.*, 418(02), 17–31, doi:10.1130/2007.2418(02), 2007.

993 Pe-Piper, G. and Piper, D. J. W.: The effect of changing regional tectonics on an arc volcano: Methana, Greece, *J. Volcanol.*  
994 *Geotherm. Res.*, 260, 146–163, doi:10.1016/j.jvolgeoes.2013.05.011, 2013.

995 Raffi, I., Wade, B. S., Pälke, H., Beu, A. G., Cooper, R., Crundwell, M. P., Krijgsman, W., Moore, T., Raine, I. and  
996 Sardella, R.: The Neogene Period, in *Geologic Time Scale 2020*, pp. 1141–1215, Elsevier., 2020.

997 Rinaldi, M. and Venuti, M. C.: The submarine eruption of the Bombarda volcano, Milos Island, Cyclades, Greece, *Bull.*  
998 *Volcanol.*, 65(4), 282–293, doi:10.1007/s00445-002-0260-z, 2003.

999 Rivera, T. A., Storey, M., Zeeden, C., Hilgen, F. J. and Kuiper, K.: A refined astronomically calibrated 40Ar/39Ar age for  
000 Fish Canyon sanidine, *Earth Planet. Sci. Lett.*, 311(3–4), 420–426, doi:10.1016/j.epsl.2011.09.017, 2011.

001 Rontogianni, S., Konstantinou, N. S., Melis, C. P. and Evangelidis: Slab stress field in the Hellenic subduction zone as  
002 inferred from intermediate-depth earthquakes, *Earth, Planets Sp.*, 63(2), 139–144, doi:10.5047/eps.2010.11.011, 2011.

003 Schaen, A., Jicha, B., Hodges, K., Vermeesch, P., Stelten, M., Mercer, C., Phillips, D., Rivera, T., Jourdan, F., Matchan, E.,  
004 Hemming, S., Morgan, L., Kelley, S., Cassata, W., Heizler, M., Vasconcelos, P., Benowitz, J., Koppers, A., Mark, D.,  
005 Niespolo, E., Sprain, C., Hames, W., Kuiper, K., Turrin, B., Renne, P., Ross, J., Nomade, S., Guillou, H., Webb, L., Cohen,  
006 B., Calvert, A., Joyce, N., Ganerød, M., Wijbrans, J., Ishizuka, O., He, H., Ramirez, A., Pfänder, J., Lopez-Martinez, M.,  
007 Qiu, H. and Singer, B.: Interpreting and reporting 40Ar/39Ar geochronologic data, *GSA Bull.*, doi:10.1130/B35560.1, 2020.

008 Singer, B. S., Thompson, R. A., Dungan, M. A., Feeley, T. C., Nelson, S. T., Pickens, J. C., Brown, L. L., Wulff, A. W.,  
009 Davidson, J. P. and Metzger, J.: Volcanism and erosion during the past 930 k.y. at the Tatara–San Pedro complex, Chilean  
010 Andes, *Geol. Soc. Am. Bull.*, 109(2), 127–142, doi:10.1130/0016-7606(1997)109<0127:VAEDTP>2.3.CO;2, 1997.

011 Sonder, R. A.: Zur Geologie and Petrographie der Inselgruppe von Milos, *Zeitschr. Volc.*, 8, 11–231, 1924.

012 Spakman, W., Wortel, M. J. R. and Vlaar, N. J.: The Hellenic Subduction Zone: A tomographic image and its geodynamic  
013 implications, *Geophys. Res. Lett.*, 15(1), 60–63, doi:10.1029/GL015i001p00060, 1988.

014 Stewart, A. L.: *Volcanic Facies Architecture and Evolution of Milos, Greece*, University of Tasmania., 2003.

015 Stewart, A. L. and McPhie, J.: Internal structure and emplacement of an Upper Pliocene dacite cryptodome, Milos Island,  
016 Greece, *J. Volcanol. Geotherm. Res.*, 124(1–2), 129–148, doi:10.1016/S0377-0273(03)00074-X, 2003.

017 Stewart, A. L. and McPhie, J.: An Upper Pliocene coarse pumice breccia generated by a shallow submarine explosive  
018 eruption, Milos, Greece, *Bull. Volcanol.*, 66(1), 15–28, doi:10.1007/s00445-003-0292-z, 2004.  
019 Stewart, A. L. and McPhie, J.: Facies architecture and Late Pliocene – Pleistocene evolution of a felsic volcanic island,  
020 Milos, Greece, *Bull. Volcanol.*, 68(7–8), 703–726, doi:10.1007/s00445-005-0045-2, 2006.  
021 Traineau, H. and Dalabakis, P.: Mise en evidence d’une eruption phreatique historique sur l’île de Milos (Grece), *CR Acad*  
022 *Sci Paris*, 1–38, 1989.  
023 Vougioukalakis, G. E., Satow, C. G. and Druitt, T. H.: Volcanism of the South Aegean volcanic arc, *Elements*, 15(3), 159–  
024 164, 2019.  
025 Wendt, I. and Carl, C.: The statistical distribution of the mean squared weighted deviation, *Chem. Geol. Isot. Geosci. Sect.*,  
026 86(4), 275–285, doi:10.1016/0168-9622(91)90010-T, 1991.  
027 White, S. M., Crisp, J. A. and Spera, F. J.: Long-term volumetric eruption rates and magma budgets, *Geochemistry,*  
028 *Geophys. Geosystems*, 7(3), 262–266, doi:10.1029/2005GC001002, 2006.  
029 York, D.: Least squares fitting of a straight line with correlated errors, *Earth Planet. Sci. Lett.*, 5(C), 320–324,  
030 doi:10.1016/s0012-821x(68)80059-7, 1968.  
031

**Table 1. Previous Published eruption ages and related stratigraphic units of the island of Milos**

Stratigraphy	Sample	Mineral	Location	Petrology	K <sub>2</sub> O (wt.%)	Age (Ma)	± 1σ
Unit IV	<sup>1</sup> Angelier_1	Unknown	Fyriplaka	Rhyolite	-	-	-
Unit III	<sup>1</sup> Angelier_2	Unknown	Halepa	Rhyolite	2.44	0.95	0.06
Unit II	<sup>1</sup> Angelier_3	Unknown	Triades	Dacite	1.47	1.71	0.08
	<sup>1</sup> Angelier_4	Unknown	Kleftico	Andesite	1.77	2.33	0.09
	<sup>1</sup> Angelier_5	Unknown	Kleftico	Andesite	1.45	2.50	0.09
Unit I	<sup>1</sup> Angelier_6	Unknown	Adamas	Rhyolite	2.90	2.15	0.08
	<sup>1</sup> Angelier_7	Unknown	Dhemeneghaki	Rhyolite	2.75	1.84	0.08
Phreatic activity	<sup>5</sup> Gif-7358&7359	Carbonized wood	Agia Kiriaki	Lahar deposits	-	200 BC-200 AD	
CFT	<sup>2</sup> M196	Unknown	Fyriplaka	Rhyolite	2.9	0.09	0.02
	<sup>2</sup> M194	Unknown	Fyriplaka	Rhyolite	2.85	0.14	0.03
	<sup>2</sup> M168	Unknown	Trachilas	Rhyolite	3.91	0.37	0.09
	<sup>2</sup> M-48	Biotite	NW of Filiplaka	Rhyolite	6.41	0.48	0.05
	<sup>3</sup> M1-1	Lava	Plakes	Dacite	2.07	0.80	0.10
	<sup>2</sup> M-OB1	Groundmass	N of Dhemenegaki	Obsidian	2.53	0.88	0.18
	<sup>2</sup> M27	Unknown	Plakes	Dacite	1.87	0.97	0.06
	<sup>3</sup> M1-4	Lava	Plakes	Dacite	2.32	1.20	0.10
	<sup>5</sup> MIL130 <sup>e</sup>	Zircon	Triades	Dacite	-	1.44	0.08
	<sup>2</sup> M-OB2	Groundmass	Bombarda	Obsidian	2.73	1.47	0.05
PSLD	<sup>6</sup> Fission track1	Groundmass	Adamas	Obsidian	-	1.54	0.18
	<sup>6</sup> Fission track2	Groundmass	Bombarda	Obsidian	-	1.57	0.15
	<sup>7</sup> Fission track3	Groundmass	Bombarda-Adamas	Obsidian	-	1.57	0.12
	<sup>2</sup> M103	Unknown	near Pollonia	Andesite	1.87	1.59	0.25
	<sup>7</sup> Fission track3	Groundmass	Dhemeneghaki	Obsidian	-	1.60	0.06
	<sup>2</sup> M146	Unknown	1km NW of Adamas	Rhyolite	3.09	1.71	0.05
	<sup>2</sup> M110	Unknown	Sarakiniko	Dacite	2.57	1.85	0.10
CDLF	<sup>2</sup> M1	Unknown	Aghios, near Triades	Rhyolite	3.32	2.04	0.09
	<sup>2</sup> M66	Unknown	~1 km NW of Adamas	Dacite	2.61	2.03	0.06
	<sup>4</sup> MIL243*	Zircon	Triades	Dacite	-	2.18	0.09
	<sup>2</sup> M156	Unknown	Angathia, near Triades	Dacite	2.84	2.38	0.10
	<sup>4</sup> MIL365*	Zircon	Filakopi	Rhyolite	-	2.66	0.07
BPS	<sup>4</sup> MIL343*	Zircon	Kalogeros cryptodome	Dacite	-	2.70	0.04
	<sup>2</sup> M164	Unknown	Kleftico	Rhyolite	2.84	3.08	0.08
	<sup>2</sup> M163	Unknown	Kleftico	Andesite	1.18	3.50	0.14

Published ages from 1=Angelier et al. (1977), 2=Fytikas et al. (1976, 1986), 3=Matsuda et al. (1999), 4=Stewart and McPhie (2006), 5=Trainau and Dalabakis (1989), 6=Bigazzi and Radi (1981), Arias et al. (2006). Angelier et al. (1977) do not provide sample names, only numbers for the sample locations. Here the location is given after "Angelier" (Angelier et al. (1977, their Fig. 3). Abbreviations: BPS=Basal pyroclastic series; CDLF=Complex of domes and lava flows; PSLD=Pyroclastic series and lava domes; CTF=Complexes of Trachilas and Fyriplaka. See more details in Fig. 4.

Commented [MOU17]: what do these numbers relate to "Angelier\_1" etc?

Commented [MOU18]: what does superscript "e" relate to?

**Table 2. Incremental heating  $^{40}\text{Ar}/^{39}\text{Ar}$  results of the Milos volcanic field.**

Volcanic Unit	Sample -ID	Irr-ID	Latitude	Age $\pm 1\sigma$ (Ma)	MS WD	$^{39}\text{Ar}_k$ (%)	n/ntotal	$^{40}\text{Ar}^*$ (%)	K/Ca $\pm 1\sigma$	Inverse isochron age (Ma)	$^{40}\text{Ar}/^{36}\text{Ar} \pm 1\sigma$	MS WD
Fyriplaka Complex	G15M0008 <sup>B</sup>	VU110-Z22a	36.6729 N 24.4670 E	0.05 $\pm$ 0.01	0.04	16.24	3/15	1.20	60.9 $\pm$ 10.6	0.05 $\pm$ 0.10	298.08 $\pm$ 8.77	0.08
		VU110-Z22b		<b>0.062 <math>\pm</math> 0.003</b>	0.91	71.81	8/11	2.69	57.3 $\pm$ 8.4	0.06 $\pm$ 0.02	299.39 $\pm$ 3.66	1.09
		Combined (Z22)		<b>0.061 <math>\pm</math> 0.004</b>	0.82	41.37	11/26	2.29	58.0 $\pm$ 6.3	0.07 $\pm$ 0.01	296.78 $\pm$ 1.78	0.83
	G15M0012 <sup>B</sup>	VU110-Z24a	36.6795 N 24.4828 E	0.05 $\pm$ 0.01	3.09	38.89	3/11	2.89	40.0 $\pm$ 6.0	0.14 $\pm$ 0.03	285.98 $\pm$ 4.76	0.07
		VU110-Z24b		0.09 $\pm$ 0.02	8.16	48.04	4/11	4.59	30.1 $\pm$ 7.1	0.09 $\pm$ 0.05	297.46 $\pm$ 10.29	12.78
		Combined (Z24)		<b>0.07 <math>\pm</math> 0.01</b>	7.44	43.53	7/22	3.86	32.3 $\pm$ 5.0	0.09 $\pm$ 0.03	295.67 $\pm$ 7.39	9.02
	G15M0009 <sup>B</sup>	VU110-Z23a	36.6716 N 24.4891 E	0.11 $\pm$ 0.02	1.37	18.33	4/12	1.65	45.4 $\pm$ 7.3	0.76 $\pm$ 0.30	268.52 $\pm$ 17.08	0.90
		VU110-Z23b		0.11 $\pm$ 0.03	6.77	41.05	4/11	3.13	19.4 $\pm$ 3.7	0.29 $\pm$ 0.14	285.17 $\pm$ 15.80	8.09
		Combined (Z23)		<b>0.11 <math>\pm</math> 0.02</b>	3.50	29.50	8/21	2.39	19.7 $\pm$ 2.6	0.15 $\pm$ 0.05	295.78 $\pm$ 4.34	4.04
Trachilas Complex	G15M0007 <sup>B</sup>	VU110-Z12a	36.7671 N 24.4124 E	0.30 $\pm$ 0.01	4.61	56.50	8/16	14.51	38.3 $\pm$ 2.4	0.28 $\pm$ 0.05	301.42 $\pm$ 9.01	5.47
		VU110-Z12b		<b>0.317 <math>\pm</math> 0.004</b>	1.29	74.05	4/11	18.30	32.0 $\pm$ 2.5	0.31 $\pm$ 0.03	299.52 $\pm$ 6.40	2.04
		Combined (Z12)		0.31 $\pm$ 0.01	5.57	65.27	12/27	15.77	33.1 $\pm$ 1.6	0.34 $\pm$ 0.03	293.05 $\pm$ 5.50	5.84
Kontaro dome	G15M0020 <sup>D</sup>	VU108-Z5a_5	36.7234 N 24.3952 E	1.52 $\pm$ 0.01	1.06	61.82	8/12	18.30	1.51 $\pm$ 0.05	1.49 $\pm$ 0.02	300.03 $\pm$ 0.86	0.95
		VU108-Z5b_1		1.56 $\pm$ 0.01	1.94	41.54	3/10	47.94	1.73 $\pm$ 0.06	1.58 $\pm$ 0.02	294.97 $\pm$ 3.74	2.17
		VU108-Z5b_2		1.52 $\pm$ 0.01	1.73	62.45	5/10	22.95	1.56 $\pm$ 0.08	1.53 $\pm$ 0.02	298.12 $\pm$ 0.89	2.34
		Combined (Z5)		<b>1.54 <math>\pm</math> 0.01</b>	3.06	57.32	16/32	25.31	1.58 $\pm$ 0.04	1.55 $\pm$ 0.01	297.41 $\pm$ 0.57	2.82
	G15M0019 <sup>D</sup>	VU108-Z6a_4	36.7211 N 24.3950 E	1.62 $\pm$ 0.01	3.80	89.75	9/11	34.28	0.91 $\pm$ 0.05	1.62 $\pm$ 0.02	297.66 $\pm$ 1.36	4.40
		VU108-Z6a_5		1.55 $\pm$ 0.01	4.50	95.41	10/12	35.26	0.88 $\pm$ 0.06	1.55 $\pm$ 0.01	298.73 $\pm$ 1.29	5.40
		VU108-Z6b_1		1.56 $\pm$ 0.01	4.05	56.64	4/10	53.19	1.02 $\pm$ 0.01	<b>1.48 <math>\pm</math> 0.02</b>	315.46 $\pm$ 5.20	0.44
				32.1								
		Combined (Z6)		1.55 $\pm$ 0.01	5	80.97	27/45	38.78	0.93 $\pm$ 0.04	1.53 $\pm$ 0.02	300.60 $\pm$ 2.27	34.25
Dheme-neghaki volcano	G15M0032B <sup>D</sup>	VU108-Z18	36.7084 N 24.5324 E	<b>1.825 <math>\pm</math> 0.002</b>	0.91	98.64	12/13	93.86	1.83 $\pm$ 0.04	1.825 $\pm$ 0.003	301.52 $\pm$ 3.34	0.93
Triades lava dome	G15M0021 <sup>B</sup>	VU110-Z4_2	36.7402 N 24.3397 E	<b>1.97 <math>\pm</math> 0.01</b>	1.66	63.83	4/12	54.72	107.55 $\pm$ 20.64	1.97 $\pm$ 0.03	299.16 $\pm$ 5.36	2.56
		VU110-Z4_2b		2.01 $\pm$ 0.01	6.76	75.39	6/16	57.84	54.43 $\pm$ 8.29	2.04 $\pm$ 0.05	293.08 $\pm$ 10.44	8.15
		Combined (Z4)		1.99 $\pm$ 0.01	9.08	69.12	10/28	56.59	73.52 $\pm$ 6.46	2.00 $\pm$ 0.04	295.64 $\pm$ 7.89	10.30
Adamas lava dome	G15M0004 <sup>A</sup>	VU108-Z10_1	36.7282 N 24.4315 E	2.99 $\pm$ 0.11	1.00	87.31	4/12	16.36	0.030 $\pm$ 0.002	7.89 $\pm$ 2.46	202.39 $\pm$ 48.47	0.01
		VU108-Z10_2		2.86 $\pm$ 0.09	1.50	86.18	7/11	17.58	0.029 $\pm$ 0.002	0.70 $\pm$ 0.29	348.91 $\pm$ 27.33	1.00
		Combined (Z10)		2.90 $\pm$ 0.07	1.31	86.74	11/23	17.13	0.029 $\pm$ 0.001	<b>1.95 <math>\pm</math> 0.45</b>	319.51 $\pm$ 14.70	1.17
The dyke of Mavro Vouni lava dome	G15M0016 <sup>D</sup>	VU108-Z8a	36.6668 N 24.3398 E	2.71 $\pm$ 0.02	2.31	79.64	8/12	16.57	0.24 $\pm$ 0.05	2.65 $\pm$ 0.10	299.84 $\pm$ 2.32	2.92
		VU108-Z8a_4		2.61 $\pm$ 0.03	0.93	57.41	7/12	16.86	0.12 $\pm$ 0.07	2.69 $\pm$ 0.10	296.44 $\pm$ 2.49	0.69
		VU108-Z8b_1		2.67 $\pm$ 0.01	1.50	65.57	7/11	17.25	0.11 $\pm$ 0.04	2.55 $\pm$ 0.05	301.53 $\pm$ 1.14	0.71
		Combined (Z8)		<b>2.66 <math>\pm</math> 0.01</b>	2.51	67.27	22/35	16.87	0.14 $\pm$ 0.02	2.61 $\pm$ 0.05	300.01 $\pm$ 1.18	2.78
Korokia dome	G15M0029 <sup>D</sup>	VU108-Z16a	36.7465 N 24.5200 E	2.67 $\pm$ 0.01	0.96	23.61	4/13	56.34	0.53 $\pm$ 0.05	2.68 $\pm$ 0.02	296.64 $\pm$ 3.18	1.25
		VU108-Z16b_1		2.69 $\pm$ 0.01	1.32	27.08	3/13	55.78	0.55 $\pm$ 0.04	2.67 $\pm$ 0.03	301.16 $\pm$ 4.72	2.13
		Combined (Z16)		2.68 $\pm$ 0.01	1.66	25.30	7/26	56.10	0.54 $\pm$ 0.03	2.67 $\pm$ 0.02	300.00 $\pm$ 2.94	1.98
Coherent dacite of Profitis Ilias volcano	G15M0015 <sup>D</sup>	VU108-Z9a	36.6629 N 24.3596 E	3.12 $\pm$ 0.02	9.07	43.07	3/12	42.73	1.31 $\pm$ 0.05	3.06 $\pm$ 0.02	304.19 $\pm$ 1.25	0.01
		VU108-Z9b_1		2.98 $\pm$ 0.02	4.53	27.00	4/14	39.35	0.98 $\pm$ 0.06	3.04 $\pm$ 0.02	293.83 $\pm$ 1.38	1.14
		Combined (Z9)		2.99 $\pm$ 0.02	5.54	22.79	6/26	41.77	1.00 $\pm$ 0.04	<b>3.06 <math>\pm</math> 0.02</b>	292.77 $\pm$ 1.62	1.90
Coherent dacite of Profitis Ilias volcano	G15M0017 <sup>D</sup>	VU108-Z7a	36.6596 N 24.3675 E	<b>3.64 <math>\pm</math> 0.08</b>	3.13	28.62	7/13	9.77	1.04 $\pm$ 0.02	4.14 $\pm$ 0.49	293.87 $\pm$ 4.77	3.44
		VU108-Z7a_4		<b>4.10 <math>\pm</math> 0.06</b>	2.13	34.71	6/17	9.08	1.10 $\pm$ 0.01	4.11 $\pm$ 1.40	298.44 $\pm$ 15.51	3.24
		VU108-Z7b_1		<b>3.41 <math>\pm</math> 0.05</b>	3.95	31.41	5/13	9.95	1.00 $\pm$ 0.03	3.68 $\pm$ 0.71	295.97 $\pm$ 7.34	7.09
		Combined (Z7)		<b>3.63 <math>\pm</math> 0.08</b>	14.04	31.40	18/43	9.59	1.04 $\pm$ 0.02	2.19 $\pm$ 0.32	311.31 $\pm$ 3.60	10.19

The age in bold is considered as the best estimate of the eruptive age.

The  $^{40}\text{Ar}^*$  (%) is the average radiogenic  $^{40}\text{Ar}$  of the analyses included in the weighted mean.

The experiment was analyzed on biotite<sup>B</sup>, obsidian<sup>D</sup>, amphibole<sup>A</sup> and groundmass<sup>G</sup> of a sample.

The same steps were used for the calculation of isochron ages as used in the weighted mean ages.

**Table 3.  $^{40}\text{Ar}/^{39}\text{Ar}$  results of single grain fusion analyses on the Milos volcanic field.**

Volcanic unit	Sample-ID	Irr-ID	Location	Age $\pm 1\sigma$ (Ma)	MS WD	$^{39}\text{Ar}_K$ (%)	n/ntotal	$^{40}\text{Ar}^*$ (%)	K/Ca $\pm 1\sigma$	Inverse isochron age (Ma)	$^{40}\text{Ar}/^{36}\text{Ar} \pm 1\sigma$	MS WD
Fyriplaka complex	G15M0008 <sup>B</sup>	VU110-Z22	36.6729 N 24.4670 E	0.71 $\pm$ 0.06	0.41	25.78	8/23	8.67	17.5 $\pm$ 1.8	0.64 $\pm$ 0.20	302.75 $\pm$ 12.62	0.46
	G15M0012 <sup>B</sup>	VU110-Z24	36.6795 N 24.4828 E	1.12 $\pm$ 0.11	2.26	60.49	14/23	7.32	14.9 $\pm$ 0.8	0.26 $\pm$ 0.07	316.75 $\pm$ 19.49	2.29
	G15M0009 <sup>B</sup>	VU110-Z23	36.6716 N 24.4891 E	0.65 $\pm$ 0.07	1.16	79.91	19/23	5.87	12.0 $\pm$ 0.5	0.28 $\pm$ 0.07	309.57 $\pm$ 16.01	1.22
Trachilas complex	G15M0007 <sup>B</sup>	VU110-Z12	36.7671 N 24.4124 E	0.47 $\pm$ 0.05	0.75	72.65	15/22	9.09	14.8 $\pm$ 0.5	0.55 $\pm$ 0.12	293.95 $\pm$ 11.30	0.80
Kalamos lava	G15M0033 <sup>B</sup>	VU108-Z19	36.6662 N 24.4652 E	<b>0.412 <math>\pm</math> 0.004</b>	1.10	77.24	8/10	22.22	20.5 $\pm$ 2.7	0.39 $\pm$ 0.02	303.32 $\pm$ 3.06	0.89
Trachilas complex	G15M0034 <sup>B</sup>	VU108-Z20	36.7550 N 24.4244 E	<b>0.51 <math>\pm</math> 0.02</b>	0.95	56.92	6/10	3.53	13.7 $\pm$ 1.2	0.61 $\pm$ 0.08	296.45 $\pm$ 1.65	0.92
	G15M0035 <sup>B</sup>	VU108-Z21	36.7550 N 24.4244 E	<b>0.63 <math>\pm</math> 0.02</b>	1.26	73.43	6/9	4.87	17.7 $\pm$ 1.1	0.77 $\pm$ 0.13	294.99 $\pm$ 3.17	1.42
Halepa lava dome	G15M0013 <sup>B</sup>	VU108-Z13	36.6716 N 24.4406 E	<b>1.04 <math>\pm</math> 0.01</b>	1.62	82.40	9/10	26.30	*15.2 $\pm$ 0.2	1.02 $\pm$ 0.04	299.77 $\pm$ 4.06	0.00
Triades lava dome	G15M0021 <sup>B</sup>	VU110-Z4	36.7402 N 24.3397 E	2.48 $\pm$ 0.04	1.49	87.08	4/12	36.09	13.00 $\pm$ 0.60	3.44 $\pm$ 0.46	228.58 $\pm$ 36.66	1.39
	G15M0022 <sup>B</sup>	VU108-Z14	36.7402 N 24.3397 E	<b>2.10 <math>\pm</math> 0.01</b>	1.37	100.00	10/10	36.04	*11.7 $\pm$ 0.2	2.08 $\pm$ 0.06	299.44 $\pm$ 4.63	1.59
	G15M0023 <sup>B</sup>	VU108-Z3	36.7263 N 24.3420 E	<b>2.10 <math>\pm</math> 0.01</b>	1.72	55.58	6/11	35.93	*76.1 $\pm$ 2.4	2.13 $\pm$ 0.06	296.12 $\pm$ 4.63	2.08
	G15M0024 <sup>B</sup>	VU108-Z15	36.7277 N 24.3415 E	<b>2.13 <math>\pm</math> 0.01</b>	0.46	63.67	6/10	29.74	22.5 $\pm$ 3.2	2.09 $\pm$ 0.03	300.50 $\pm$ 1.58	0.23
Mavros Kavos lava dome	G15M0025 <sup>B</sup>	VU108-Z2	36.6876 N 24.3515 E	<b>2.36 <math>\pm</math> 0.01</b>	0.70	84.62	9/10	37.62	43.2 $\pm$ 2.7	2.34 $\pm$ 0.04	300.57 $\pm$ 3.49	0.78
	G15M0026 <sup>B</sup>	VU108-Z1b	36.6848 N 24.3500 E	2.35 $\pm$ 0.01	1.36	95.23	9/10	38.56	12.8 $\pm$ 2.3	<b>2.42 <math>\pm</math> 0.04</b>	292.01 $\pm$ 2.92	0.93
Kalegeros crypto-dome	G15M0006 <sup>B</sup>	VU108-Z11	36.7643 N 24.5157 E	2.72 $\pm$ 0.01	1.95	87.67	9/10	47.90	*28.3 $\pm$ 0.5	<b>2.62 <math>\pm</math> 0.04</b>	310.21 $\pm$ 4.04	0.99

The age in bold is considered as the best estimate of the eruptive age.

The  $^{40}\text{Ar}^*$  (%) is the average radiogenic  $^{40}\text{Ar}$  of the analyses included in the weighted mean.

\*The K/Ca ratio is calibrated by removing the total fusion with excess  $^{37}\text{Ar}$  (Ca) (fA>1).

<sup>B</sup>The experiment was analyzed on biotite of the sample.

The same steps were used for the calculation of isochron ages as used in the weighted mean ages.

**Table 4. Major-element composition of volcanic samples from the Milos Volcanic Field.**

Sample-ID	Rock Types	SiO <sub>2</sub> wt.%	TiO <sub>2</sub> wt.%	Al <sub>2</sub> O <sub>3</sub> wt.%	Fe <sub>2</sub> O <sub>3</sub> T wt.%	MnO wt.%	MgO wt.%	CaO wt.%	Na <sub>2</sub> O wt.%	K <sub>2</sub> O wt.%	P <sub>2</sub> O <sub>5</sub> wt.%	BaO wt.%	LOI wt.%
G15M0008	Pumice	76.71	0.14	12.96	1.11	0.058	0.22	1.27	4.04	3.22	0.021	0.056	0.16
G15M0012	Pumice	75.47	0.13	12.77	1.08	0.057	0.22	1.27	4.12	3.15	0.024	0.055	0.35
G15M0009	Pumice	76.02	0.13	12.91	1.04	0.059	0.23	1.19	3.99	3.41	0.022	0.056	0.16
G15M0007	Pumice	76.68	0.08	12.60	0.85	0.084	0.11	0.75	3.58	4.74	0.009	0.051	0.17
G15M0033	Rhyolite	76.68	0.10	12.86	0.88	0.087	0.18	0.85	3.71	4.46	0.014	0.045	0.14
G15M0034	Pumice	76.89	0.08	12.64	0.84	0.085	0.11	0.74	3.50	4.85	0.009	0.050	0.33
G15M0035	Pumice	78.40	0.08	12.93	0.85	0.087	0.11	0.76	3.49	4.95	0.010	0.052	0.06
G15M0013	Rhyolite	72.87	0.22	14.11	1.95	0.071	0.51	2.23	3.73	3.43	0.044	0.055	0.13
G15M0020	unknown	-	-	-	-	-	-	-	-	-	-	-	-
G15M0019	Dacite	64.26	0.56	16.08	5.33	0.112	2.42	5.33	3.60	1.69	0.038	0.038	0.09
G15M0032 B	Obsidian	75.57	0.20	13.32	1.46	0.062	0.33	1.71	3.95	3.26	0.033	0.055	0.07
G15M0004	Dacite	63.56	0.57	16.09	5.70	0.114	2.81	6.01	3.49	1.57	0.090	0.036	0.04
G15M0021	Trachy- dacite	64.98	0.35	16.82	3.69	0.075	1.50	2.19	2.61	7.24	0.049	0.353	0.17
G15M0022	Enclave	53.87	0.60	19.91	7.61	0.157	3.93	5.45	1.73	6.11	0.075	0.34	0.21
G15M0023	Rhyolite	73.05	0.29	14.24	3.23	0.017	0.53	2.35	3.28	3.36	0.043	0.064	0.12
G15M0024	Rhyolite	76.57	0.23	11.73	1.69	0.025	0.46	2.36	2.85	2.31	0.045	0.046	0.20
G15M0025	Rhyodacite	69.56	0.42	15.30	3.15	0.106	0.88	3.67	3.49	2.98	0.105	0.059	0.19
G15M0026	Rhyodacite	69.57	0.43	16.08	3.38	0.037	0.62	3.43	3.56	2.63	0.087	0.061	0.09
G15M0006	Rhyodacite	68.58	0.40	15.90	2.67	0.074	0.81	2.89	4.19	3.61	0.108	0.099	0.12
G15M0016	Basaltic Andesite	55.72	0.66	18.43	7.70	0.135	4.42	8.78	2.90	1.41	0.090	0.030	0.06
G15M0029	Dacite	61.91	0.79	17.09	5.90	0.087	1.84	6.07	3.57	2.71	0.200	0.126	0.09
G15M0015	Andesite	63.77	0.64	16.33	5.42	0.097	2.48	5.91	3.35	1.91	0.089	0.036	0.04
G15M0017	Dacite	68.03	0.58	15.90	3.47	0.066	1.34	4.31	3.76	2.69	0.101	0.044	0.48

The classification of rock type for each sample is on the basis of field observation and SiO<sub>2</sub> versus K<sub>2</sub>O plot of Le Bas et al. (1986). All iron expressed as Fe<sub>2</sub>O<sub>3</sub>T(otal).

**Table 4. Major-element composition of volcanic samples from the Milos Volcanic Field.**

Sample-ID	G15M0 008	G15M0 012	G15M0 009	G15M0 007	G15M0 033	G15M0 034	G15M0 035	G15M0 013	G15M 0020	G15M 0019	G15M00 32B	G15M0 004
Rock Types	Pumice	Pumice	Pumice	Pumice	Pumice	Pumice	Pumice	Rhyolite	-	Dacite	Obsidian	Dacite
Major elements (wt.%)												
SiO <sub>2</sub>	76.71	75.47	76.02	76.68	76.68	76.89	78.40	72.87	-	64.26	75.57	63.56
TiO <sub>2</sub>	0.14	0.13	0.13	0.08	0.10	0.08	0.08	0.22	-	0.56	0.20	0.57
Al <sub>2</sub> O <sub>3</sub>	12.96	12.77	12.91	12.60	12.86	12.64	12.93	14.11	-	16.08	13.32	16.09
Fe <sub>2</sub> O <sub>3</sub>	1.11	1.08	1.04	0.85	0.88	0.84	0.85	1.95	-	5.33	1.46	5.70
MnO	0.06	0.06	0.06	0.08	0.09	0.09	0.07	0.07	-	0.11	0.06	0.11
MgO	0.22	0.22	0.23	0.11	0.18	0.11	0.11	0.51	-	2.42	0.33	2.81
CaO	1.27	1.27	1.19	0.75	0.85	0.74	0.76	2.23	-	5.33	1.71	6.01
Na <sub>2</sub> O	4.04	4.12	3.99	3.58	3.71	3.50	3.49	3.73	-	3.60	3.95	3.49
K <sub>2</sub> O	3.22	3.15	3.41	4.74	4.46	4.85	4.95	3.43	-	1.69	3.26	1.57
P <sub>2</sub> O <sub>5</sub>	0.02	0.02	0.02	0.01	0.01	0.01	0.01	0.04	-	0.04	0.03	0.09
BaO	0.06	0.06	0.06	0.05	0.05	0.05	0.05	0.06	-	0.04	0.06	0.04
L.O.I.	0.16	0.35	0.16	0.17	0.14	0.33	0.06	0.13	-	0.09	0.07	0.04
Total	99.97	98.70	99.22	99.70	100.01	100.13	101.78	99.35	-	99.55	100.02	100.08

Commented [MOU19]: should give totals of major element oxides.

should have samples across the top and major elements down the side.

Sample-ID	G15M0 021	G15M0 022	G15M0 023	G15M0 024	G15M0 025	G15M0 026	G15M0 006	G15M0 016	G15M0 029	G15M0 015	G15M0 017
Rock Types	Trachy- dacite	Enclave	Dacite	Rhyolite	Dacite	Dacite	Dacite	Basaltic Andesite	Dacite	Dacite	Dacite
Major elements (wt.%)											
SiO <sub>2</sub>	64.98	53.87	73.05	76.57	69.56	69.57	68.58	<b>55.72</b>	61.91	63.77	68.03
TiO <sub>2</sub>	0.35	0.60	0.29	0.23	0.42	0.43	0.40	0.66	0.79	0.64	0.58
Al <sub>2</sub> O <sub>3</sub>	16.82	19.91	14.24	11.73	15.30	16.08	15.90	18.43	17.09	16.33	15.90
Fe <sub>2</sub> O <sub>3</sub>	3.69	7.61	3.23	1.69	3.15	3.38	2.67	7.70	5.90	5.42	3.47
MnO	0.08	0.16	0.02	0.03	0.11	0.04	0.07	0.14	0.09	0.10	0.07
MgO	1.50	3.93	0.53	0.46	0.88	0.62	0.81	4.42	1.84	2.48	1.34
CaO	2.19	5.45	2.35	2.36	3.67	3.43	2.89	8.78	6.07	5.91	4.31
Na <sub>2</sub> O	2.61	1.73	3.28	2.85	3.49	3.56	4.19	2.90	3.57	3.35	3.76
K <sub>2</sub> O	7.24	6.11	3.36	2.31	2.98	2.63	3.61	1.41	2.71	1.91	2.69
P <sub>2</sub> O <sub>5</sub>	0.05	0.08	0.04	0.05	0.11	0.09	0.11	0.09	0.20	0.09	0.10
BaO	0.35	0.34	0.06	0.05	0.06	0.06	0.10	0.03	0.13	0.04	0.04
L.O.I.	0.17	0.21	0.12	0.20	0.19	0.09	0.12	0.06	0.09	0.04	0.48
Total	100.03	100.00	100.57	98.53	99.92	99.98	99.45	100.34	100.39	100.08	100.77

The classification of rock type for each sample is on the basis of field observation and SiO<sub>2</sub> versus K<sub>2</sub>O plot of Le Bas et al. (1986). All iron expressed as Fe<sub>2</sub>O<sub>3</sub>T(otal).

**Table 5. Summary of the eruption ages of the Milos volcanic field**

No.	Name of volcanic centre	Age (Ma)	Reference
1	Kimlos volcano	3.34	Fytikas et al., 1986
2	Profitis Ilias crypto/pumice cone	3.08	Fytikas et al., 1986
3	coherent dacite of Profitis Ilias volcano	3.06	This study
4	Filakopi volcano	2.66	Stewart and McPhie, 2006
5	Kalegeros cryptodome	2.62	This study
6	Mavro Vouini lava dome	2.5	Angelier et al., 1977
7	Mavros Kavos lava dome	2.42-2.36	This study
8	Polyegos lava dome	2.34	Fytikas et al., 1986
9	Triades lava dome	2.13-2.10 and 1.97	This study
10	Adamas lava dome	2.03	Fytikas et al., 1986
11	Dhemeneghaki volcano	1.83	This study
12	Bombardo volcano	1.71	Fytikas et al., 1986
13	Korakia dome	1.59	Fytikas et al., 1986
14	Komntaro dome	1.52-1.48	This study
15	Halepa lava dome	1.04	This study
16	Plakes lava dome	0.97	Fytikas et al., 1986
17	Trachilias complex	0.63, 0.51 and 0.317	This study
18	Kalamos lava dome	0.41	This study
19	Antimilos domes	0.32	Fytikas et al., 1986
20	Fyriplaka complex	0.11 and 0.07-0.06	This study
21	Phreatic activity	200 AD-200 BC	Trainau and Dalabakis, 1989

Appendix (supplements I: field images, II: <sup>40</sup>Ar/<sup>39</sup>Ar analytical data and III: X-Ray reports).

**Commented [X20]:** This Table is a new Table for indicating the number of the left panel of new Figure 14.

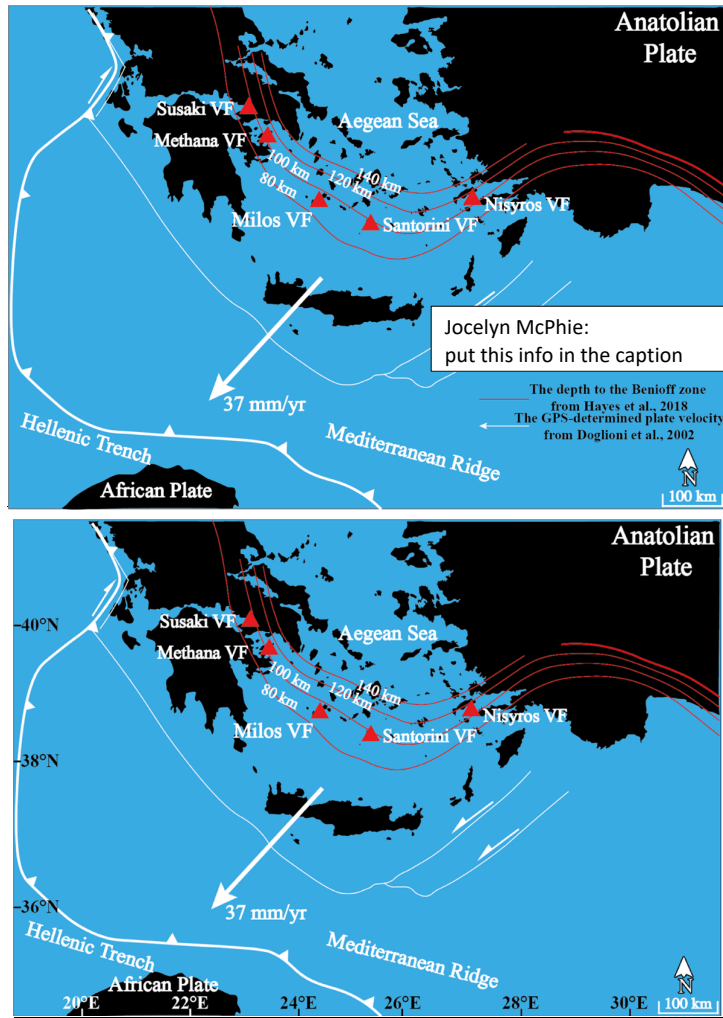
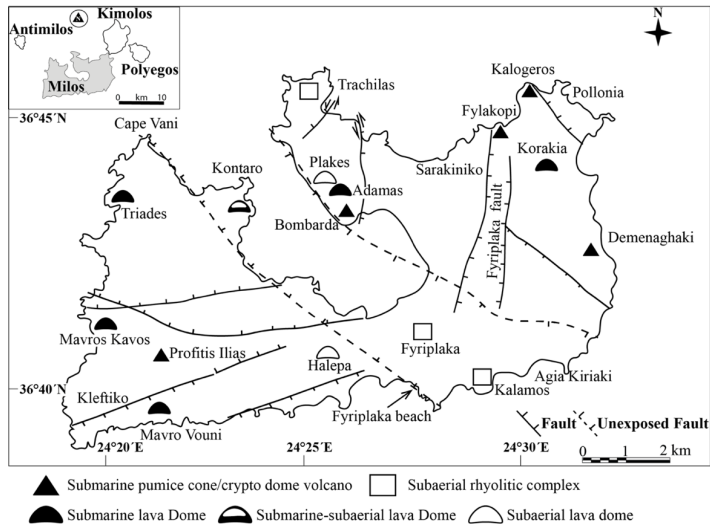


**Figure 1.** Map of the South Aegean Volcanic Arc (SAVA). Volcanic fields (VF) are indicated by red triangles: Susaki, Methana and Milos VFs in the western SAVA, Santorini VF in the centre and Nisyros VF in the eastern SAVA. Red contour lines show the depth to the Benioff zone (Hayes et al., 2018). White arrow represents the GPS-determined plate velocity of the Aegean microplate relative to the African plate from Doglioni et al. (2002).





**Commented [MOU21]:** This figure is misleading, especially for the pumice cone volcanoes. What you have shown is the only the approximate centre of areas where the different facies associations have been mapped. There is in fact a lot of overlap and interfingering of different associations. Also, the map implies that the various "volcano" types shown are discrete - they are shown separated by something that isn't actually defined. Any map presented at this stage should support the text.

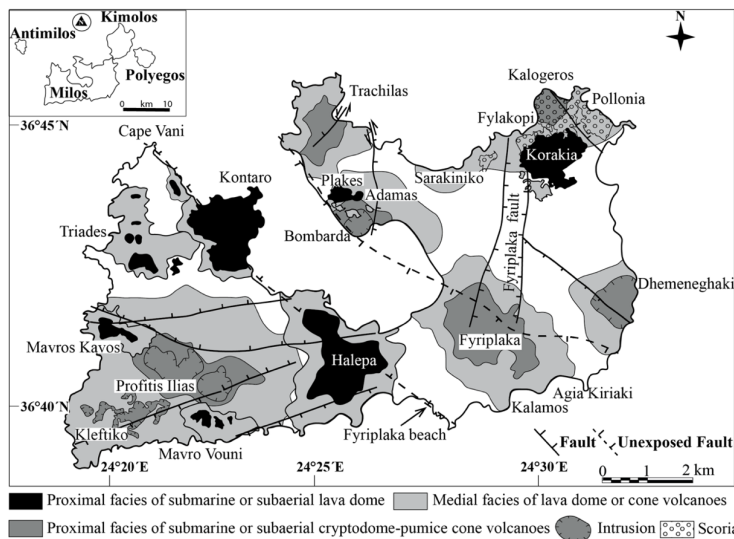


**Figure 2.** Distribution of the proximal and medial facies of the submarine pumice cone/crypto dome volcanoes, submarine, submarine-subaerial and subaerial domes and rhyolitic complexes (tuff cone and associated lava) of Milos, modified after Fytikas et al. (1986) and Stewart and McPhie (2006). The distal facies of Stewart and McPhie (2006) is not shown.

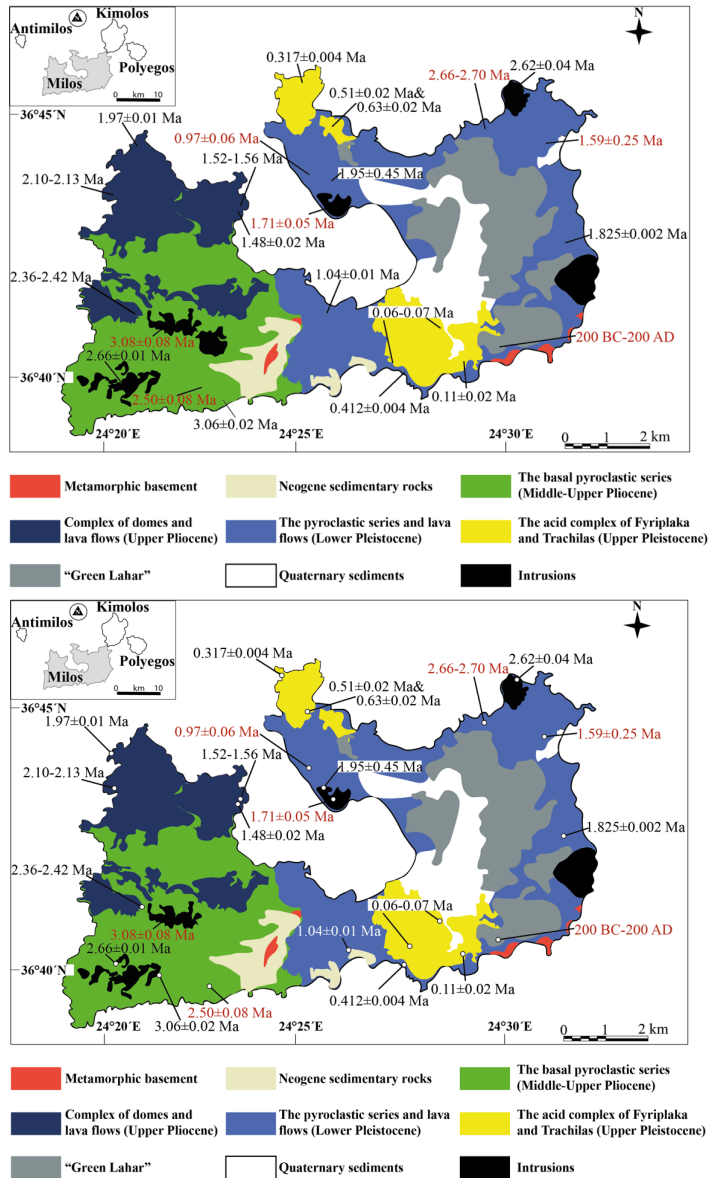
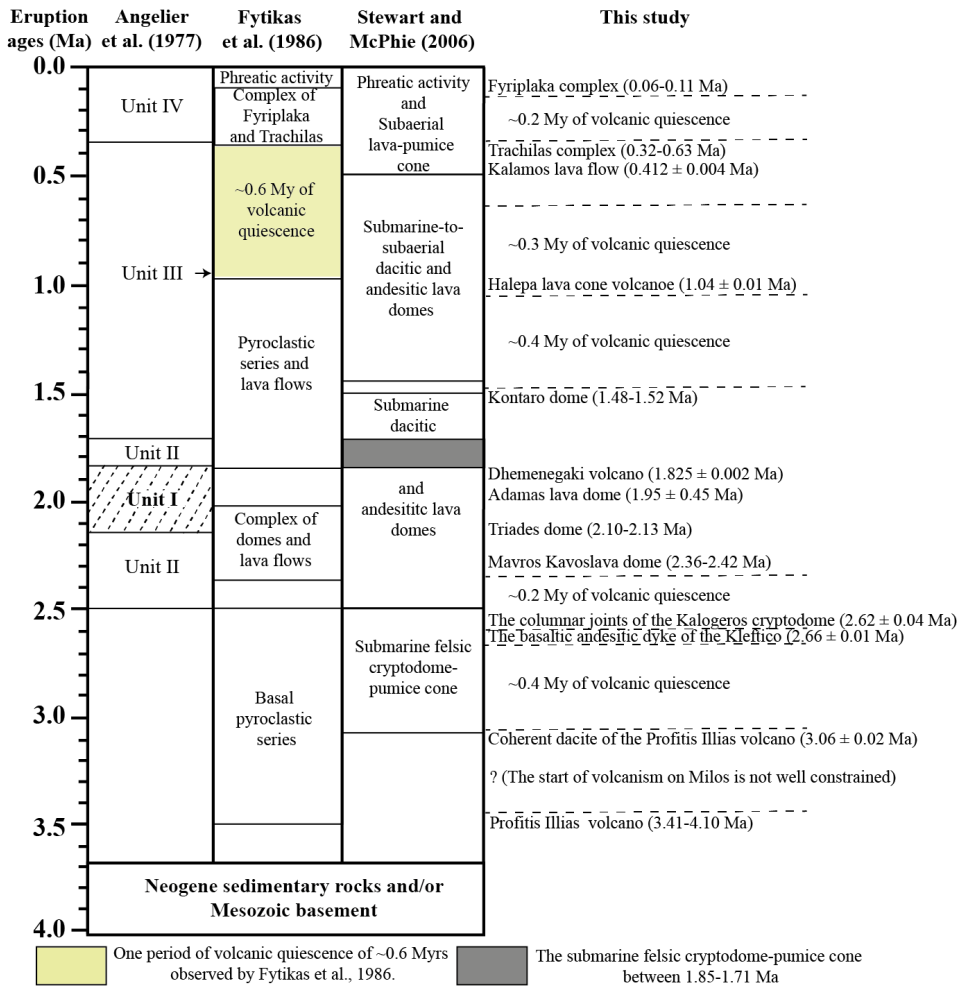


**Figure 3. Simplified geological map of Milos with our  $^{40}\text{Ar}/^{39}\text{Ar}$  ages and sample locations of key volcanic deposits, modified after Stewart and McPhie (2006) and Grasemann et al. (2018). The stratigraphic units of Milos are from Fytikas et al. (1986). Age data from this study are in black, published ages are shown in red (Angelier et al., 1977, Fytikas et al., 1986, Traineau and Dalabakis, 1989, and Stewart and McPhie, 2006). The "Green Lahar" (Fytikas, 1977) consists of deposits from multiple phreatic explosions and contains fragments of metamorphic, sedimentary and volcanic rocks.**



**Commented [MOU22]:** typo volcanoe; should be "lava", not "lava flow"; Most volcanic units actually take at most months to a few years to form, and the rest of the time is repose. So "quiescence" is the norm, "quiescence" is what goes on most of the time. Eruptions are brief (instantaneous) interruptions to that "quiescence". some of the more complex units that have multiple subdivisions probably take longer but certainly not the single domes. It is thus misleading to block out certain intervals as quiescence when almost all the time is "quiescence". Should remove these labels and explain this situation in the text.

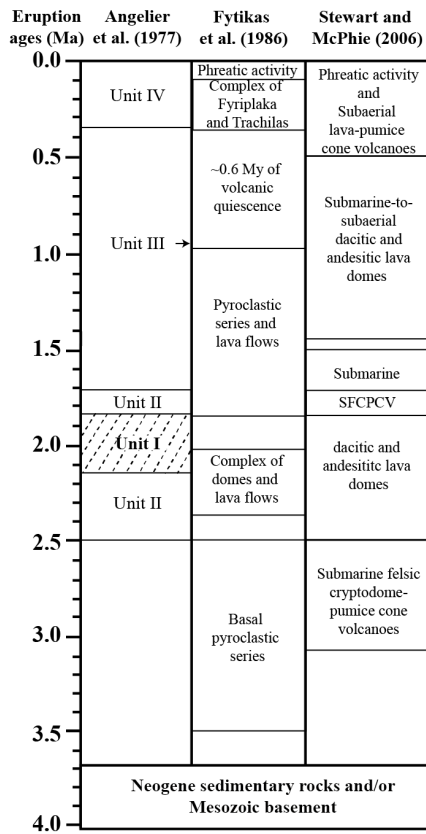
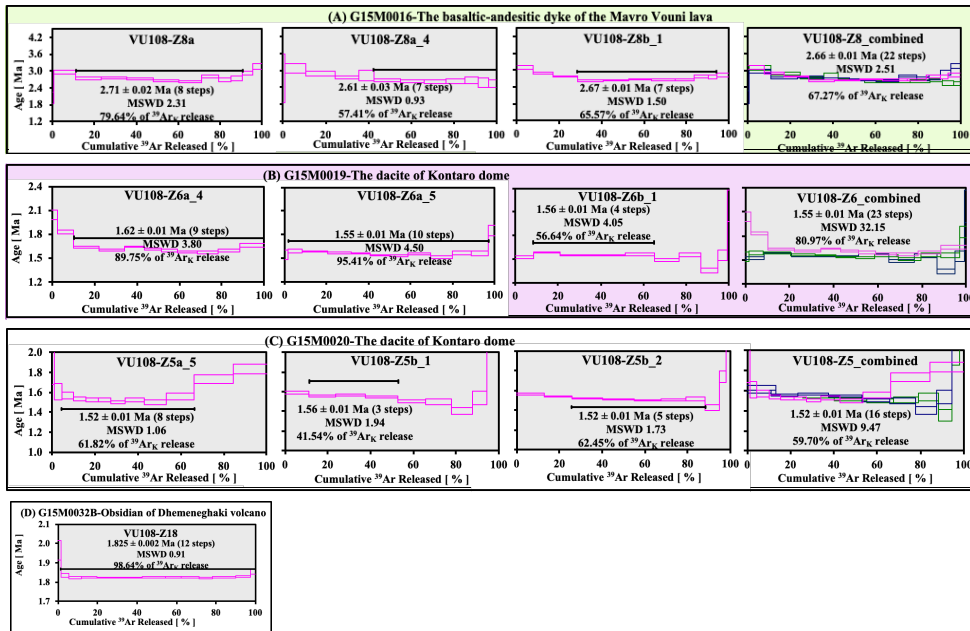


Figure 4. Previous proposed stratigraphic frameworks for Milos by Angelier et al. (1977), Fytikas et al. (1986) and Stewart and McPhie (2006). Volcanic unit II of Angelier et al. (1977) contains unit I. Stewart and McPhie (2006) described the volcanic faces of Milos mainly based on the geochronological works of Angelier et al. (1977) and Fytikas et al. (1986). Abbreviation: SFCPCV=Submarine felsic cryptodome-pumice cone volcanoes.



Commented [MOU23]: the title does not make sense

Commented [MOU24]: Jörn Wotzlaw: Fig. 5-8 look like supplementary figures that I think need some editing to make them even useful. The Ar release spec- tra are alright but they are many and in many cases are shown as individual samples and as combines spectra. Maybe it would be more useful to have larger panels only with the combined data and move the individual ones into the supplementary material. It would just make things less messy. Similarly, the ranked age plots for total fusion analyses have loads of text in each panel but the scaling of the axes is so stretched out, that it is difficult to assess the dispersion of the data.

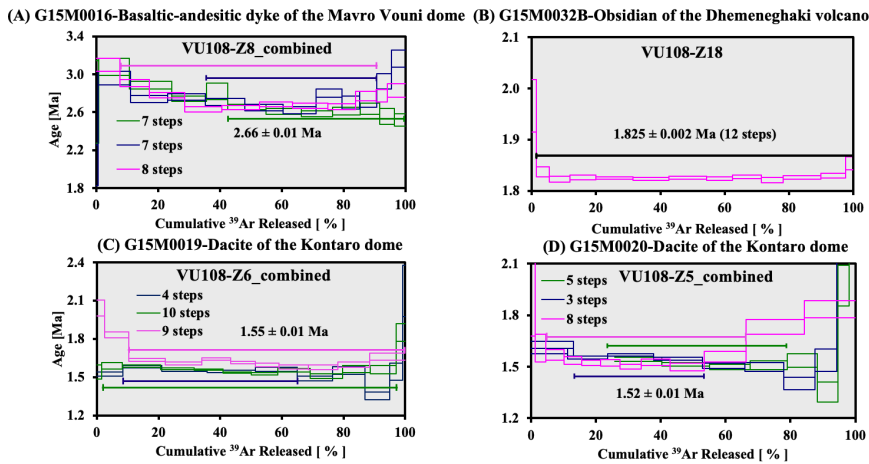
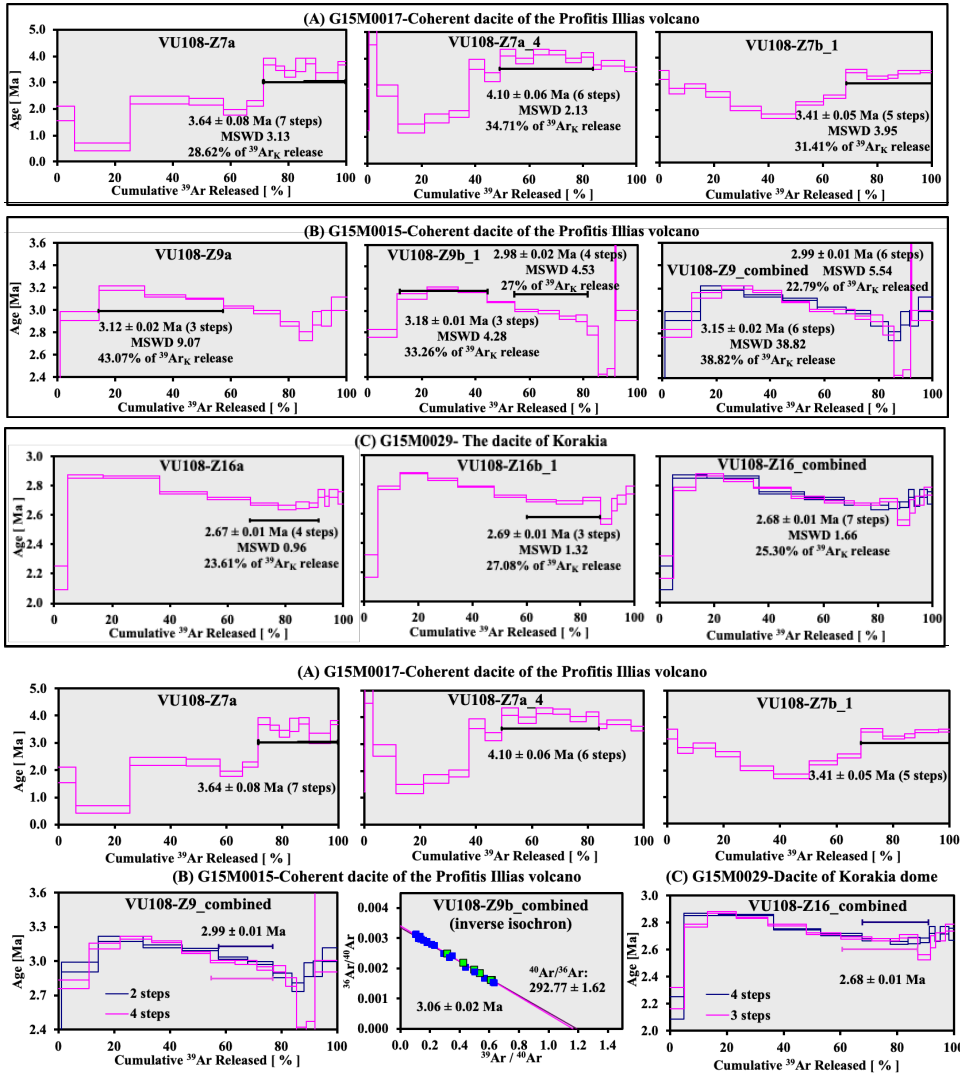
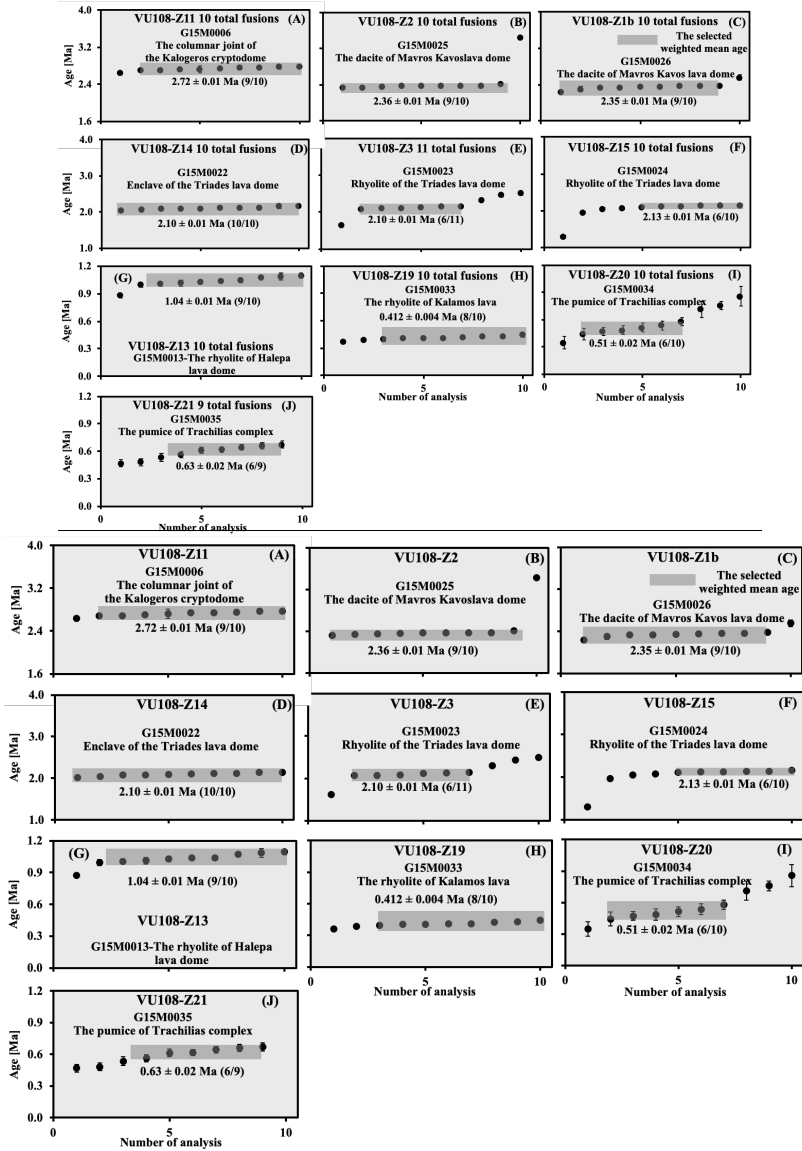


Figure 5. Groundmass  $^{40}\text{Ar}/^{39}\text{Ar}$  plateau ages for samples G15M0016 (A), G15M0032B (B), G15M0019 (C) and G15M0020 (D). The Mavro Vouni dome (A), Dhemenehaki volcano (B) and Kontaro dacitic dome (C, D) are located in respectively the south-western, north-eastern and eastern parts of Milos VF (see Fig. 2). Final age calculation is reported with  $1\sigma$  errors. See the individual steps of sample G15M0016, G15M0019 and G15M0029 in supplementary material II.



**Figure 6. Groundmass  $^{40}\text{Ar}/^{39}\text{Ar}$  plateau or inverse isochron ages for samples G15M0017 (A), G15M0015 (B) and G15M0029 (C). Individual steps and final age calculation are reported with  $1\sigma$  errors. The Profitis Ilias volcano (A, B) and dacitic Korakia dome (C) are located in the south-western and north-eastern parts of Milos VF, respectively (see Fig. 2). See the individual steps of sample G15M0015 and G15M0029 in supplementary material II.**



**Figure 7.** Biotite  $^{40}\text{Ar}/^{39}\text{Ar}$  total fusion ages for samples G15M0006 (A) and G15M0025-26 (B, C), G15M0022-24 (D-F), G15M0013 (G) and G15M0033-35 (H-J). Data outside shaded area are not included in the weighted mean. Individual steps and final age calculation are reported with  $1\sigma$  errors. The Kalogeros cryptodome and Mavros Kavos lava dome are located in the north-eastern and south-western parts of Milos VF, respectively, and Triades lava dome, Halepa lava dome, Trachilias complex and the Kalamos lava are situated in the southern, northern and south-eastern parts of Milos VF, respectively (see Fig. 2).

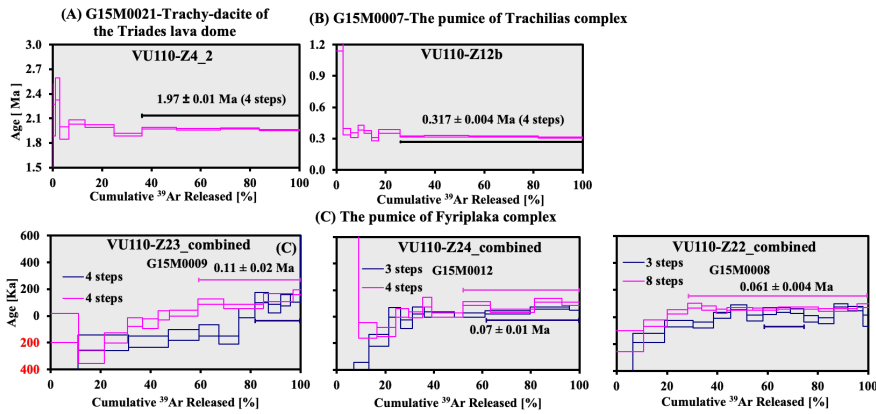
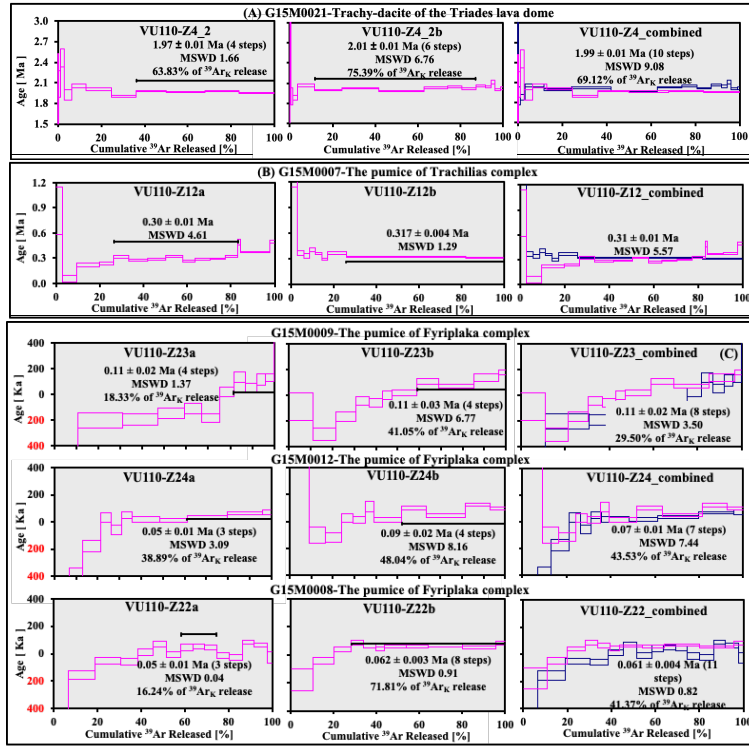


**Figure 8.** Biotite  $^{40}\text{Ar}/^{39}\text{Ar}$  plateau ages for samples G15M0021 (A), G15M0007 (B), and G15M0009 (VU110-Z23 combined), G15M0012 (VU110-Z24 combined) and G15M0008 (VU110-Z22 combined) (C). The numbers in red represent negative ages. Individual steps and final age calculation are reported with  $1\sigma$  errors. The Triades lava dome, Trachilias and Fyriplaka complexes are located in the north-western, northern and south-eastern parts of Milos VF, respectively (see Fig. 2). See the individual steps of sample G15M0021, G15M0007, G15M0009, G15M0012 and G15M0008 in supplementary material II.



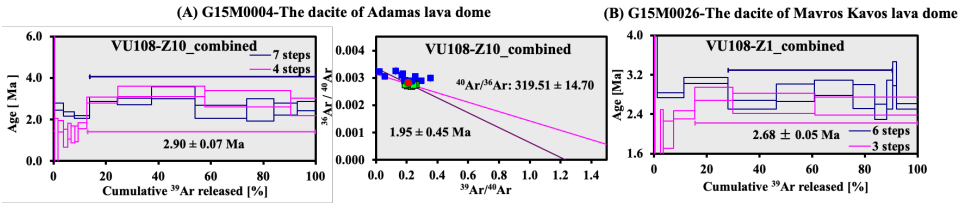
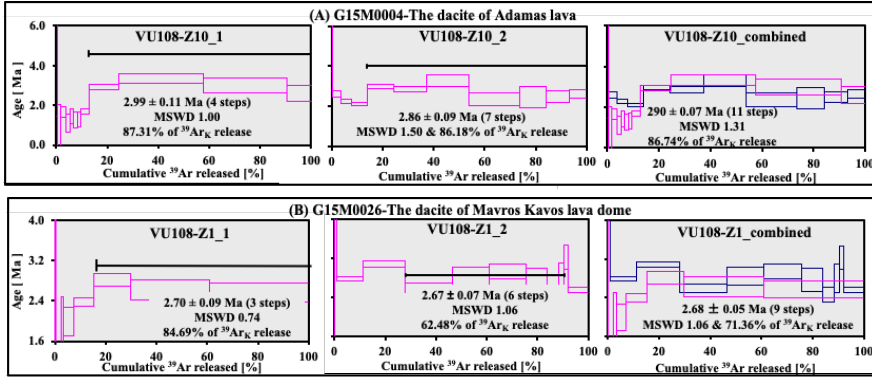


**Figure 9.** Amphibole  $^{40}\text{Ar}/^{39}\text{Ar}$  plateau or inverse isochron ages for samples G15M0004 (A) and G15M0026 (B). Final age calculation is reported with  $1\sigma$  errors. The Adamas and Mavros Kavos lava domes are located in the northern and south-western parts of Milos VF, respectively (see Fig. 2). See the individual steps of sample G15M0004 and G15M0026 in in supplementary material II.

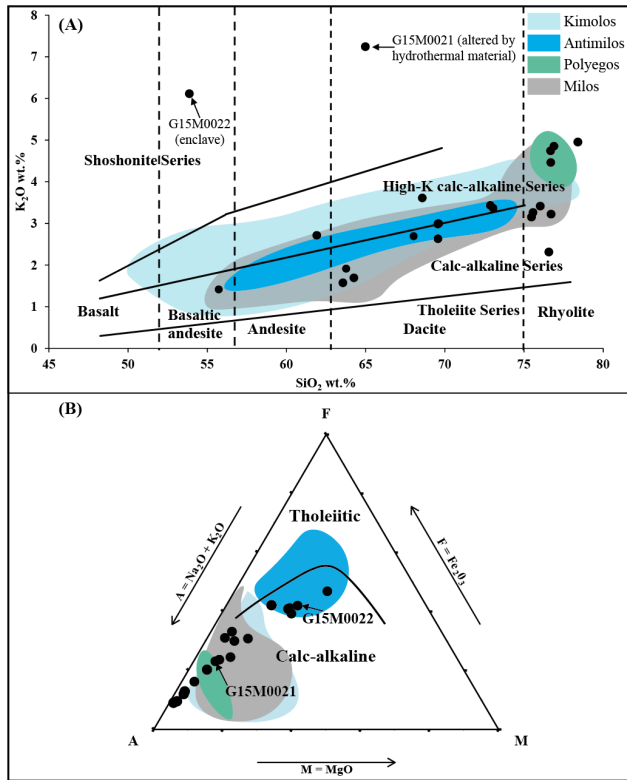


Figure 10.  $\text{SiO}_2$  versus  $\text{K}_2\text{O}$  (A) and AFM (B) diagrams for the Milos volcanic field with data of this study as solid circles. Published data are represented by shaded fields (Francalanci and Zelmer, 2019 and reference therein). Fields for the tholeiite, calc-alkaline, high-K calc-alkaline and shoshonitic series are from Peccerillo and Taylor (1976). Vertical lines defining fields for basalt, basaltic-andesite, andesite, dacite and rhyolite are from Le Bas et al. (1986). The solid line dividing tholeiitic and calc-alkaline fields is from Irvine and Baragar (1971).

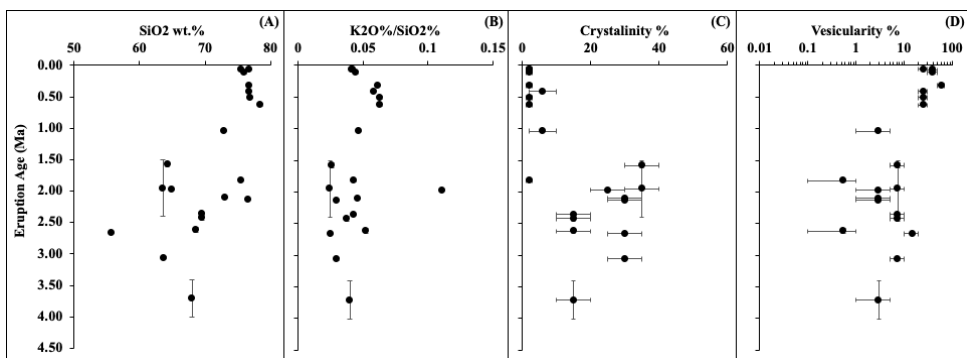


Figure 11. Eruption age versus (A) SiO<sub>2</sub> wt.%, (B) K<sub>2</sub>O%/SiO<sub>2</sub>%, (C) Crystallinity % and (D) Vesicularity % of Milos volcanic units of this study. The estimations of crystallinity and vesicularity on the older samples (>1.0 Ma) are all from lava and domes. The younger samples (<1.0 Ma) are pumiceous pyroclastic units. Data of the old pumices of the Profitis Ilias (~3.08 Ma) and Filakopi volcanoes (2.66 Ma) are lacking due to the severe alteration.

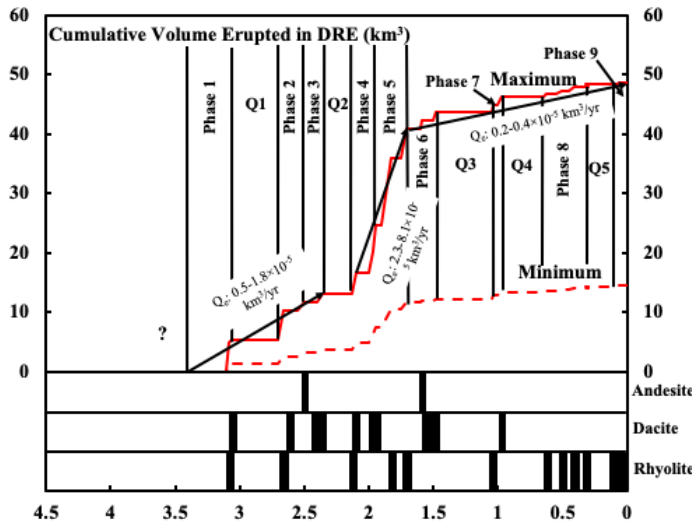


Figure 12. Cumulative eruption volume versus time for the volcanic deposits of Milos. The maximum (Max; red line) and minimum (Min; dashed red line) cumulative eruption volume curves were estimated from Campos et al. (1996) and Stewart and McPhie (2006); see discussion for more details. In the lower part of the figure the composition of the erupted products is shown (data from this study and Fytikas et al., 1986). The exact volume of volcanic products between 4.1 and 3.06 Ma is not well constrained and indicated with a question mark. Note the shift to more felsic compositions over time and the decrease in erupted volumes after 1.6 Ma. Q1-5 are the four periods of volcanic quiescence that lasted more than 200 kyr. Q<sub>v</sub> is the long term volumetric volcanic output rate explained in discussion.

Commented [MOU25]: McPhie: Because the data are so incomplete, these plots are of little value.

Commented [MOU26R25]: After adding the data of Filakopi pumice breccia, the so incomplete data should not be called in this study.

Commented [MOU27]: McPhie: what is the vertical scale? Add a label.

Commented [MOU28R27]: The vertical scales have been removed.

Commented [MOU29]: Jörn Morzlaw: I would recommend to combine figures 11 and 12 to display the eruptive flux and compositional variations together on the same scale. I think this would be quite illustrative (e.g. it seems like the transition from the high-flux to late low flux interval coincides with a rather sudden change in magma composition, crystal content etc. This has some important petrological implications and reveals some important change in the magma plumbing system from producing crystal-rich (20-40%) intermediate eruptions to crystal-poor (<5%) rhyolitic magmas that represent the extracted residual liquids. Describing and discussing this in detail in a short paragraph on the petrologic implication I think would be very interesting.

Commented [MOU30R29]: Agree. I combined figures 11 and 12 after adding the additional data from Plake and Filakopi volcanic centres.

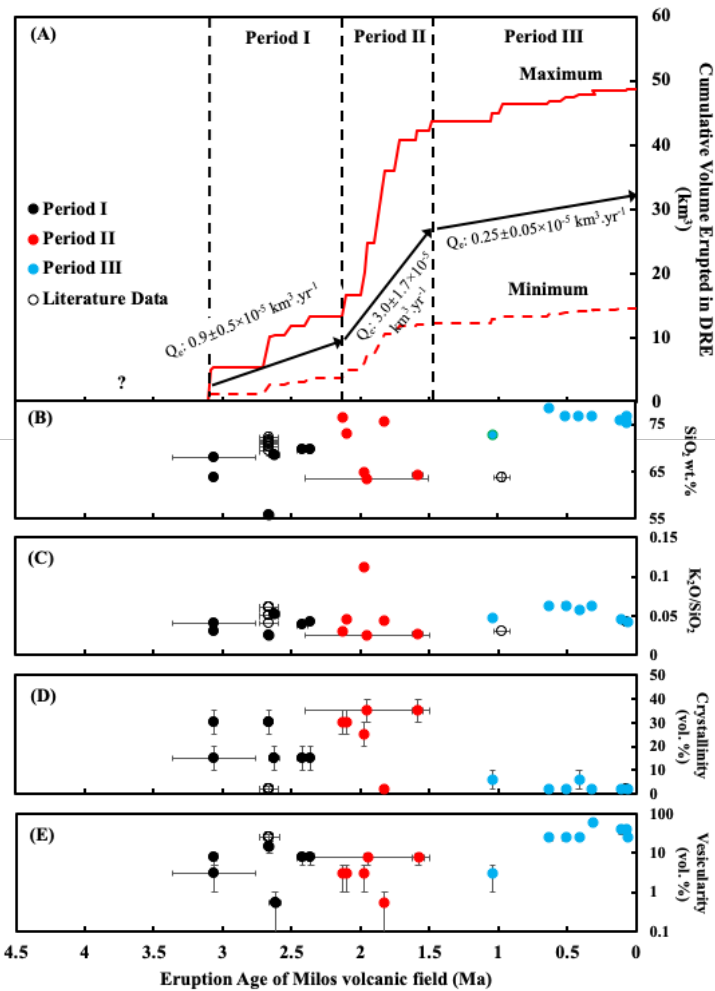
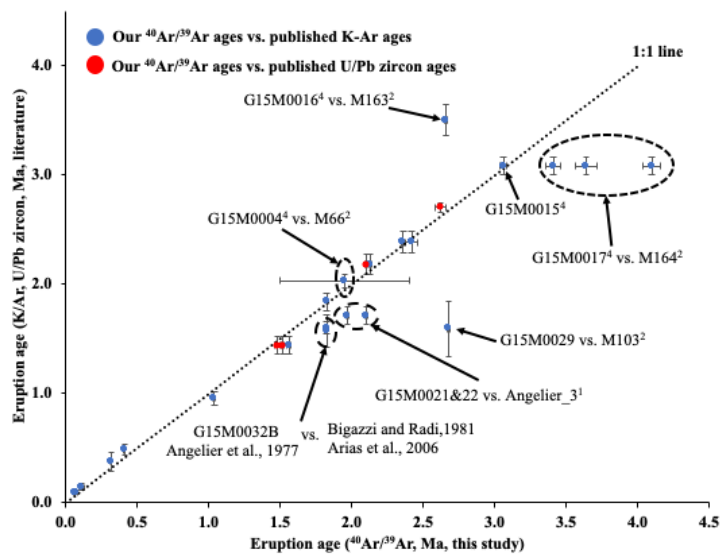


**Figure 11. Eruption age versus (A) cumulative eruption volume for the volcanic deposits of Milos, (B) SiO<sub>2</sub> wt.%, (C) K<sub>2</sub>O/SiO<sub>2</sub>%, (D) crystallinity vol. % and (E) vesicularity vol. % of Milos volcanic units of this study and previous studies. The maximum (Max; red line) and minimum (Min; dashed red line) cumulative eruption volume curves were estimated from Campos et al. (1996) and Stewart and McPhie (2006).  $Q_v$  is the long term volumetric volcanic output rate (see discussion). The exact volume of volcanic products between 4.1 and 3.08 Ma is not well constraint and indicated with a question mark. In this study, the estimations of crystallinity and vesicularity on the older samples (>1.0 Ma) are all from lava and domes. Most of the younger samples (<1.0 Ma) are pumiceous pyroclastic units. The major element, crystallinity and vesicularity data of the old pumices of Filakopi volcanoes (2.66 Ma) are from Stewart (2003). The major element data of the Plakes lava dome is from Fytikas et al. (1986). Geochemical, crystallinity and vesicularity data of the old pumices of the Profitis Ilias (~3.08 Ma) is lacking due to the severe alteration.**



<sup>1</sup>=Angelier et al., 1977; <sup>2</sup>= Fytikas et al., 1986; <sup>3</sup>= Matsuda et al., 1999; <sup>4</sup>=Stewart and McPhie, 2006.

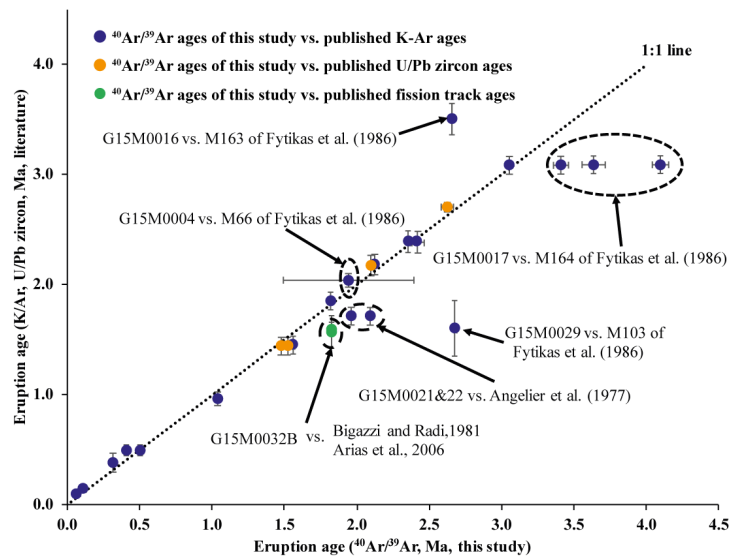
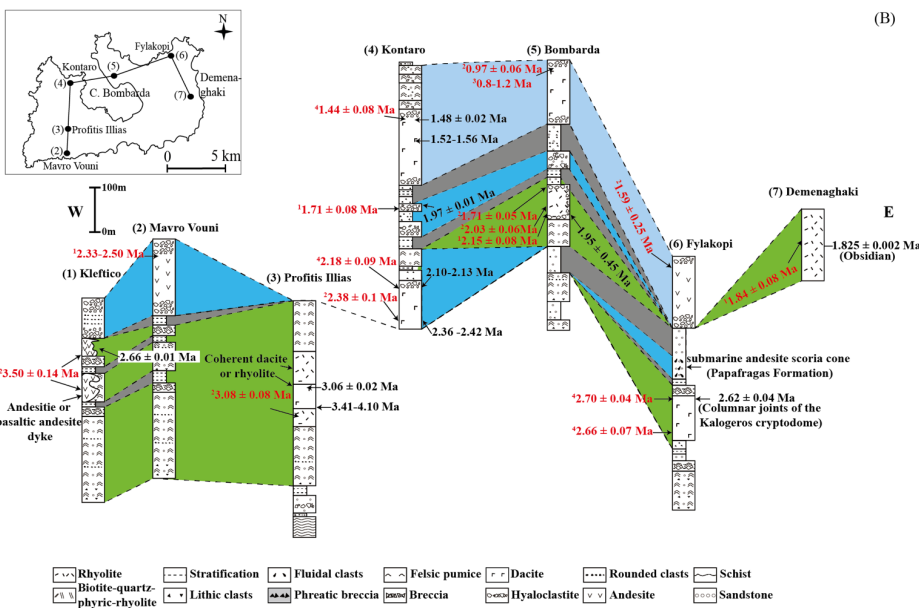
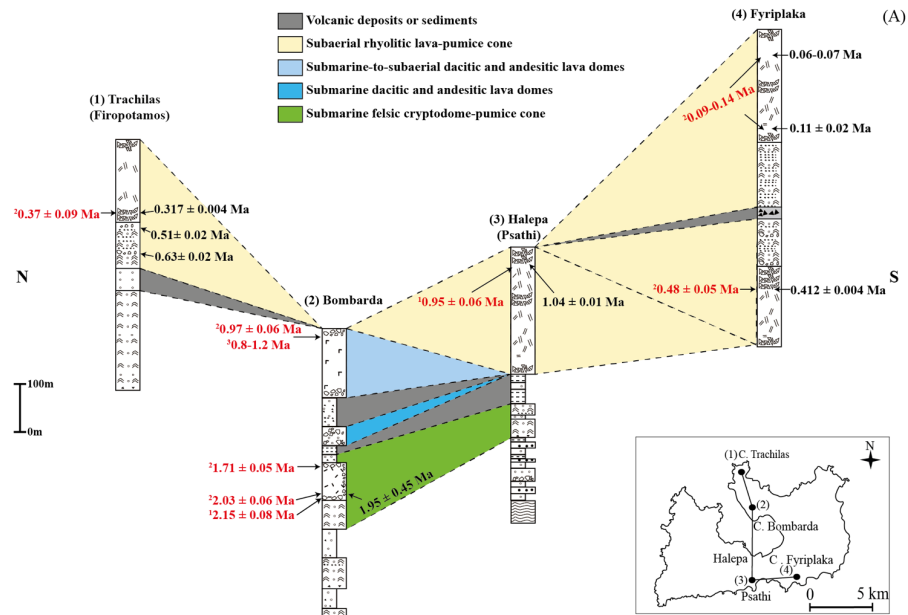


Figure 12. The  $^{40}\text{Ar}/^{39}\text{Ar}$  ages of this study (x-axis) compared to the K/Ar ages (Angelier et al., 1977; Fytikas et al., 1986), U/Pb zircon ages (Stewart and McPhie, 2006) and fission track ages (Bigazzi and Radi, 1981; Arias et al., 2006) (y-axis) for the same volcanic units. Ages which deviate from the 1:1 correlation line are discussed in section 4.1.

Commented [MOU31]: McPhie: The superscripts seem to not make any sense. why is this sample of yours (G15M0004) referred to Stewart and McPhie? Same problem to G15M0016 and 17. There is lack of information of fission track ages.




**Commented [MOU32]:** McPhie: logs 1 and 4 are not consistent with the other logs; they are not graphic logs whereas all the other ones (copied from Stewart and McPhie) are graphic.

the schist pattern doesn't match the legend

**Commented [MOU33R32]:** These will be fixed. The schist pattern legend should be consistent.

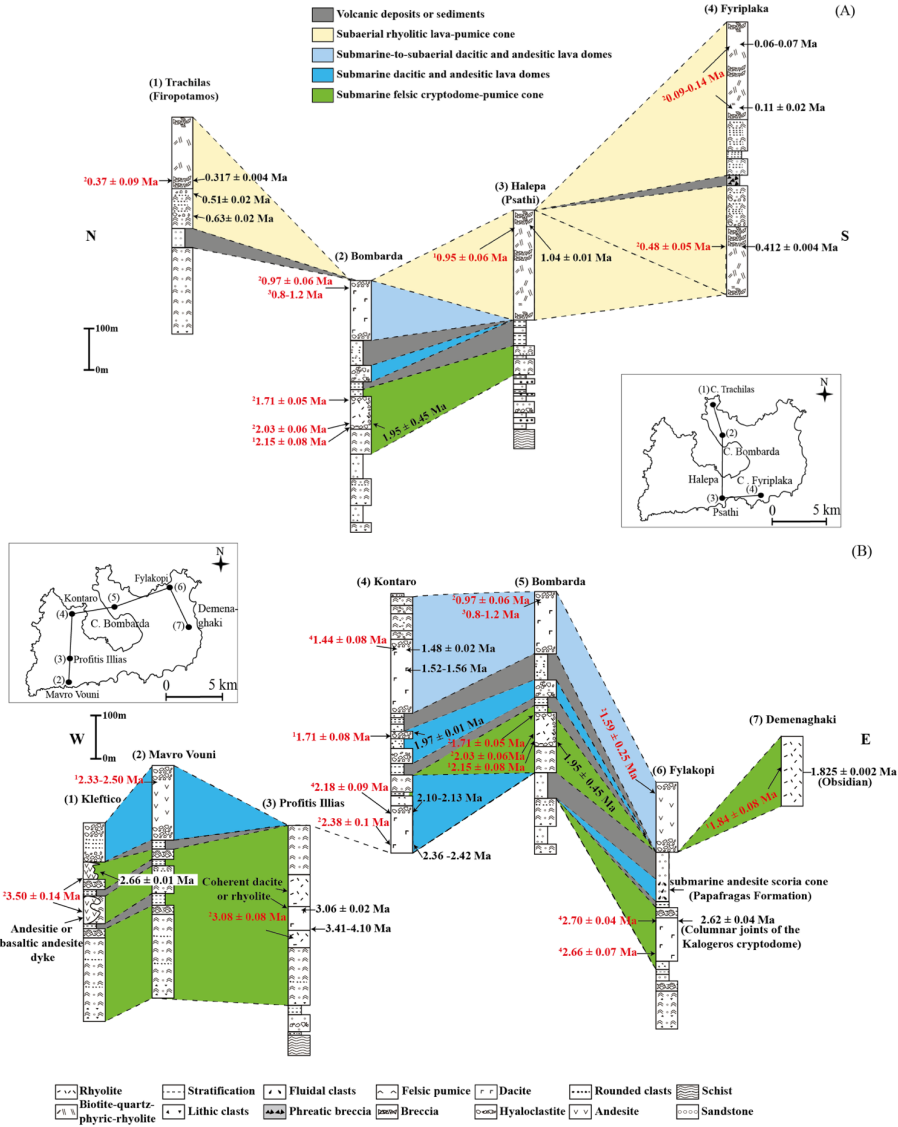


Figure 14. Nine selected stratigraphic columns covering the (A) young (<1.4 Ma) old (>1.4 Ma) and (B) old (>1.4 Ma) young (<1.4 Ma) volcanic deposits of Milos modified after Stewart and McPhie (2006), except for (7) Demenaghaki. Age data in black are from this study and in red are from: 1=Angelier et al. (1977), 2=Fytikas et al. (1976, 1986), 3=Matsuda et al. (1999), 4=Stewart and McPhie (2006).

Commented [MOU34]: McPhie: seems to be the reverse - A is young and B is old

Commented [MOU35R34]: Fixed.

Commented [MOU36]: McPhie: seems to be the reverse - A is young and B is old

Commented [MOU37R36]: Fixed.

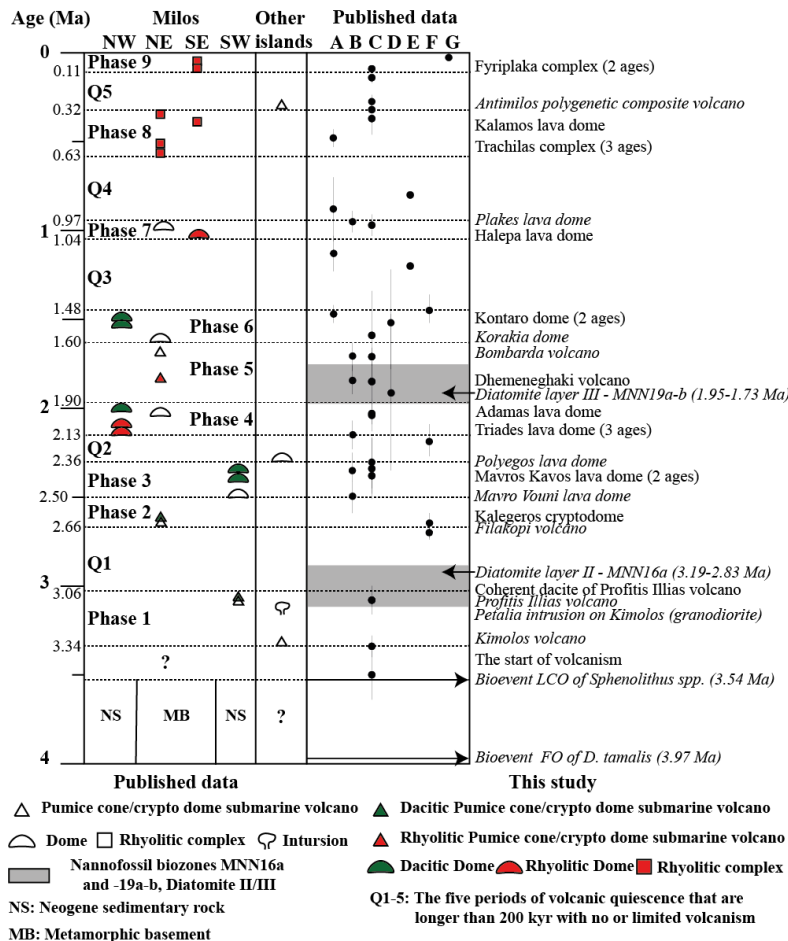


**Figure 15.** Diagram comparing the proposed nine volcanic phases and four periods of quiescence of Milos based on the new  $^{40}\text{Ar}/^{39}\text{Ar}$  data of this study (indicated by solid symbols) and published age data (indicated by open symbols, names in italic). The volcano types for the different volcanic units (left panel) are from Stewart and McPhie (2006). The location of the different volcanoes is given in Fig 3, and indicated in the left panel (from left to right: NW, NE, SE and SW of Milos). The right panel corresponds to published data: [A]=Fytikas et al., 1976, [B]=Angelier et al., 1977, [C]=Fytikas et al., 1986, [D]=Bigazzi & Radi, 1981, [E]=Matsuda, 1999, [F]=Stewart and McPhie (2006) and [G]=Principle 2002. Biostratigraphic data of the Neogene sediments (NG) is from Van Hinsbergen et al. (2004) calibrated to Gradstein et al. (2012) (LCO of *Sphenolithus* spp. and FO of *D. tamalis*) and Calvo et al. (2012). The start of volcanism (3.34-3.54 Ma) on Milos and the basement underneath Kimolos, Polyegos and Antimilos islands is not well constrained and indicated with question marks (see text for discussion).

**Commented [MOU38]: Jörn:** Fig. 15 is a bit of a mess and I don't find that this figure is doing the amount of new high-quality data justice. A better-quality summary figure that integrates all the new and published data would sum up this work nicely for any reader.

**Commented [MOU39R38]:** I hope this problem has been solved.

**Commented [MOU40]: McPhie:** the legend implies that you attribute the composition and volcano type to this study when in fact, this study has not contributed any new data on volcano types or composition. The text of legend should be Published age data and Age data, this study.

**Commented [MOU41R40]:** Partly agree. We did contribute geochemical data to Milos volcanic field. We agree with the confusing legend and modified it.

**Commented [MOU42]: McPhie:** This figure only makes sense if you remove the "volcanic phases" and remove the "periods of quiescence".

Neither the compositions nor eruption styles of the volcanoes grouped in the "volcanic phases" show any connections or relationship. eg. "phase 4" groups rhyolite and andesite and "phase 2" groups a cryptodome and pumice cone.

**Commented [MOU43R42]:** "Phases" and "quiescence" have been removed.

**Commented [MOU44]: McPhie:** typo should be constrained

**Commented [MOU45R44]:** Agree



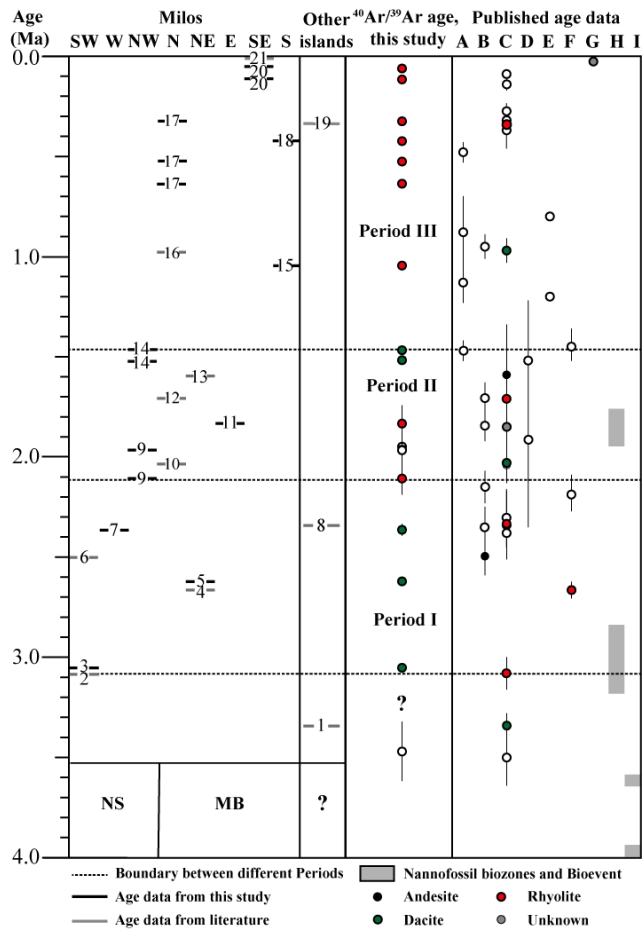
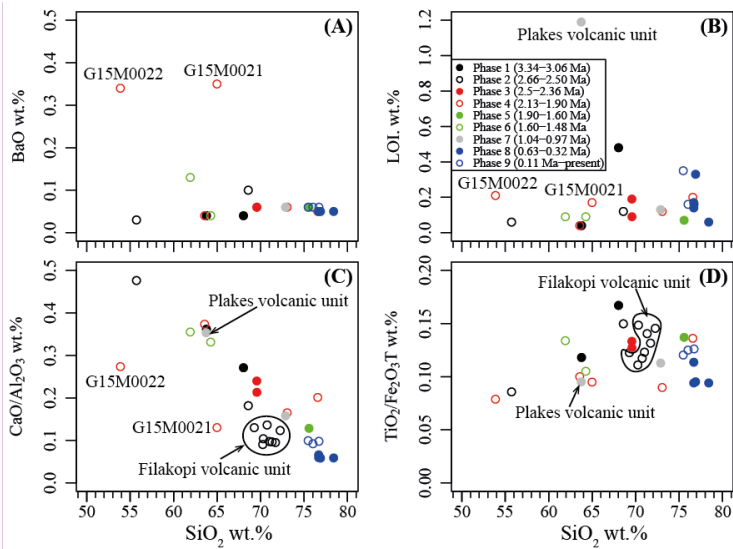


**Figure 14. Diagram presenting three periods of different long term volumetric volcanic output rate on Milos volcanic field based on the new  $^{40}\text{Ar}/^{39}\text{Ar}$  Ar data of this study and published data. The location of the different volcanoes is given in Fig 2 and indicated in the left panel (from left to right: SW, W, NW, N, NE, E, SE and S of Milos). The right panel corresponds to published age data: [A]=Fytikas et al., 1976, [B]=Angelier et al., 1977, [C]=Fytikas et al., 1986, [D]= Bigazzi & Radi, 1981, [E]=Matsuda, 1999, [F]=Stewart and McPhie (2006), [G]= Trainau and Dalabakis, 1989, and Biostratigraphic data of the Neogene sediments (NG) is from [H]=Calvo et al. (2012) and [I]=Van Hinsbergen et al. (2004) calibrated to Raffi et al. (2020) (LCO of *Sphenolithus* spp. and FO of *D. tamalis*). The number in the left panel represents the volcanic centres of Milos (see details in Table 5). The start of volcanism (3.08-3.61 Ma) on Milos and the basement of the other Islands (Antimilos, Kimolos and Polyegos) are not well constraint and indicated with question marks (see text for discussion). The simplified basement cross-section (NS: Neogene sedimentary rock; MB: Metamorphic basement) under Milos volcanic units is based on Fytikas et al. (1989). We used the filled symbols as the best estimate for the eruption ages at the different volcanic**



centres.

**Figure 16.**  $\text{SiO}_2$  wt.% versus (A) BaO wt.%, (B) LOI wt.%, (C)  $\text{CaO}/\text{Al}_2\text{O}_3$  and (D)  $\text{TiO}_2/\text{Fe}_2\text{O}_3\text{T}$  for the nine volcanic phases of the Milos volcanic field. The published data of Filakopi and Plakes volcanic units are from Stewart and McPhie (2003) and Fytikas et al. (1986), respectively.

**Commented [MOU46]:** McPhie: remove "Phase" labels. Replace with measured ages.

**Commented [MOU47R46]:** This figure was removed from this manuscript.